RSC Sustainability

Accepted Manuscript

This article can be cited before page numbers have been issued, to do this please use: S. A. Thomas, J. Cherusseri and D. N. Rajendran, *RSC Sustain.*, 2024, DOI: 10.1039/D4SU00146J.

ROYAL SOCIETY OF CHEMISTRY

View Article Online
DOI: 10.1039/D4SU00146J

Sustainability Spotlight Statement

Wearable electronic devices necessitate sustainable and safe energy storage devices to power them. Flexibility, bendability, twistability are the required features need to be adapted for the wearable supercapacitors. The increasing demand for sustainable energy storage devices are manifested by UN Sustainable Development Goal: 7: Affordable and Clean Energy. Carbon fibers-based hybrid/nanocomposite electrodes are highly sustainable materials for developing high-performance flexible and wearable supercapacitors.

View Article Online
DOI: 10.1039/D4SU00146J

Data Availability Statement

Data sharing not applicable – no new data generated. Data availability is not applicable to this article as no new data were created or analysed in this study.

Recent Advancements on Carbon Fibers-Based Sustainable Electrodes for Flexible and Wearable Supercapacitors

Susmi Anna Thomas[1], Jayesh Cherusseri[2,3*] and Deepthi N. Rajendran[1*]

[1]Department of Physics, Government College for Women (Affiliated to University of Kerala), Thiruvananthapuram, Kerala 695014, India
[2]Research Centre for Nanomaterials and Energy Technology (RCNMET), School of Engineering and Technology, Sunway University, No. 5 Jalan University, Bandar Sunway, 47500 Selangor Darul Ehsan, Malaysia
[3]School of Engineering and Technology, Sunway University, No. 5 Jalan University, Bandar Sunway, 47500 Selangor Darul Ehsan, Malaysia

***Corresponding Author**
E-Mail Address: drjayeshpuli@gmail.com (JC); deepthinrphysics@gmail.com (DNR)

Abstract

Electrochemical energy storage devices such as rechargeable batteries and supercapacitors have replaced conventional batteries and dielectric capacitors due to their excellent charge storage capabilities. Supercapacitors (SCs) are excellent in their high-power density and can deliver high-power on demand in fraction of seconds. SCs utilize water-based electrolytes, hence are safe and reliable energy storage devices for application in portable and wearable electronic devices. A major challenge in fabricating a flexible and wearable SC is the rigidity of electrodes prepared due to the usage of rigid metallic current collectors. This hinders SCs in their successful implementation to power the commercial wearable electronic device. The flexibility to a SC is mainly imparted by its electrodes hence the preparation of electrode is utmost important. In this review, we report the facile fabrication of SCs using carbon fiber (CF) including carbon microfiber and carbon nanofiber. CF is a sustainable environment-friendly material that can be used in electrochemical energy storage devices. CF functions as both an electrode-active material and a current collector during the fabrication of a SC. A major bottle-neck in using the CF as an electrode-active material in SCs is their low specific capacitance. The specific capacitance of CF-based SCs can be enhanced by preparing hybrid or nanocomposite electrodes by combining CF with other high-performing electrode-active materials such as electronically conducting polymers, nanocarbons, MXenes, transition metal oxides, etc. We have provided a detailed discussion on the various strategies adopted for the synthesis of CF-based hybrid/nanocomposite flexible electrodes for SC application. The electrochemical performance evaluation of CF-based SC electrodes is reviewed and emphasis is given to their flexible and wearable features. This article helps to get an in-depth insight about the preparation of sustainable CF-based flexible electrodes for the next-generation wearable SCs.

Keywords: Supercapacitor, Carbon Fiber, Wearable Electronics, Electrochemical Energy Storage, MXene

1. Introduction

Tremendous development in portable and wearable electronics have triggered the research and development of flexible energy storage devices to power them [1, 2]. The increased explorations in the field of energy science and technology helped the consumer electronic industry to emphasize design and manufacture consumer electronic products with features such as flexibility, portability and a miniaturized size. Such products hold various fantastic

View Article Online
DOI: 10.1039/D4SU00146J

functionalities like rolling-up display, on-body sensors, wearable cloth fabric with self-charging utility, etc. to name a few [3-5]. The efforts put forwarded in the field of consumer electronics necessitated gigantic modifications to the energy storage systems in terms of their flexibility and safety in implementation rather than merely possessing high energy density, power density and long cyclic stability. Hence importance has been given to the mechanical features such as flexibility, bendability, stretchability, etc in fabricating energy storage devices for wearable electronic devices [6-8]. Among the various available choices, rechargeable metal-ion batteries and supercapacitors (SCs) are the two contemporary choices that evolved to save the current energy demand due to energy scarcity [9-11]. Rechargeable metal-ion batteries such as lithium-ion batteries, sodium-ion batteries, etc are excellent in their energy densities but they fail to deliver high-power on demand. On the other hand, SCs are best in their high-power density but exhibit low energy density. A major demerit of using rechargeable metal-ion batteries is their recyclability where the disposal become a nightmare. In contrary, SCs utilizing water-based electrolytes are environment-friendly candidates and can be made sustainable devices if the components used are sustainable materials. Hence, water-based SCs become a major focus of research now-a-days. The rapid development in the field of portable electronic devices, it is mandatory to develop flexible energy storage devices such as flexible SCs where the SC can be bendable, twistable etc during its operation [12]. The stress-strain relationship of a flexible energy storage device can be linearly elastic, anelastic or plastic [13]. A flexible SC should necessary to hold the features such as bendability, foldability, stretchability characteristics and safest operation [14, 15]. Recently, researchers are dedicated their efforts to introduce mechanical flexibility in rechargeable batteries by imparting flexibility to their individual components in order to demonstrate it for practical industrial applications but their flammability remains a major challenge [16, 17].

With respect to the features of flexible electronic devices, the power sources are needed to be mechanically flexible in terms of their bendable and twistable features. The bulky and cumbersome architecture of the energy storage devices are not encouraged as it will be difficult to integrate with the available portable electronic device [18]. The development of planar energy storage devices that can easily be integrated with textile fabrics by weaving or other means become an area of research for both the materials scientists as well as the energy researchers [19]. There are large number of studies reported in the literature that discuss the design and mechanism underlying with the flexible energy storage systems when there is a mechanical deformation [20]. To make flexible energy storage systems for practical purposes, each component in the system must be sustainable, conformable with shape, hold higher efficiency, heat resistant, cost-effective, and scalable but majority of the materials doesn't fully satisfy the criteria [21, 22]. One of the major challenges facing in the development of these sustainable materials is the availability of the material. The other features such as easiness in their synthesis, reliability and shape-conformability are also equally important. The current developments in the field of nanostructured materials for application as electrode-active materials made a stimulation in the field of electrochemical energy storage devices [23, 24]. The different types of electrode-active materials used are electronically conducting polymers, transition metal oxides, carbon nanomaterials, biomass nanofibers, etc. Among the various choices, carbon nanomaterials have achieved great interest due to their efficient chemical, thermal, mechanical and electronic properties [25]. In the family of carbon materials, carbon fiber (CF), including carbon nanofiber (CNF) and carbon microfiber (CMF), have achieved great acceptance in developing flexible electrode fabrication.

CF is a unique type of carbon materials contains a carbon content of >90 wt%. This fibril form of the carbon consists of tubostratic carbon layers with graphite crystallites oriented in the fiber axis. With respect to its structural and compositional features, these materials are extraordinary tensile strength, higher value of modulus and stiffness, efficient temperature and

View Article Online
DOI: 10.1039/D4SU00146J

fatigue resistance, good electrical conductivity and low specific density [14]. CF-based materials are developed at an industrial scale from sources such as polyacrylonitrile (PAN) and pitch precursors and the production has begun from the year 1960. CF and CF-reinforced composites become a fascinating substrate for high-performing and indispensable structural combinations. Since CF exhibits excellent mechanical strength and lightweight, it become an inevitable material of choice in the field of aerospace, automobiles, biomedical, electrical components, etc. Commercially available CF consists of thousands of monofilaments in a diameter range of 5-10 μm. In accordance with the synthesis approaches, various forms of CF-based components such as CF fabric, CF paper, CF textile, CNF fabric, etc are developed in the recent past [26]. CF prepared in both laboratory and industry is classified in accordance with the precursors used for its synthesis. PAN, isotropic pitch and mesophase pitch are synthesized by the spinning of the individual precursors such as PAN, isotropic pitch and anisotropic mesophase pitch, etc., followed by the reactions such as stabilization and carbonization at an elevated temperature, such as 1300ºC [20]. Mechanical and other fundamental properties of CF depend upon the characteristic features of precursors used in the synthesis and also the method adopted. The precursors should be easily spun to a filamentary architecture, which can able to decompose to a stable form without producing any melting at a slow rate. The carbon content of the product should be very high after the pyrolysis procedure and produce a maximum yield [26]. The CF hold good crystallinity in the direction of fiber axis.

Flexible electronic devices are bendable and twistable, sometimes twistable hence the SCs integrated with such devices also should possess the same features. SCs utilizing water-based electrolytes and flexible electrodes are highly preferred for wearable electronic device application due to their safe in application and easiness in integration [8] A term called “smart electronics” is also evolved in the recent past, which has more functional features to attract the market such as wifi-charging, facial recognition monitoring, etc [27]. SCs can be coupled with renewable energy conversion technologies such as solar cells, piezoelectric/triboelectric nanogenerators, etc. for the effective utilization of waste energy for charging the SC instantaneously. But a proper design is mandatory and the charging capability of the energy conversion device should be matched with the electronic device which is going to utilize the power from the SC. In the case of flexible SCs, these energy conversion devices should be flexible too for their easy integration with wearable electronic devices. The main components of a SC are electrodes, current collector, electrolyte separator, electrolyte and sealing material. The main component that determines the performance of a SC is the electrode-active material. But the main component in a flexible SC is the supporting substrate at which the electrode-active material is composed with. During the fabrication of SC electrode, the electrode-active material is coated over an electronically conducting substrate (such as metal sheet, metal foil, metal foam, etc). Hence the flexibility to the electrode is actually imparted by the substrate used in the fabrication process. If metal substrates are used for the fabrication of Sc electrode, the prepared electrodes become rigid and hence become non-flexible. Hence flexible substrates are mandatory in developing flexible electrodes for SCs. The choices for flexible electronically conducting substrates are plastics (such as indium-doped tin oxide coated polyethylene terephthalate), carbon cloth, CMF sheet/mat, CNF sheet/mat, etc. Among the limited available choices, CF is the best option to use as substrates for fabricating flexible electrodes due to their environment-friendliness, low specific gravity, biodegradability, sustainability, low cost, easy processing, etc. CF-based SC electrodes with planar architecture are highly preferred for sustainable energy conversion and energy storage devices due to their extraordinary flexibility [20]. CF can easily be integrated with wearable electronic textiles by simple weaving procedures, which has boosted their demand in developing wearable SCs [11]. To compete with the requirements of current wearable devices with varying sizes and shapes, it is necessary

View Article Online
DOI: 10.1039/D4SU00146J

to introduce CF-based fibrous electrodes with efficient physical, chemical, mechanical and electrochemical properties [28]. The CF can be used in SC electrodes in three different ways: (i) substrate for the electrode-active material, (ii) current collector for the electrode-active material, and (iii) an electrode-active material for the SC. In some cases, CF is used as electrode-cum-current collector for developing SCs [29]. There are number of studies carried out using CF-based SCs in the literature. But a comprehensive review in the field of CF-based SCs is lacking in the literature. This motivated us to write this review article. A graphical analysis of number of publications based on CF-based SCs from 2004 to 2023 is given in **Figure 1**. It can be seen that a rise in number of publications happened from the year 2013 and received an exponential growth towards year 2019 and become stable thenafter. The reason for this saturation can be considered as the limited electrode designs that can be applied to the SC electrode as well as to the SC devices using CF as the flexible component in it. In this review article, we discuss the synthesis of CF such as CMF and CNF, and their successful implementation in SC electrodes. The recent progresses and challenges of various nanocomposite electrodes based on CF such as CF/electronically conducting polymer nanocomposites, CF/layered double-hydroxide nanocomposites, CF/carbon nanostructures nanocomposites, etc. are emphasized with their preparation methods and characterizations. The electrochemical performance evaluations of CF-based nanocomposite electrodes for SC application are discussed in detail using various tools such as electrochemical impedance spectroscopy, cyclic voltammetry (CV), and galvanostatic charge/discharge (GCD) measurement, etc. The major contents of the present review are schematically shown in **Figure 2**.

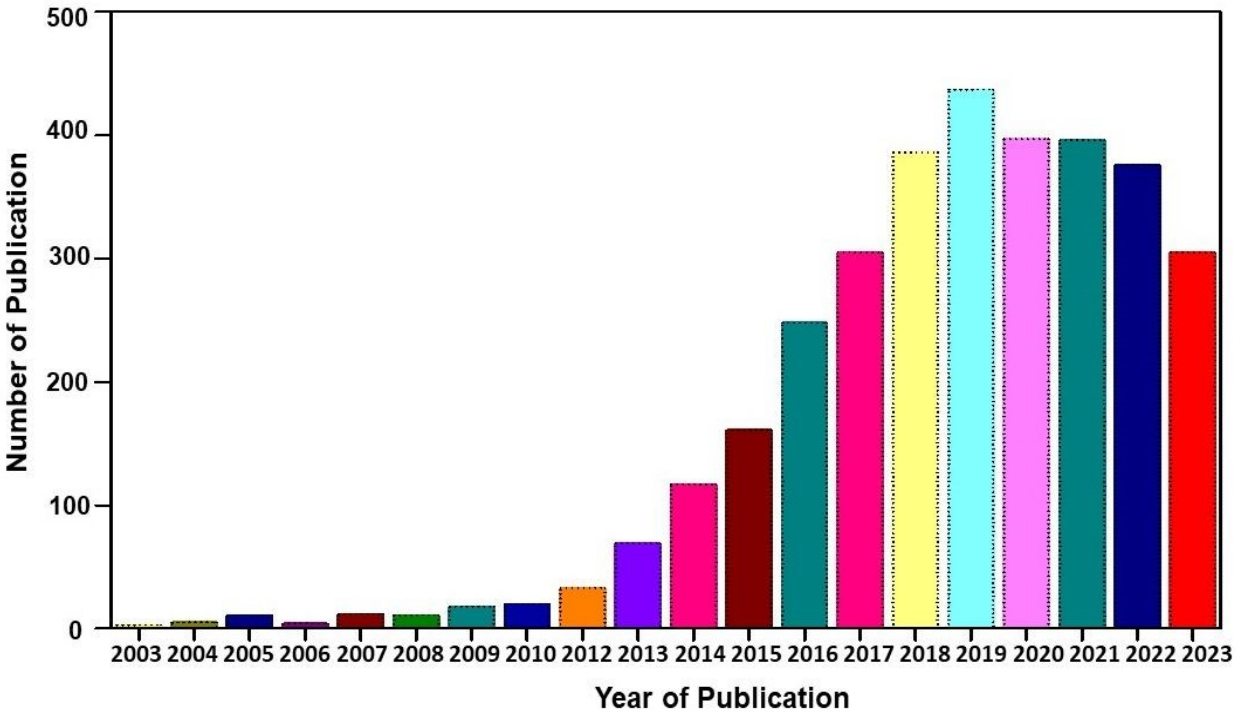

Figure 1: Statistical analysis of number of publications based on CF for SC application from the year 2004 to 2023 [Source: Web of Science].

View Article Online
DOI: 10.1039/D4SU00146J

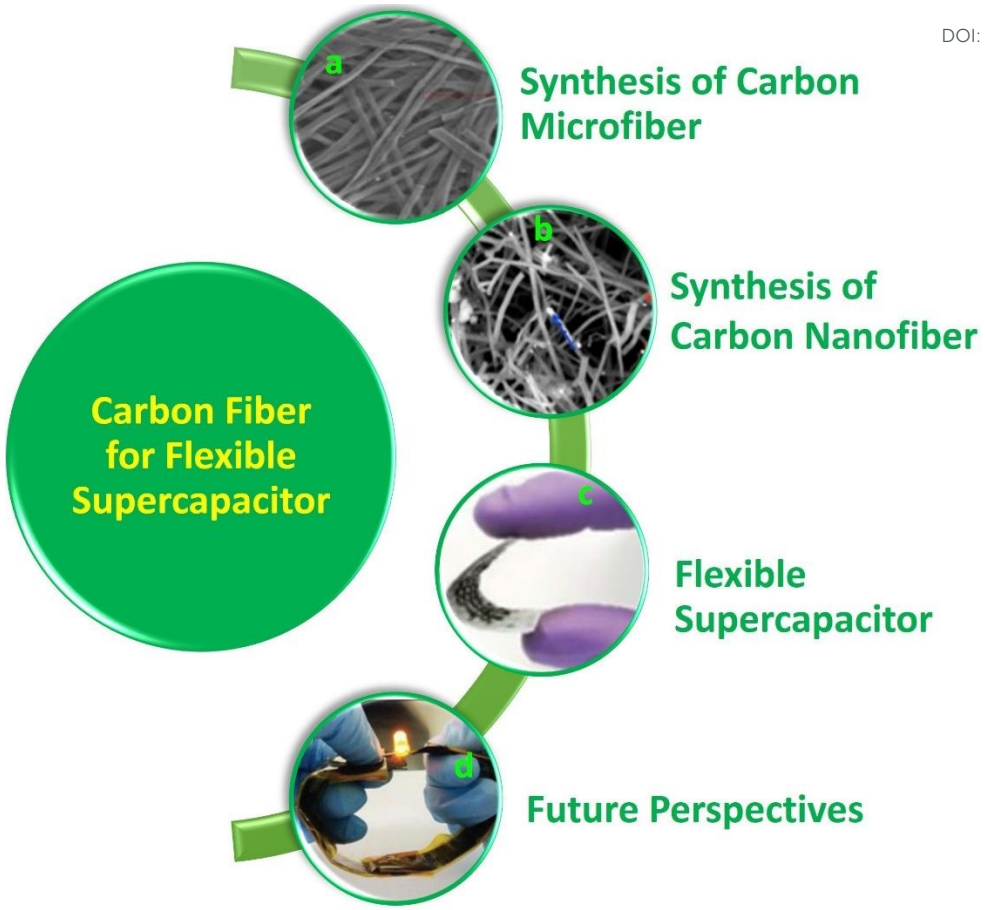

Figure 2: Contents of the present review; (a) SEM image of carbon microfiber. Reproduced with permission from [30] Copyright(2013) Nature Scientific Reports; (b) SEM image of carbon nanofiber. Reproduced with permission from [31] Copyright (2015) American Chemical Society; (c) digital photograph of carbon fiber based flexible supercapacitor. Reproduced with permission from [32] Copyright (2019) WILEY-VCH Verlag GmbH & Co. KGaA, Weinheim; (d) LED indicator lighted by two $(Ni_{0.1}Co_{0.9})_9Se_8$@CFC//PVA/KOH//rGO@ carbon fiber cloth asymmetric supercapacitors connected in series. Reproduced with permission from [33] Copyright (2018) WILEY-VCH Verlag GmbH & Co. KGaA, Weinheim.

2. Synthesis of Carbon Microfibers

Lopez et al. [34] introduced the synthesis of CMF from the polymer, PAN using N,N-dimethylformamide as solvent. Here, the PAN microfiber is synthesized by electrospinning by varying the PAN concentration and it possess high porosity when is carbonized at a temperature range of 800 - 900ºC with a polymer concentration greater than or equal to 10%. Using mechanical wood fibers, Wang et al. [35] synthesized a liganocellulose nanofibrils (LCNF) and it further kept for wet spinning in order to prepare CMF. Cellulose and lignin present in the LCNF producing a direct route of synthesizing CMF by carbonization procedure thus eliminates the thermal stabilization procedure. The authors of this work found that this LCNF as such doesn't produce a microfiber or filament by wet spinning. Thus, it needs a smaller quantity of lignin-free nanofiber, like anionic cellulose nanofibrils (TOCNF) which improves the spinnability of LCNF. Improving the quantity of TOCNF is truly influencing the spun fiber properties, before and after performing the carbonization steps. It can be observed that the TOCNF contributing to the evolution of pores through carbonization, conserving the

procedures such as surface activation, electrochemical treatment and particle deposition. The surface morphology of the as-synthesized LCNF/TOCNF microfibers before and after performing carbonization analysed by scanning electron microscope (SEM) imaging is given in **Figure 3**. With higher TOCNF content, the microfiber holds thinner and it holds a smooth surface, as shown in the first column. After the carbonization step, the microfibers shrunk in transverse axis given as second column. High-magnification SEM image of CMF is given as third column in **Figure 3**. The SEM images clearly shows that the CMF exhibits a porous morphology. Introduction of pores with improved addition of TOCNF resulting the glycoside bond cleavage and gasification. Saxena et al. [36] synthesized CMF by chemical vapour deposition (CVD) using turpentine oil decomposition with the presence of nickel sulfate catalyst on graphite host. The authors of this work obtained CMF with diameter in the range of 3-5 μm with a length of 5 mm with a twisted morphology. By using natural electrospun fiber silk cocoon, Liang et al. [30] synthesized a one-dimensional (1D) porous CMF. In this report, the authors of this work synthesized a biopolymer from silkworm by inartificial electrospinning approach, where silkworm spin like microfiber producing a cocoon through it. It is observed that by applying a feasible carbonization treatment, the electrospun natural cocoon microfiber is directly transfer to a 1D CMF having average diameter of 6 μm, as shown in **Figure 4**.

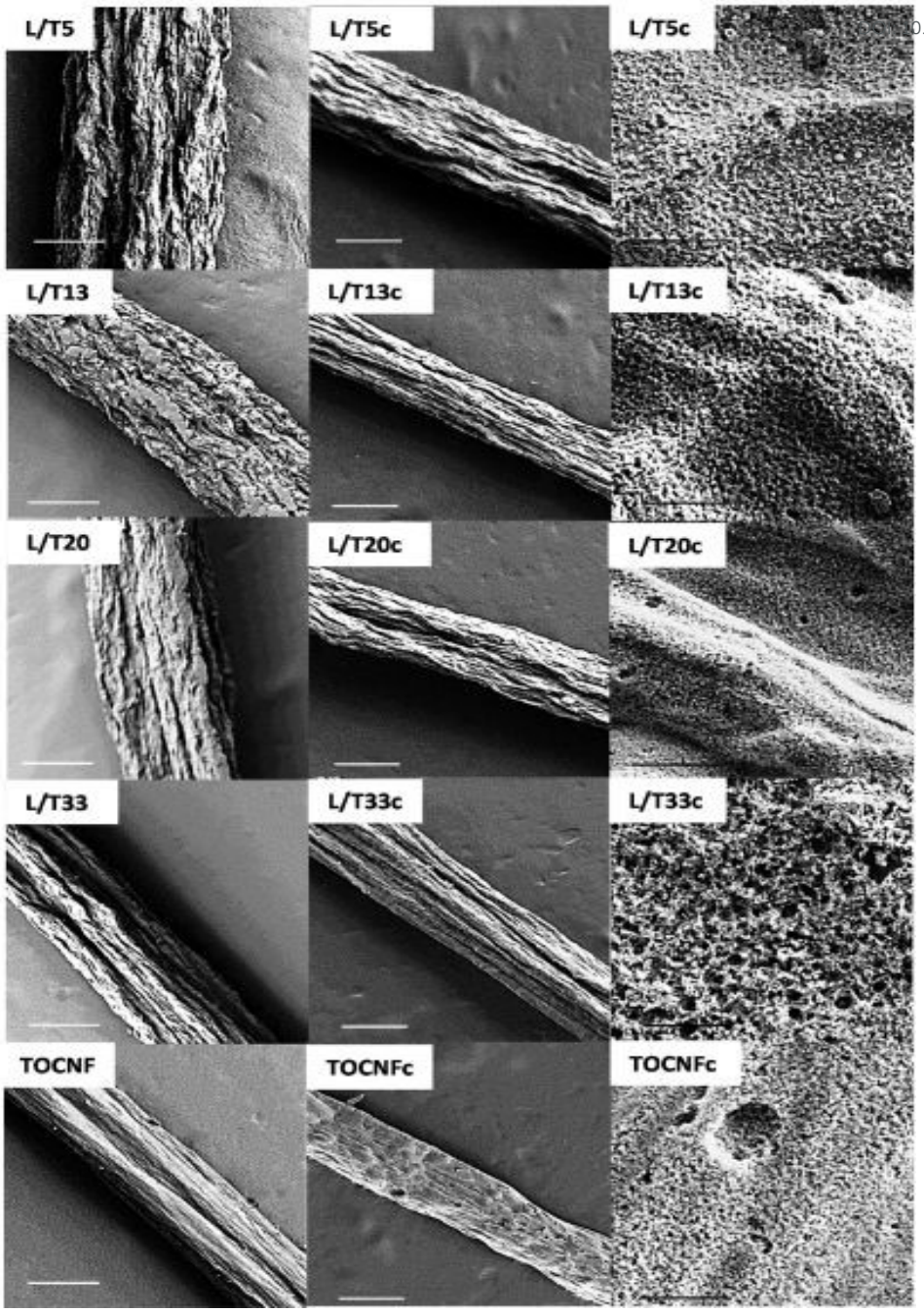

Figure 3: SEM images show LCNF/TOCNF microfiber surface morphology before (first column) and after (second column) carbonization. High-magnification SEM images of CMF is given in third column. Reproduced with permission from [35] Copyright (2020) American Chemical Society.

From this study, it is found that these 1D CMF hold large number of carbon nanoparticles with a size ranging from 10 to 40 nm and it interconnected with each one to introduce a three-dimensional (3D) porous network architecture. These carbon nanoparticle units possess majorly a microporous structure, with compact and loose aggregation points to a mesoporous to microporous structure. A direct carbonization of this natural biopolymer without holding any harsh environment directs the introduction of micro/nanostructure. Synthesis of CMF from natural polymers envisages the environment-friendliness and hence its acceptance.

View Article Online
DOI: 10.1039/D4SU00146J

Figure 4: Pictorial representation of preparation of hierarchical porous CMF from silk cocoon. Reproduced with permission from [30] Copyright (2013) Nature Scientific Reports.

The SEM and transmission electron microscope (TEM) images of the as-prepared porous CMF are given in **Figure 5**. After performing the carbonization treatment at a temperature of 900ºC, the prepared CMF holds a uniform fibrous morphology, as depicted in **Figure 5a**. A CMF with diameter of 6 µm can be observed from this image, it exhibits a smaller diameter than silk microfibers, represents that this fibrous network producing a shrinkage as part of carbonization due to the burning of non-carbon element and other carbon-containing components. From the high-magnification SEM image (**Figure 5b**), it can be seen that the CMF possesses a fibrous framework which is interconnected with diameter of 10-40 nm formed during high-temperature pyrolysis. A CMF obtained through this procedure hold a prominent network of porous network architecture, which can be clearly visible from the TEM images given in **Figure 5c,d**. Using carbonization and activation approach, Taer et al. [37] synthesized a MCF from spiderweb. In this report, the carbonisation is performed under nitrogen atmosphere by adopting a multi-step heating profile to a temperature of **400ºC**. The activation procedure is performed using potassium hydroxide as active agent. A CMF with a diameter of 0.5-25 µm is obtained and it found that the CMF possesses an amorphous character with a carbon content of about 84%. There are various reports in the literature that describes the synthesis of CMF-based nanocomposites such as the formation with FeS using molten salt approach [38], ZnO through green template procedure [39], single template approach [40], etc.

View Article Online
DOI: 10.1039/D4SU00146J

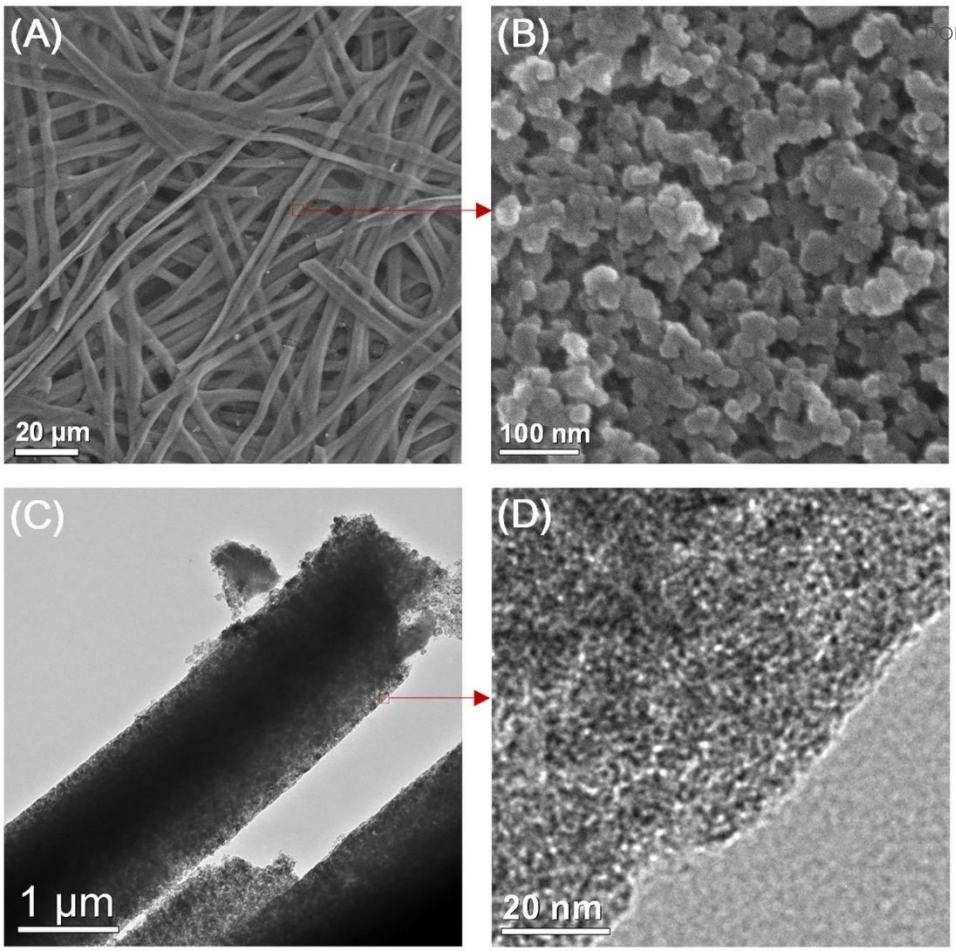

Figure 5: a) and b) SEM image; c) and d) TEM image of highly porous CMF. Reproduced with permission from [30] Copyright(2013) Nature Scientific Reports.

3. Synthesis of Carbon Nanofibers

CNF is hydrophobic in nature. The surface chemistry of CNF can be tailored with the help of various functional groups and are used in a variety of fields such as electrochemical energy storage, sensors, water purification, etc. The major synthesis methods of CNF include chemical vapour deposition [41-43], template-assisted approach [44-46], filament assisted-sputtering [47, 48], etc. Ahmed et al. [49] synthesized CNF by the impregnation of nickel ion (Ni^{2+}) in powdered activated carbon. CVD approach with the application of acetylene gas, and hydrogen gas are employed for this synthesis procedure. The as-synthesized CNF possessed an average diameter in the range of 100 - 160 nm and the presence of Ni particles are confirmed by energy dispersive X-ray spectroscopy (EDX) analysis. Ren et al. [31] reported a large-scale synthesis of CNF with higher strength, flexibility and conductivity using facile approach of electrolytic conversion of CO_2 dissolved in atmosphere molten carbonates. The molten carbonates consisting of almost 20 mol/L of reducible tetravalent carbon but air contains tetravalent carbon only about $1.7x10^{-5}$ mol/L. This approach eliminates any other procedures to concentrate CO_2. With the adsorption of CO_2 from air, these molten carbonates introduce an increase in the reducible tetravalent concentration to million-fold, which is available for splitting to carbon inside electrolysis chamber. Here, the higher concentration of reducible tetravalent carbon sites logarithmically reduces the electrolysis potential and facilitates the transfer of charges at a lower electrolysis potential. In this procedure, CO_2 is bubbled into molten carbonates, and during electrolysis, oxygen is going to evolve into anode, but a thick solid carbon is built in

View Article Online
DOI: 10.1039/D4SU00146J

cathode (**Figure 6**). It is observed that the molten carbonate is splitted into carbon which approaches to 100% Coulombic efficiency, otherwise carbonates are mixing with hydroxides. In another case, there exists a co-generation of oxygen and carbon and it sustains the formation of carbon with higher current densities and a similar phenomenon at the cathodes of carbon, platinum or steel **can also be observed**. Fuel cell electrolysis potential is happened at higher temperature and higher amount of oxide concentration with respect to a higher current density. It is found that the dissolved carbon dioxide in molten carbonates is going to be an uncontrolled mixture of graphite and amorphous carbon. The product introduced by cathode electrolysis, as shown in the SEM image **(Figure)** contains controlled carbon fiber with points of metal nucleation. The majority of Ni particles are located in the nanofiber tip, but some of the particles are stayed aside and not associated with the CNF growth. This fiber is found to be homogeneous in the cathode, which hold a diameter of 200 - 300 nm with length in the range of 20 - 200 µm. Here, the fibers are synthesized through electrolysis at 10 cm^2 galvanized coil steel wire cathode and the generation of oxygen by nickel anode in a molten Li_2CO_3 fixed at a temperature of 730ºC initiated with a low current of 5 mA/cm^2 in cathode, followed by a constant current electrolysis phenomenon at higher current range of 100 mA/cm^2 for a duration **2 to 4 h**. Here, the cooled product consists of fibers mixed by solidified electrolyte. The resultant product readily falls in cooled cathode when it became uncoiled. A Coulombic efficiency of greater than 80% is achieved and the as-synthesized product after washing the electrolyte contains more than 80% of pure CNFs.

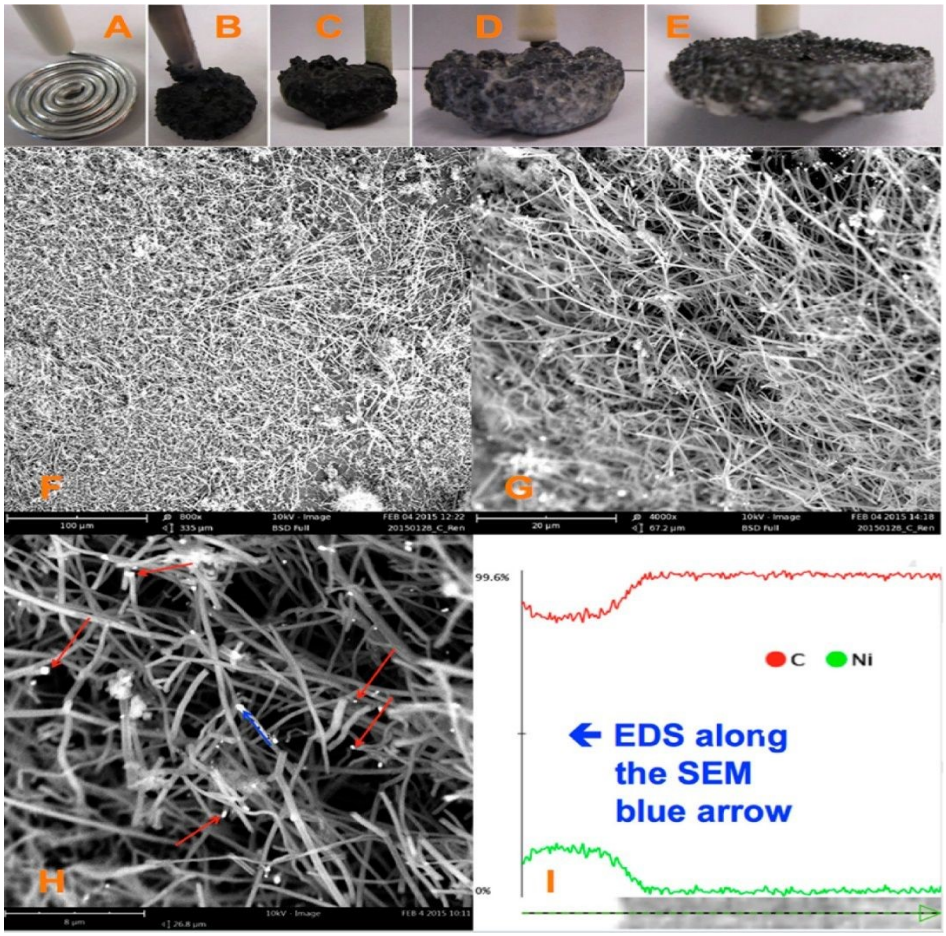

Figure 6: Formation of CO_2 to CNF introduced in a coiled galvanized steel cathode with anode as nickel at 0.05 A, then a constant current electrolysis at 1 A. There is no addition of Li_2O to molten Li_2CO_3 electrolyte at 730ºC; f)-h) SEM images holding different magnifications of

View Article Online
DOI: 10.1039/D4SU00146J

product removed from cooled and washed cathode; a) SEM image of 10 cm^2 coiled nanowire with diameter of 0.12 cm cathode which is prior to electrolysis. Anode material is the inner wall of 20 mL Ni crucible which consists of electrolyte; b)-e) maximum amount of variation in cathode which is subsequent to the removal of carbonate electrolyte after 4 Ah electrolysis in molten carbonate. Red arrow contained in h) corresponds to Ni nucleation sites and the blue coloured arrow corresponds to introduction at one of the Ni sites and which moving in CNF path; i) EDS mapping in 6 µ blue arrow path which is represented in SEM image h). Reproduced with permission from [31] Copyright (2015) American Chemical Society.

Gaud et al. [50] synthesized CNF from organic waste product such as plant waste in a cost-effective and eco-friendly way. The morphological analysis of the CNF showed that CNF with diameter lie in the range of 40 - 60 nm and a few micrometers in length. The as-synthesized CNF possessed a smooth surface. The EDX analysis reveals that it doesn't contain any impurities such as halides and oxides. Kotanjac et al. [51] synthesized CNF on woven cloth using CVD approach with nanoscale metal catalyst with the decomposition of hot hydrocarbon vapour. This report showed that an effective production of thin single layer fibers with a dimension of 25 x 30 cm.

4. Carbon Fibers for Flexible Supercapacitors

SCs are new-generation electrochemical energy storage devices exhibiting high power density, high charge/discharge rates, long cycle life, etc. Based on the charge storage mechanism, SCs are classified in to three types: electrochemical double layer capacitors, pseudocapacitors (or redox capacitors) and battery-type hybrid SCs. SCs have received great attention in the field of energy storage devices. Wearable electronic devices necessitate flexible and wearable SCs to power them. Wearable SCs must possess features such as flexibility, bendability, twistability to a higher extend in order to integrate with the wearable electronic devices. But the limited availability of a flexible substrate, shedding effect, and non-uniform distribution in the electrode-active materials limit their potential integration. To eradicate these issues, CF-based SCs have been developed in the recent past. This section describes the CF-based nanocomposite electrodes for application in high-performance SCs.

4.1 Carbon Fiber/Electronically Conducting Polymer Nanocomposite Electrodes

Electronically conducting polymers are the best candidates for SC electrode application due to their intrinsic conductivity, easy in synthesis, good redox activity, etc. Examples of electronically conducting polymers used in SC electrodes are polyaniline (PANI), polypyrrole (PPY), poly(3,4-ethylenedioxythiophene) (PEDOT), poly(3,4-ethylenedioxythiophene): polystyrenesulfonate (PEDOT:PSS), poly(3-hexylthiophene), etc. Ling et al. [52] prepared a flexible, foldable and light-weight CF paper substrate using wet-lay technique and it possesses a reduced internal resistance and large porosity. Here, a γ-MnO_2 wrapped over PANI led to a core-shell architecture, and a step-wise modified in-situ polymerization approach is applied for the uniform distribution of the polymer. The SC electrode thus prepared exhibited a high specific capacitance of 642.5 F/g at a current density of 1 A/g. A SC was fabricated using these nanocomposite electrodes, which delivered an energy density of 114.2 Wh/kg at a corresponding power density of 798.6 W/kg. This SC exhibited a capacitance retention of 81.3% even after completing 5000 cycles. Introduction of an electronically conductive polymer to a flexible substrate makes it electrically conducting and it can be further used for fabricating SC electrode with good mechanical properties. Niu et al. [53] used electrochemical polymerization technique to prepare SC electrode comprising of coral-like PEDOT nanotube array over textile CF (TCs). In this study, ZnO nanowire grown over TCs act as a sacrificial template. PEDOT polymerization follows by the removal of ZnO nanowire

template creates a composite of PEDOT nanotube which was vertically grown over TC. Morphology hold by PEDOT is highly depends upon the time for deposition as given in SEM image **Figure 7**. During a smaller deposition time of about 5 minute (**Figure 7(a-c)**), PEDOT possesses a nanofiber-like structure with a diameter of ~200 nm and length of ~10µm (**Figure 7d-f**). Fibers are interconnected each other and generating a highly porous network of CF. But a longer duration of deposition (~10 minutes), PEDOT formed a coral-like structure where the PEDOT nanorods are forming a growth in vertical direction and it helps in rapid transport of electrons. Like ZnO nanowire structure, the PEDOT showed a reduction in its diameter from base to tip (**Figure 7f**). Also, the PEDOT nanotubes achieve a length in the range of tens of micrometers, where its diameter increases within a range of ~0.5 - 1 µm (**Figure 7f**). If the deposition time increases to 15 minutes (**Figure 7g-i**), PEDOT is increasing its diameter in a continuous manner and reaches upto 800 nm (**Figure 7i**). The coral-like PEDOT nanotube exhibits efficient conductivity that make the TC@PEDOT-10 as an efficient electrode material. To introduce the prepared electrode material for practical applications, the authors of this work developed two SCs consisting of TC@PEDOT-10 as an electrode with 1 M aqueous H_2SO_4 and PVA-H_2SO_4 as electrolytes. From this study, it is found that the two SCs hold an ideal behaviour with rectangular shape possessing a similar current response at a constant rate of 50 mV/s (**Figure 8a**), indicating the similarity in the electrochemical characteristics due to similar ionic conductivity introduced by the PVA-H_2SO_4 gel electrolyte. The charge/discharge characteristics of SCs are examined using GCD measurements performed at different current densities (**Figure 8b**). The triangular-shaped GCD curves possessing coincident curves that represent a complete doping/de-doping reaction in reversible style, that executes in an electrochemical method. From the variation in specific capacitance of SCs at different current densities (**Figure 8c**) show that the SCs with H_2SO_4 aqueous electrolyte exhibited a capacitance of 22.1 F/g at 0.25 A/g and it holds a capacity retention of 86.4% at 8 A/g.

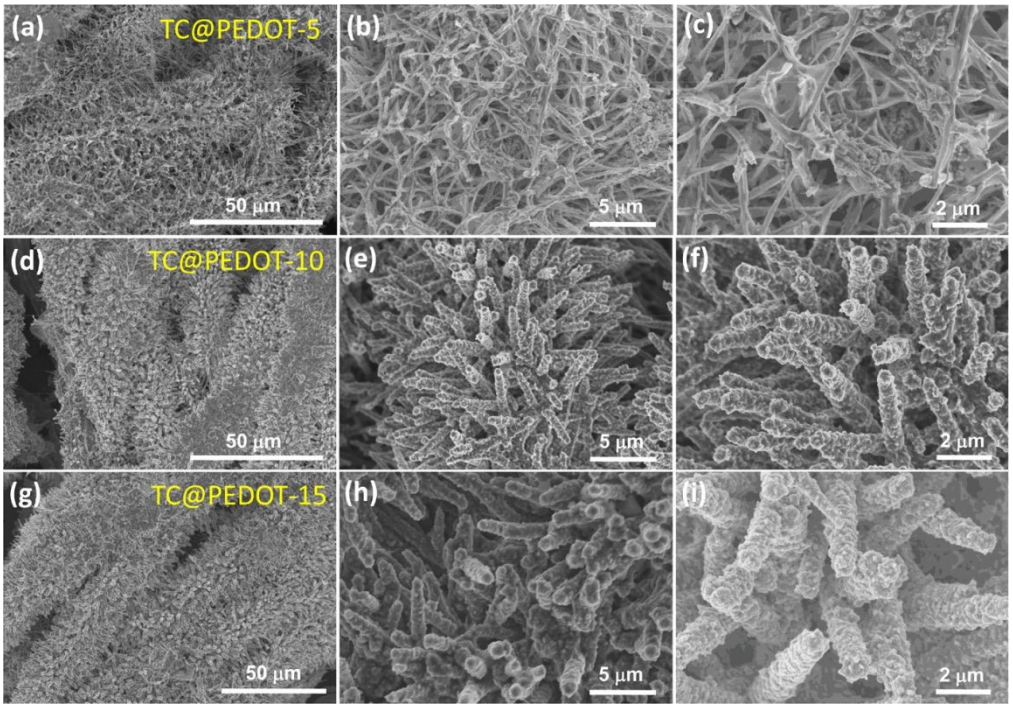

Figure 7: TC@PEDOT SEM images in various magnifications (a-c) TC@PEDOT-5 (d-f) TC@PEDOT-10 and (g-i) TC@PEDOT-15 electrode. Reproduced with permission from[53] Copyright (2020) American Chemical Society.

View Article Online
DOI: 10.1039/D4SU00146J

The specific capacitance obtained for this SC is found to be higher than the SC fabricated with PVA-H_2SO_4 gel electrolyte holding a specific capacitance of 21.7 F/g with a capacity retention of 83.8%. A plot that shows the variation in the capacitance with respect to frequency is given in **Figure 8d**. With maximum C´´ and corresponding f_o, relaxation time constant □o of device in both these electrolytes can able to introduce, it reveals the shortest time taken for the discharging of all energy in an efficiency greater than 50%. The '□$_o$' value calculated for the SC utilizing H_2SO_4 and the SC utilizing PVA-H_2SO_4 gel electrolyte are 0.87 s and 0.96 s, respectively. The flexibility of SC utilizing PVA-H_2SO_4 gel electrolyte was tested by bending the SC at different bending angles and recovered its initial state after the bending test. When the SC bend at an angle of 160º, the CV profiles correspond to SC utilizing PVA-H_2SO_4 gel electrolyte found to be unaltered (**Figure 8e**), which reveals the integrity of the SC electrode and the high flexibility of the SC. The cyclic stability of SC utilizing PVA-H_2SO_4 gel electrolyte was examined by carrying out CV analysis for 500 bending cycles at a constant scan rate of 50 mV/s and shown in **Figure 8f**. The CV profile of SC utilizing PVA-H_2SO_4 gel electrolyte shows a retention of ~92%, even it is bending at 120º for 500 cycles.

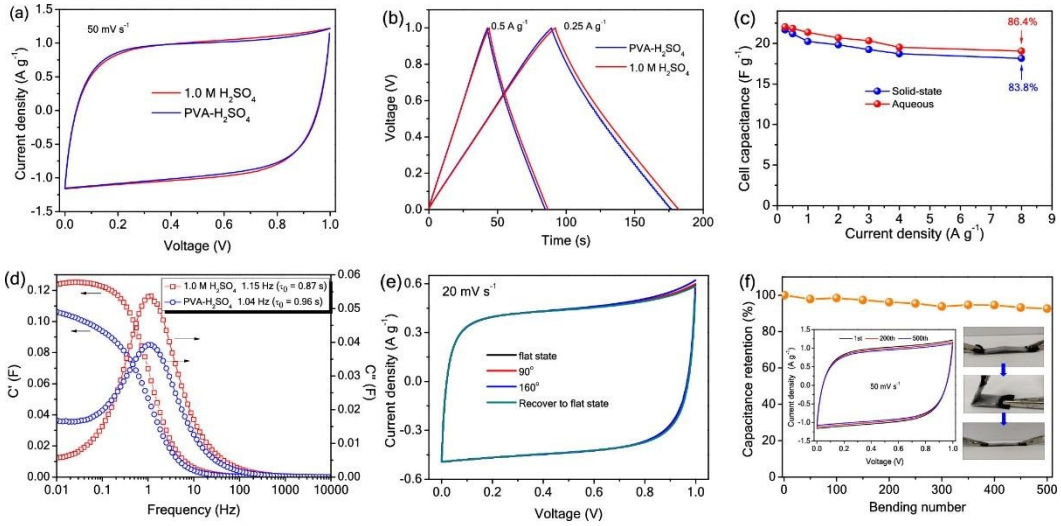

Figure 8: (a) CV curve at 50 mV/s; (b)GCD profiles at 0.5A/g and 0.25A/g; (c) rate capability diagram in the range 0.25-8 A/g; (d) real (C´) and imaginary part of (C´´) specific capacitance as a function of frequency (f_o); (e) CV curve representing solid state SC device with various bending state; (f) retention in capacity after bending device for 500 cycles at 120º. Reproduced with permission from [53] Copyright (2020) American Chemical Society.

An ultra-flexible SC using oxidized carbon nanotubes (CNTs) grown over CF (OCNTF)/PPY brush-like electrode was reported recently [54]. Initially, the OCNTF was synthesized using CVD method followed by air-oxidation. Further, PPY was coated over the OCNTF substrate by electrochemical polymerization method with varied deposition time. **Figure 9** represents the steps involved in the synthesis of OCNTF/PPY nanocomposite.

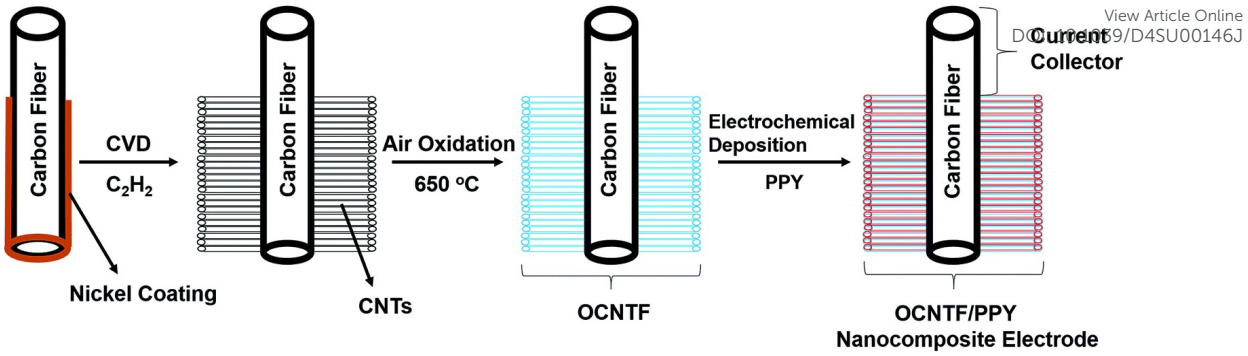

Figure 9: Pictorial representation of fabrication of electrode. Reproduced with permission from [54] Copyright (2016) Royal Society of Chemistry.

The SEM images of CNTs synthesized over CF by CVD is given in **Figure 10**(**a-c**) and (**e**). From these images it can be observed that there exists a higher density of CNTs grown over the CF substrate vertically. The oxidation of CNTs is introduced by the high-temperature annealing under oxygen environment. The SEM images of OCNTF are shown in **Figure 10d** and **f**.

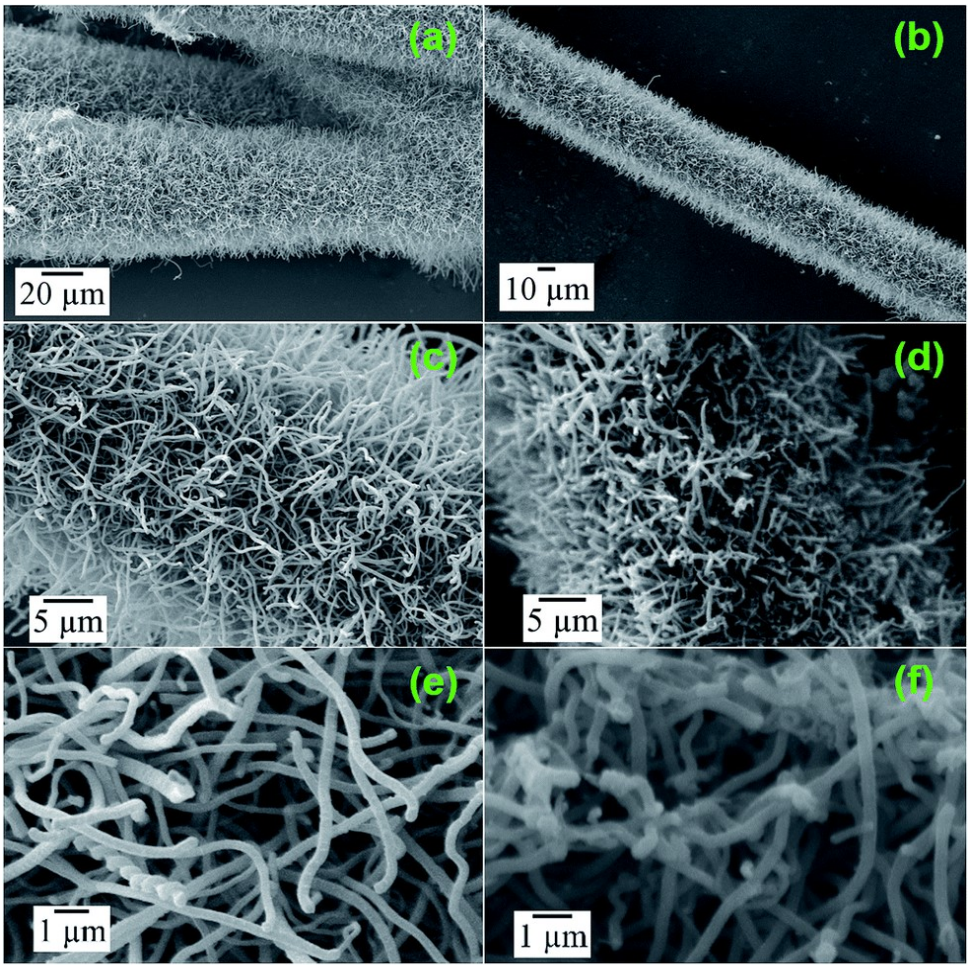

Figure 10: SEM images of CNTF (a-c) and e) and OCNTF (d and f). Reproduced with permission from [54] Copyright (2016) Royal Society of Chemistry.

View Article Online
DOI: 10.1039/D4SU00146J

The OCNTF/PPY nanocomposites are prepared at different deposition intervals. The electrochemical deposition performed at a deposition time of 50 minutes show a dendritic structured PPY over the OCNTF. This OCNTF/PPY nanocomposite is further used as an electrode-active material for the fabrication of a flexible SC. In order to analyse flexibility of fabricated electrode, GCD measurements are performed by bending the SC electrode at different bending angles of 0º (straight position), 30º, 60º, 90º, 120º and 180º at a constant current density of 2.5 mA/cm^2. From the GCD curves (**Figure 11a**) it is clear that there is no change in the curve while it bends from the straight position towards 180º. Also, there no change in its volume specific capacitance (**Figure 11b**) and gravimetric capacitance (**Figure 11c**) was observed during the bending towards 180º. The fabricated electrode exhibited a higher cyclic stability after 5000 charge/discharge cycles (**Figure 11d**). A schematic diagram representing the solid-state SC fabricated with this electrode material is given in **Figure 11e** and its digital image is provided in **Figure 11f**. This working of the as-fabricated solid-state SC is studied by lighting-up a red light-emitting diode (LED) and depicted in **Figure 11g**. By using these solid-state SCs, a flexible SC module with two similar SCs connected in series is fabricated and its digital image is given as **Figure 11h**. This module is charging to a voltage of 4 V initially, and it efficiently lighting a white LED (**Figure 11i**). The flexibility of this SC module is verified at its straight position as well as by bending it at an angle of 180º (**Figure 11i** and **j**). In order to verify its flexibility in terms of twisting the SC, the fabricated SC module is rolled to the shape of a cylinder on discharging it through a white LED (**Figure 11k**) and no significant variation in the intensity of lighting the LED is observed. This shows the high efficiency of OCNTF/PPY nanocomposite-based SC for practical applications.

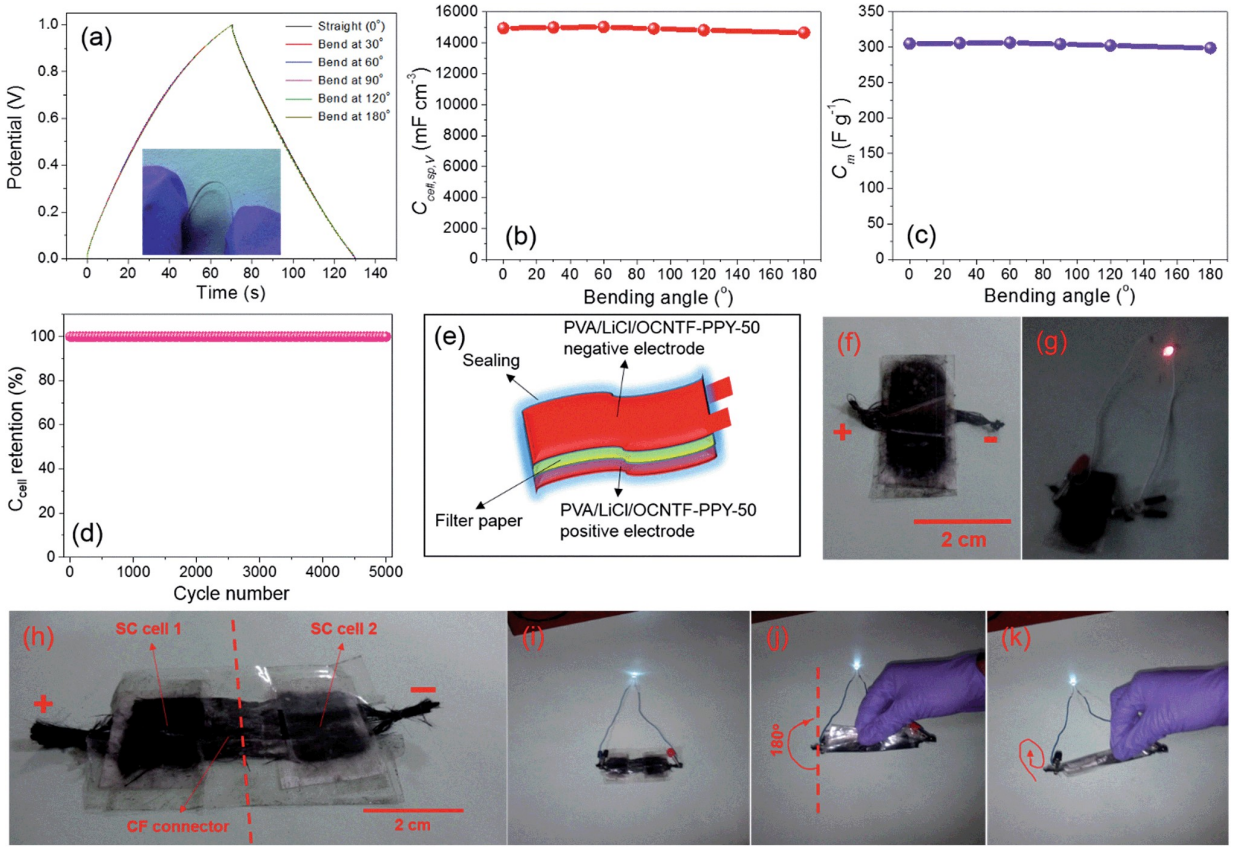

Figure 11: (a) GCD curve at a current density of 2.5 mA/cm^2 for the fabricated SC electrode bending at different angles; (b) volumetric specific capacitance; (c) gravimetric specific capacitance in various angles; (d) capacitance retention with cycle number; (e) diagrammatic

and (f) digital image of SC; (g) digital image of lighting a red LED; (h) module lighting up a white LED; (i) module lighting the white LED bending at 180º; (j) module rolling in form of cylinder and (k) lighting a white LED. Reproduced with permission from [54] Copyright (2016) Royal Society of Chemistry.

Using an aerobic pyrolysis method, Zhou et al. [55] extracted CF from a CF-reinforced polymer under oxygen atmosphere. During the pyrolysis, the reclaimed fiber surface is etched to a surface of groove-shape and it is modified by creating oxygen-containing surface functional groups, which produces an enhancement in the negative potential window of the reclaimed CF to -1.4 V. By increasing the working potential to 2.4 V, it produces a capacitance retention of **93.6%** after completing 10000 cycles in Na_2SO_4 aqueous electrolyte. Manikandan Ramu and team [56] synthesized hierarchical VS_4 nanostructures over CF by hydrothermal method and the procedure is schematically shown in **Figure 12**. During the synthesis process, the growth solution containing $VOSO_4.xH_2O$ and C_2H_5NS with complexing agent CH_3COOH were prepared. It created a VS_4 nanostructure without any binder on CF cloth substrate with good adhesion. The authors of this work synthesized various samples at different growth conditions by varying pH and are labelled as VS4-CC@VS-1 (pH 2.5), VS4-CC@VS-2 (pH 2.3) and VS4-CC@VS-3 (pH 2.1). The microstructure and morphology of these samples are studied by using FESEM imaging and it is given in **Figure 13**.

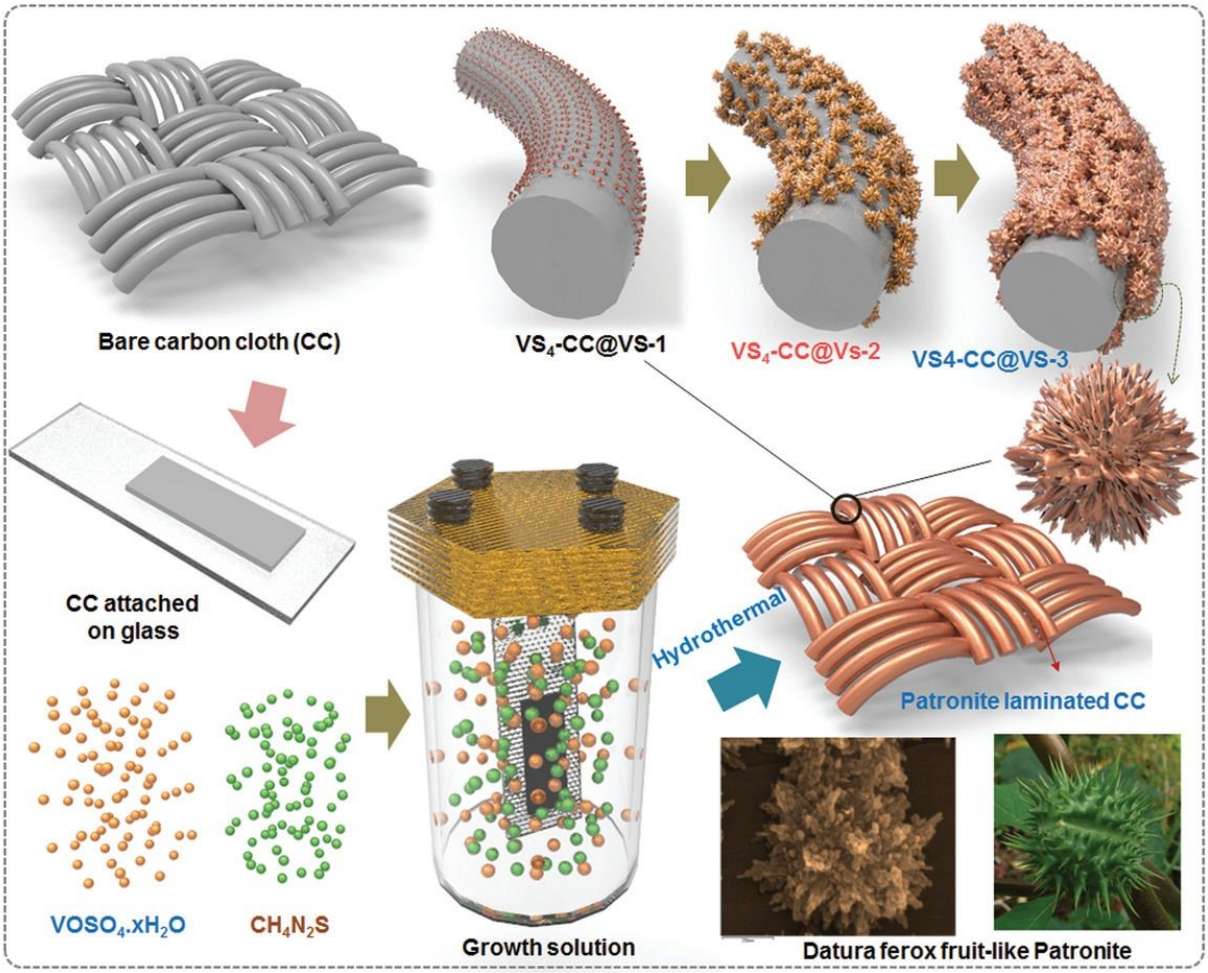

View Article Online
DOI: 10.1039/D4SU00146J

Figure 12: Pictorial representation of synthesis procedure of ferox-fruit like patronite (VS_4) nanostructure over a flexible carbon cloth substrate in a growth medium with controlled pH. Reproduced with permission from [56] Copyright (2020) WILEY-VCH Verlag GmbH & Co. KGaA, Weinheim.

The SEM images of VS4-CC@VS-1 are shown in **Figure 13a(i-iii**). In this sample, the VS_4 holds a nanospike-like agglomerated particles, which produces a non-uniform distribution over the CF cloth substrate. With an increase in concentration to twice, the VS4-CC@VS-2, an increased growth of VS4 over CF cloth was observed, as depicted in **Figure 13b(i-iii)**. A discreetness in nanospike bunches visible in the first sample, which exhibits a flower-like morphology. Due to the non-uniformity in alignment over CF cloth surface, the concentration was further increased and VS4-CC@VS-3 was prepared. **Figure 13c(i-iii**) shows the SEM images, which portraits a large growth with datura ferox fruit-like morphology with the availability of large number of electrochemically active sites. Further, SC electrodes were fabricated using these three different samples and the electrochemical performances were examined. The electrochemical performance of the SC electrodes is analysed in a three-electrode cell using 1 M 1-ethyl-3-methylimidazolium trifluoro methane sulfonate in acetonitrile ([EMIM][Otf]) ionic liquid electrolyte. The pictorial representation of fabrication of symmetric SC constructed VS4-CC@VS-3 electrodes is given in **Figure 14a**. A comparison of CV curves of the three SC electrodes (VS4-CC@VS-1, VS4-CC@VS-2 and VS4-CC@VS-3) showed that the electrode-active materials exhibit a pair of redox peaks and possess a quasi-rectangular shape, which portraits their pseudocapacitive charge storage (**Figure 14b**). A comparison of GCD measurement of the three SC electrodes (VS4-CC@VS-1, VS4-CC@VS-2 and VS4-CC@VS-3) showed that the electrode-active materials exhibit a symmetric with nearly distorted triangular curves showing the reversibility and pseudocapacitive nature of material, as shown in **Figure 14c**. The CV curves obtained for VS4-CC@VS-3 at different scan rates is given in **Figure 14d**. These CV curves consist of broad redox peaks, arises due to the intercalation/deintercalation of $[EMIM]^+$-ions, which represents that the SC electrode is pseudocapacitive in nature. The GCD curves obtained for VS4-CC@VS-3 at different current densities (1 to 10 mA/cm^2) is given in **Figure 14e**. The charge/discharge cures shows that the SC electrode exhibited efficient electrochemical performance.

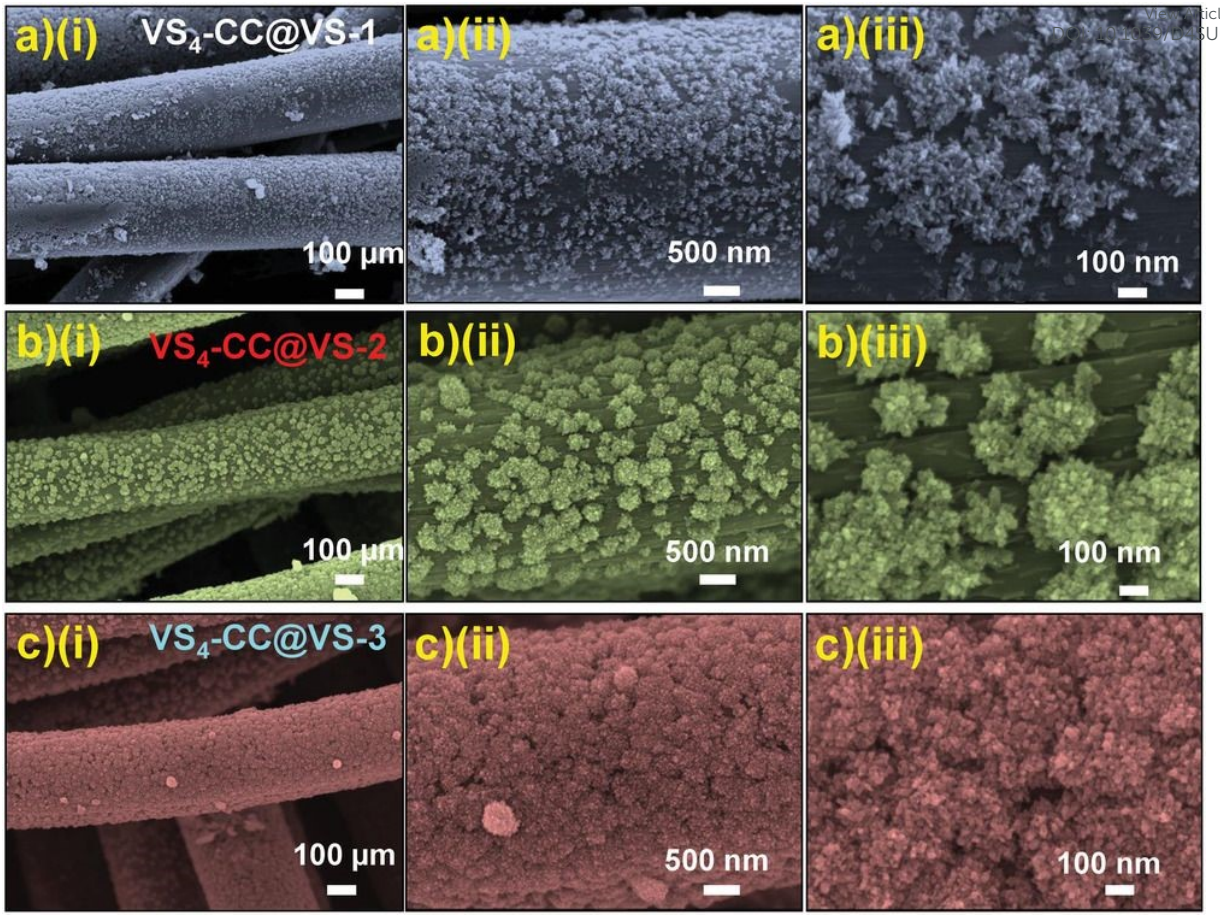

Figure 13: FESEM image of (a) VS4-CC@VS-1; b) VS4-CC@VS-2, and c) VS4-CC@VS-3 samples with various magnifications. Reproduced with permission from [56] Copyright (2020) WILEY-VCH Verlag GmbH & Co. KGaA, Weinheim.

The area specific capacitance obtained for the three SC electrodes is calculated from the GCD curves measured at different current densities and plotted in **Figure 14f**. The SCs hold a maximum area specific capacitance of 119 mF/cm^2 for VS4-CC@VS-1, 277 mF/cm^{-2} for VS4-CC@VS-2 and 536 mF/cm^{-2} for VS4-CC@VS-3, from this it can be seen that the VS4-CC@VS-3 SC exhibited a superior performance when compared to that of the other two SCs. The VS4-CC@VS-3 SC possess area specific capacitances of 536, 452, 335, 254, 194, and 149 mF/cm^2 at a current density of x,y,.., respectively. This superior electrochemical characteristics of VS4-CC@VS-3 SC is due to the dense growth of VS_4 nanoflower on CF cloth which enabled large interaction area for the rapid diffusion of electrolyte-ions. The Nyquist plot (**Figure 14g**) and bode plot (**Figure 14h**) showed that the VS4-CC@VS-1, VS4-CC@VS-2, and VS4-CC@VS-3 SCs exhibited a series resistance of 4.629, 4.14, and 3.765 Ω cm^2, respectively. Ragone plot of these three SCs (**Figure 14i**) revealed that the VS4-CC@VS-3 SC exhibited a high energy density of 28.6 Wh/kg at a corresponding power density of 9340 W/kg. This report envisages to design a binder-free electrode that facilitates a rapid diffusion of electrolyte ions thereby delivers high performance. A schematic representation of mechanism of binder-free VS4-CC@VS-3 SC electrode is depicted in **Figure 14j**.

View Article Online
DOI: 10.1039/D4SU00146J

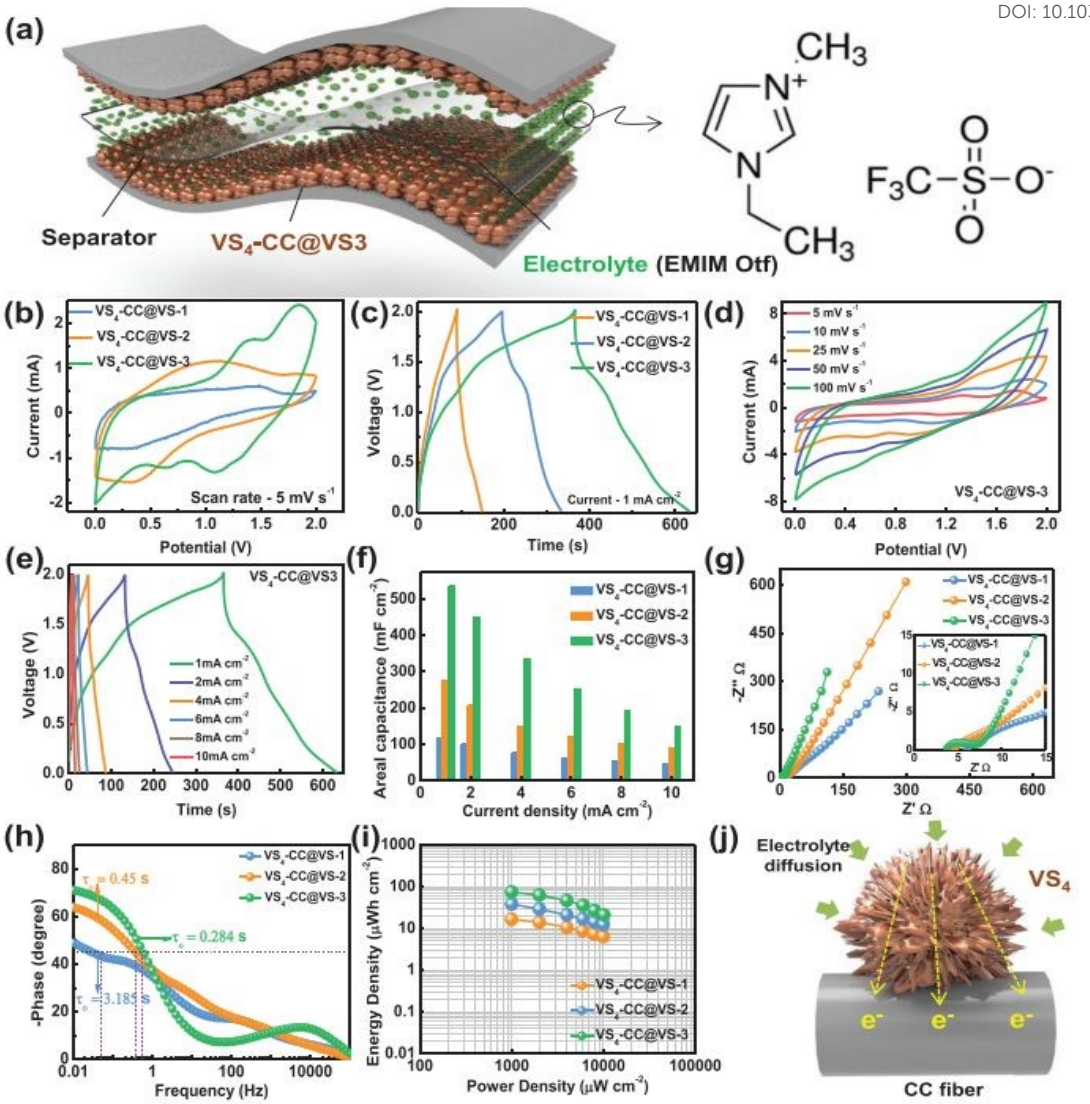

Figure 14: (a) Pictorial representation of symmetric SC with ionic liquid electrolyte; (b) CVs of electrode at a scan rate of 5 mV/s ;(c) GCD curve at 1 mA/cm^2 current density; (d) CV at different scan rates; (e) GCD at different current density; (f) variation of area specific capacitance at various current density; (g) Nyquist plot and (h) bode plot of device; (i) Ragone plot of symmetric device; (j) pictorial representation of mechanism of binder free electrode SC device with VS4-CC@VS-3. Reproduced with permission from [56] Copyright (2020) WILEY-VCH Verlag GmbH & Co. KGaA, Weinheim.

CF have prominent applications in energy fields due to its large surface area, large tolerance in temperature, reduced thermal expansion coefficient, high electrochemically active interfaces and a 1D pathway for the transportation of electrons. But the difficulty in synthesizing CNF-based SC electrodes in a green and cost-effective methods stand as a demerit for its further explorations. Li et al. [57] suggested a copolymerization approach where an oxygen-rich monomer named itaconic acid (IA) is introduced to molecular chain of PAN. This introduction does not produce any damage to the uniformity of trapezoidal structure formed in thermal stabilization approach. But it is found to create a large number of functional groups such as oxygen-containing functional groups, as shown in **Figure 15a,b**. It is found that the carbonization procedure led to a microporous structure by creating vacancy-effect in CNF. The

degradation of a segment increases by the substitution of N atom introducing higher redox activity to the material. After a stabilization period of 48 h, the prepared CNF membrane has received high flexibility and found stable even it is bent at a bending angle of 180º (inset image of **Figure 15c**). The SEM images of CNF obtained at different magnifications are depicted in **Figure 15c-e**. The HRTEM images of CNF exhibited a less graphitic structure, can be seen from **Figure 15f,g**. The selected area electron diffraction pattern (SAED) pattern which possesses a diffused rings shows an amorphous nature (**Figure 15h**). The elemental mapping analysis showed the even distribution of carbon, oxygen and nitrogen in the CNF (**Figure 15 i**). The authors of this work fabricated a flexible symmetric SC using gel electrolyte and it is shown schematically shown in **Figure 16a**. The gel electrolyte exhibits low ionic conductivity, hence a small deviation in the CV curves can be observed from its normal rectangular shape but it still maintains a uniformity in symmetry even at a scan rate of 100 mV/s (**Figure 16b**). **Figure 16c** shows the CV curves obtained at different bending angles such as 0º, 90º, and 180º and no variation in the area under the curve was observed. This shows the excellent stability of the SC even at a severe bending of 180º. The GCD curves obtained for the solid-state SC is shown in **Figure 16d**, which represents a linearity in GCD curves with a symmetric triangular shape. The Ragone plot of assembled SC is depicted in **Figure 16e** exhibits an area power density of 2142 $\mu W/cm^2$ with a corresponding energy density of 23.8 $\mu Wh/cm^2$.

View Article Online
DOI: 10.1039/D4SU00146J

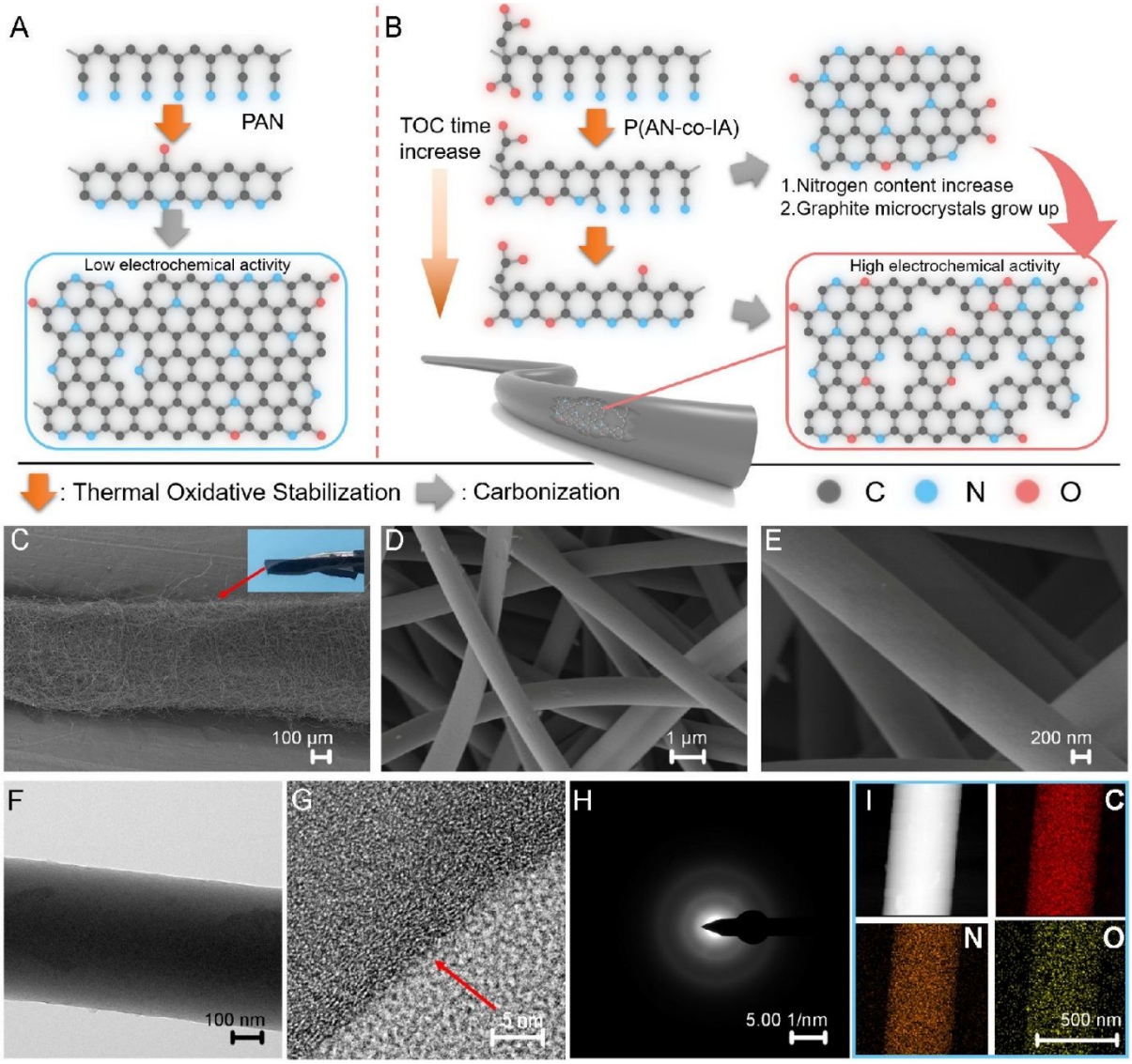

Figure 15: (a) Pictorial representation of carbonization procedure of PAN; (b) image of PAN copolymer carbonization. When the cyclization of precursor increases, pre-nitrogen content and material graphitization also increase. SEM image (c-e) carbonized CNF and image of piece of CNF. HRTEM image of CNF (f, g), (h) SAED image; (i) electron loss spectroscopy (EELS) elemental mapping. Reproduced with permission from [57] Copyright (2021) American Chemical Society.

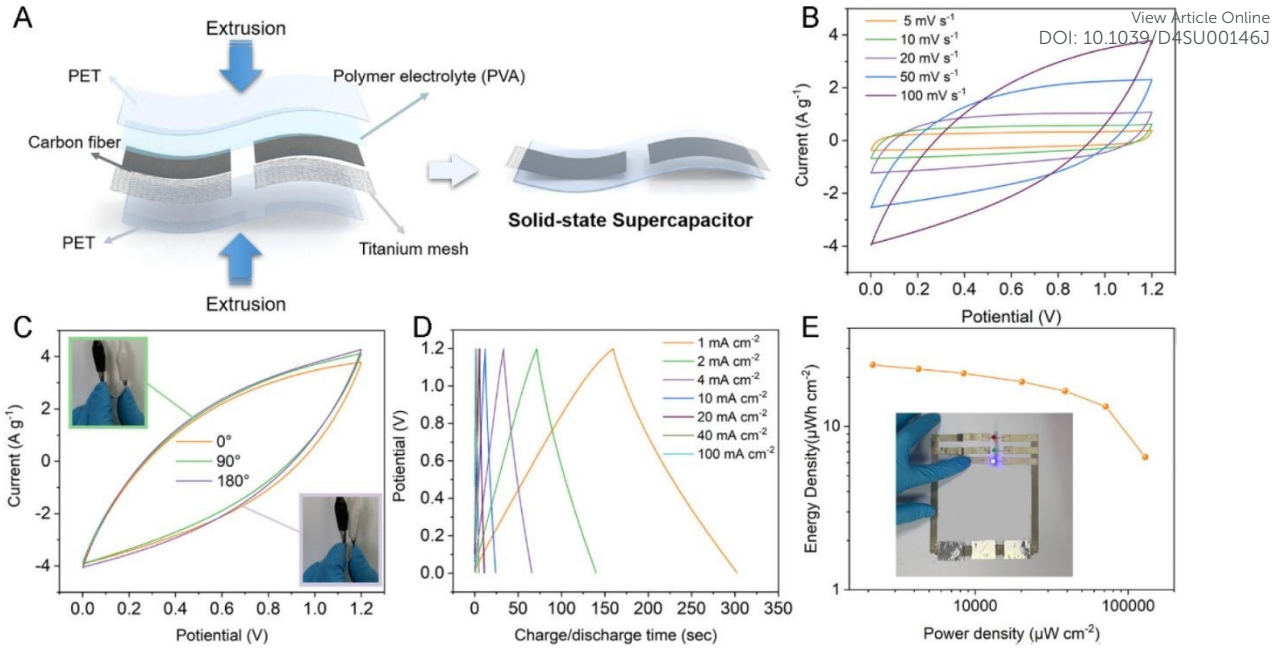

Figure 16: (a) Preparation of SC; (b) CV curve of device; (c) CV curve of device in different bending angles; (d) GCD curve; (e) Ragone plot with inset showing a blue LED constructed powered by the device. Reproduced with permission from [57] Copyright (2021) American Chemical Society.

A novel carbon nanostructure termed carbon nanopetals (CNPs) is reported in the literature [58]. The CNPs were grown over unidirectional CF (UCF) by CVD method and further used as a flexible electrode for SC application. The CNP/UCF hybrid material was further used as electrode-cum-current collector for the fabrication of a flexible SC. For the synthesis of CNPs, initially nickel is coated over UCF by electroless coating method. The electroless coating bath contains nickel sulphate hexahydrate, sodium hypophosphate, ammonium chloride, trisodium citrate and liquor ammonia. Firstly, UCF is dipped inside the electroless coating bath fixed at a temperature of 85ºC under constant stirring for a duration of 10 minutes followed by rinsing it several times using ethanol and de-ionized water and subsequently dried at 85ºC for 24 h. The UCF strands coated with nickel nanoparticles are further oxidized at a temperature of 550ºC in air-bed reactor for 30 minutes to make nickel oxide nanoparticles. The proposed oxidized nickel-coated UCF is acted as a substrate to synthesize CNPs using catalytic CVD. During this process, oxidized, nickel-coated UCF is heated to a temperature of 500ºC in a horizontal quartz furnace under continuous flow of N_2. To avoid excess generation of oxides on nickel nanoparticles, H_2 is introduced at a flow rate of 100 mL/min for a duration of 15 minutes. The temperature is then increased to 700ºC and introduced acetylene gas at a flow rate of 90 mL/minute for 15 min, by keeping fixed the N_2 flow at a rate of 200 mL/minute. Later, thiophene is introduced inside the CVD reactor simultaneously by heating a round bottom flask kept at a temperature of 80ºC on the route of N_2 flow. The CNPs grown over UCF is collected after cooling down the CVD reactor to the room temperature under N_2 flow. The entire procedure involved in synthesis of CNPs over UCF is shown in **Figure 17a**. A proposed mechanism of growth executed for CNP over the UCF is depicted in **Figure 17b**. The CVD growth established for CNPs consists of four sequential procedures which involves transportation of mass and reaction in gas phase, dissociative absorption of carbon atom on the surfaces of nickel oxide nanoparticles, carbon atom diffusion over its surface and carbon atom precipitation from nickel oxide nanoparticles.

View Article Online
DOI: 10.1039/D4SU00146J

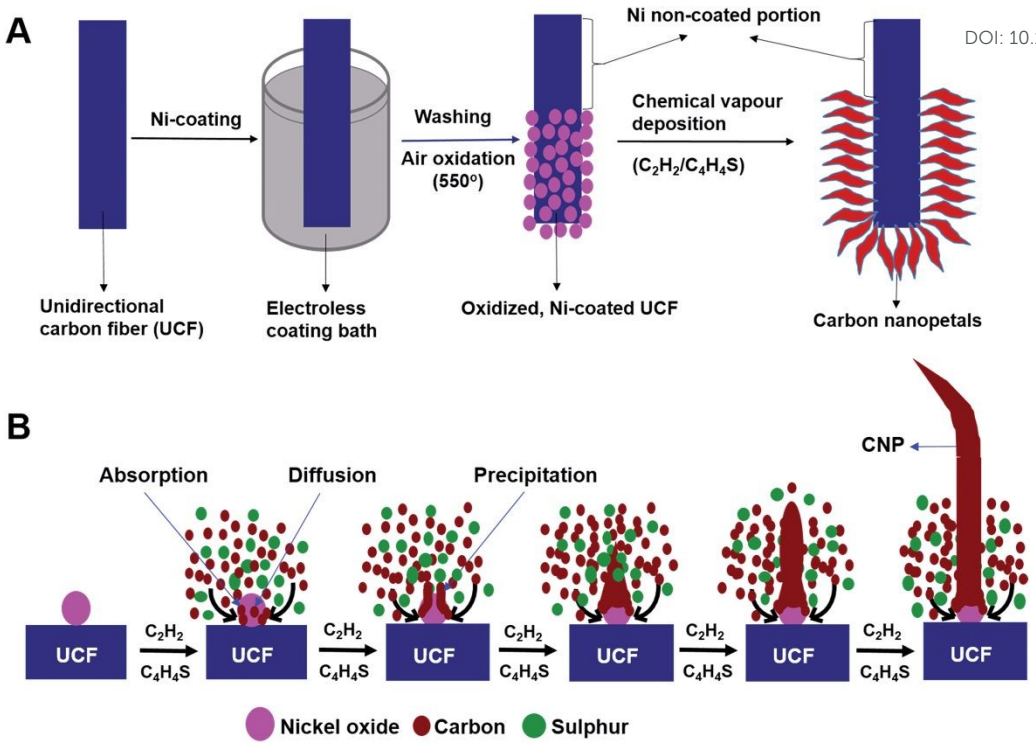

Figure 17: (a) Pictorial representation of procedures involved in the synthesis of CNPs on UCF, (b) mechanism of growth of CNPs on UCF. Reproduced with permission from [58] Copyright (2016) Royal Society of Chemistry.

The CNPs grown on UCF is further used as an electrode-active material for fabricating a SC. From the Nyquist plot (**Figure 18a**), it is found that the SC exhibits a bulk electrolyte resistance of about 6.2 Ω, and this smaller value of resistance indicates a high ionic conductivity possessed by the electrode-active material. The CV curves measured with a variation in the loading content of carbon nanopetals (258, 208, 158, 108, and 58 μg/cm^2) for the hybrid SC electrode (**Figure 18b**). The CV curves exhibited by CNP/UCF SC with the electrode having a CNP loading density of 258 μg/cm^2 at different scan rates is given in **Figure 18c**. The CV curves possess a near rectangular shape that representing the efficient double layer charge storage mechanism in accordance to the efficient propagation of charges through electrode-cum-current collector. To examine the electrochemical characteristics of pristine UCF SC electrode-active material, the CV analysis was performed in a two-electrode cell configuration at different scan rates and it is given in **Figure 18d**. From this analysis, it is clear that there exists only a slight contribution to charge storage introduced with pristine UCF. The GCD analysis of CNP/UCF SC electrode with respect to different current densities is given in **Figure 18e**. From the given analysis, it is clear that the SC possesses a high discharge capacitance of 102.6 mF at a current density of 2.77 mA/cm^2 and 69.9 mF at a comparatively high current density of 11.11 mA/cm^2. The porous architecture of the SC electrode along with the CNP orientation helps in the rapid movement of electrolyte-ions thereby an accelerated charge transfer happened which leads to high-performance. To demonstrate the practical applicability of the CNP/SC in flexible electronic devices, the SC is undergone a bending test in which the CNP/UCF SC was bend at different bending angles (**Figure 18f**). The GCD curves obtained for the SC at different bending angles such as 0º, 45º, 90º, and 110º are depicted in **Figure 18f**. The bending test display no significant variation in the charge/discharge profiles, which represents the excellent flexibility of the SC. An areal capacitance of 39.8 mF/cm^2 is obtained at 0º and it is found unaltered even at a severe bend of 180º. By increasing the loading content

View Article Online
DOI: 10.1039/D4SU00146J

of CNP, the CV curve consists large area under the curves where an area gets reduced upon lowering the CNP content in the electrode. A volume specific energy density obtained for the CNF/UCP SC is 0.753 mWh/cm^3 with a corresponding gravimetric energy density of 30 W h/kg at a constant current density of 2.77 mA/cm^2.

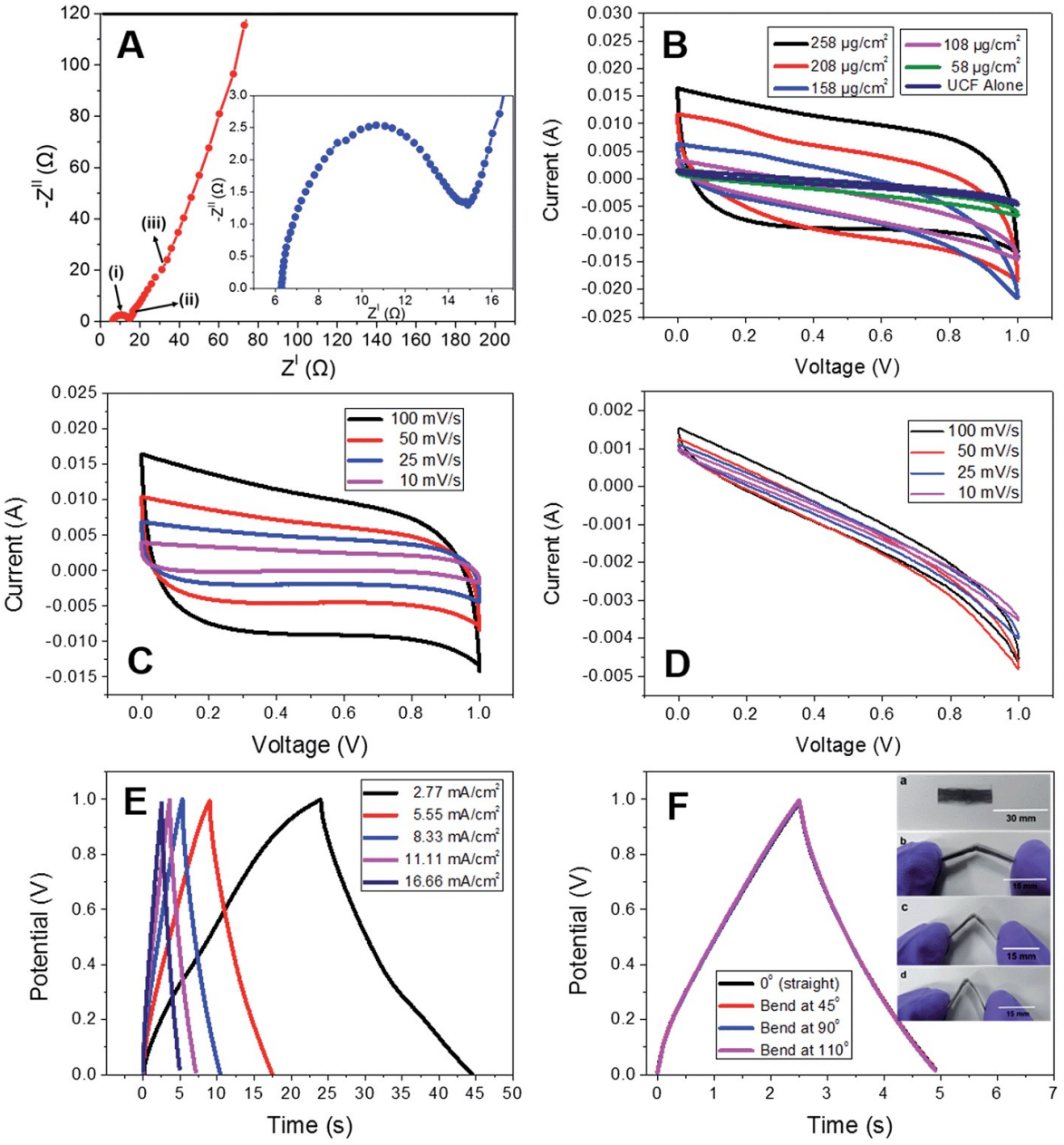

Figure 18: a) Nyquist plot (inset represents Nyquist in high frequency region); b) CV curve in different loading density; c) CV curve for different scan rate having CNP loading density of 258 µg/cm^2 of CNP/UCF SC; d) CV curve of UCF at various scan rate. GCD curve at e) various current density and f) various bending angles of CNP/UCF SC (inset shows the digital photograph of CNP/UCF SC bent for 0° (a), 45° (b), 90° (c), and 110° (d)]. Reproduced with permission from [58] Copyright (2016) Royal Society of Chemistry.

Carbon-based flexible SCs are promising candidates for powering up the smart textile wearable electronics. But their reduced energy density hindering its industrial applications especially due to the limitation of efficient synthesis approach for a highly conductive fiber electrode

exhibiting high specific capacitance. Hu et al. [59] developed a sustainable, cost-effective approach in a scalable way to develop lignin-based carbon/graphene fiber (CG@GF) hybrid with a porous structure and further used it as an electrode-active material for SC. This environment-friendly approach has envisaged the large-scale preparation of CG@GF hybrids for a variety of application including SC electrode preparation. A schematic representation of CG@GF hybrid depicting the overall synthesis procedure of CG@GF hybrid and the CG@GF SC is given in **Figure 19**. Here, the lignin powder is firstly dissolving in a 5 mL aqueous KOH solution by fixing the KOH to lignin mass ratio as 2:1. KOH is added to the lignin solution in order to introduce the dissolution of lignin in alkaline environment and to create a homogeneously arranged spinning dope. Under 0% lignin, solvent is stand as water without any KOH content. The as-prepared alkaline solution is added to the GO solution drop-wise and the concentration was fixed to be 15 mg/mL. Later, the CG@GF hybrid fibers are synthesized by coaxial wet spinning method.

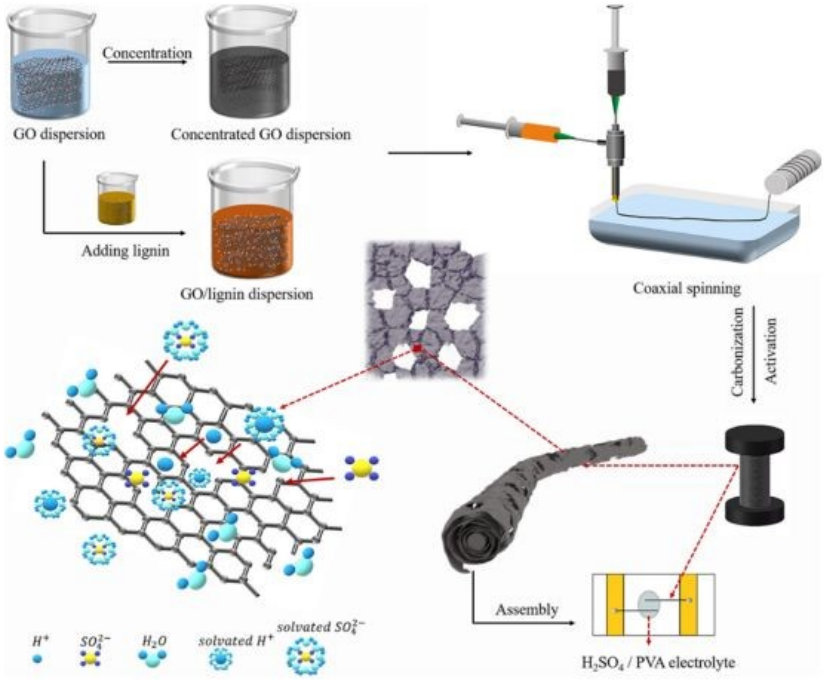

Figure 19: Pictorial representation of synthesis procedure of CG@GF electrode and fabrication of flexible SC. Reproduced with permission from [59] Copyright (2021) American Chemical Society.

The significance of carbon with lignin on the electrochemical performance in the CG@GF SC electrode is evaluated by CV measurement and shown in **Figure 20a**. It can be observed from the CV curves that that the CG@GF SC electrode exhibited a rectangular curve with a rapid propagation of charges at a scan rate of 5 mV/s. Also, the coaxially wet spun fiber in a ratio of 0% CG@GF possessed a smaller area due to an increase in the fiber diameter. The GCD curves of CG@GF hybrid-based fiber SC electrode (**Figure 20b**) shows an almost symmetric isosceles with a triangular shaped correlation between the time and charge/discharge potential at a current density of 0.1 mA/cm^2 within a potential window of 0 - 0.8 V. These features indicate that the CG@GF hybrid-based fiber SC electrode holds efficient charge/discharge characteristics. The area specific capacitance of CG@GF hybrid-based fiber SC electrode calculated from GCD curve is given in **Figure 20c**. The pure graphene fiber electrode exhibited an area specific capacitance of 23.9 mF/cm^2 at a current density of 0.1 mA/cm^2. It is also

observed that with an increase in the current density from 0.1 to 1 mA/cm^2, there exhibits a retention of capacitance of wet-spun coaxial carbon-based fiber of 60%, 57%, 65%, and 49% for 0%, 3%, 5%, and 10% CG@GF hybrid electrodes, respectively. The Nyquist plots show that (**Figure 20d**) the wet spun fiber holds a large semi-circle at the high-frequency region, depicting a high charge transfer resistance.

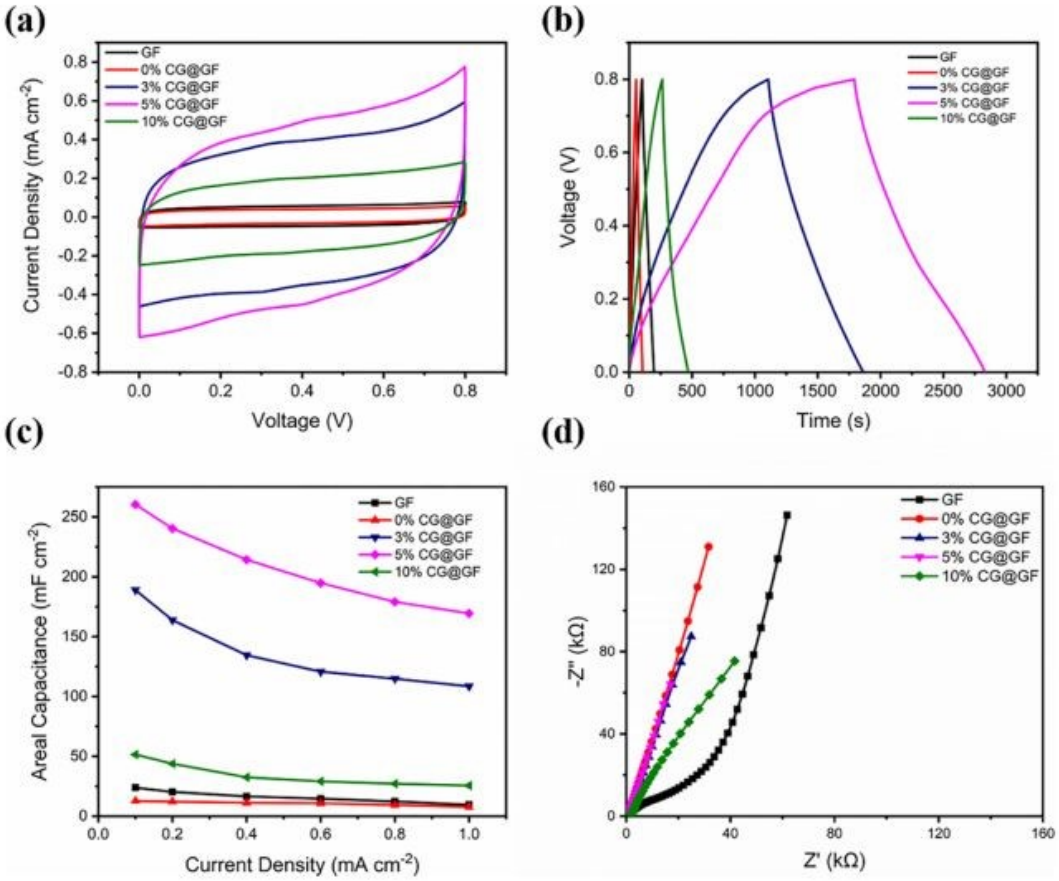

Figure 20: (a) CV curve with scan rate of 5 mV/s; (b) GCD curve at a current density 0.1mA/cm^2; (c) area specific capacitance obtained from GCD curve in different current density; (d) Nyquist plot of flexible SC. Reproduced with permission from [59] Copyright (2021) American Chemical Society.

4.2 Carbon Fibers/Layered Double Hydroxide Nanocomposite Electrodes

Layered double hydroxides are excellent candidates for SC electrode application due to their pseudocapacitive charge storage. Layered nanostructured electrodes envisages the diffusion of electrolyte-ions through it thereby an enhanced charge storage can be achieved. Gao et al. [60] fabricated a flexible SC with nickel-cobalt double hydroxide (Ni-Co LDHS) using pen ink electrodes constructed using a CF substrate. Fabrication of solid-state asymmetric SC with these electrodes is depicted in **Figure 21a**. Here, a CF thread holding small diameter range of 200-400 µm is selected as the primary electrode due to its better stiffness, light-in-weight and good conductivity. The electrical conductivity of CF thread is enhanced when it was coated with a thin layer of nickel by electrodeposition technique. The resultant electrode possesses an increase in the conductivity when compared to that of pristine CF, is evident from **Figure 21b**, it increased by a factor of 3.3 and it is found to be lighter than corresponding pure metal yarns. This is due to a thin deposition of nickel layer (about 820 nm) and it creates an improvement in the mass of electrode. Also, there exist a reduction in tensile strength of the fabricated SC

electrode from 2.05 to 1.47 GPa, mainly due to adverse effect introduced by interaction of surface carbon filament and deposited nickel atoms and the tensile test results are shown in **Figure 21c**.

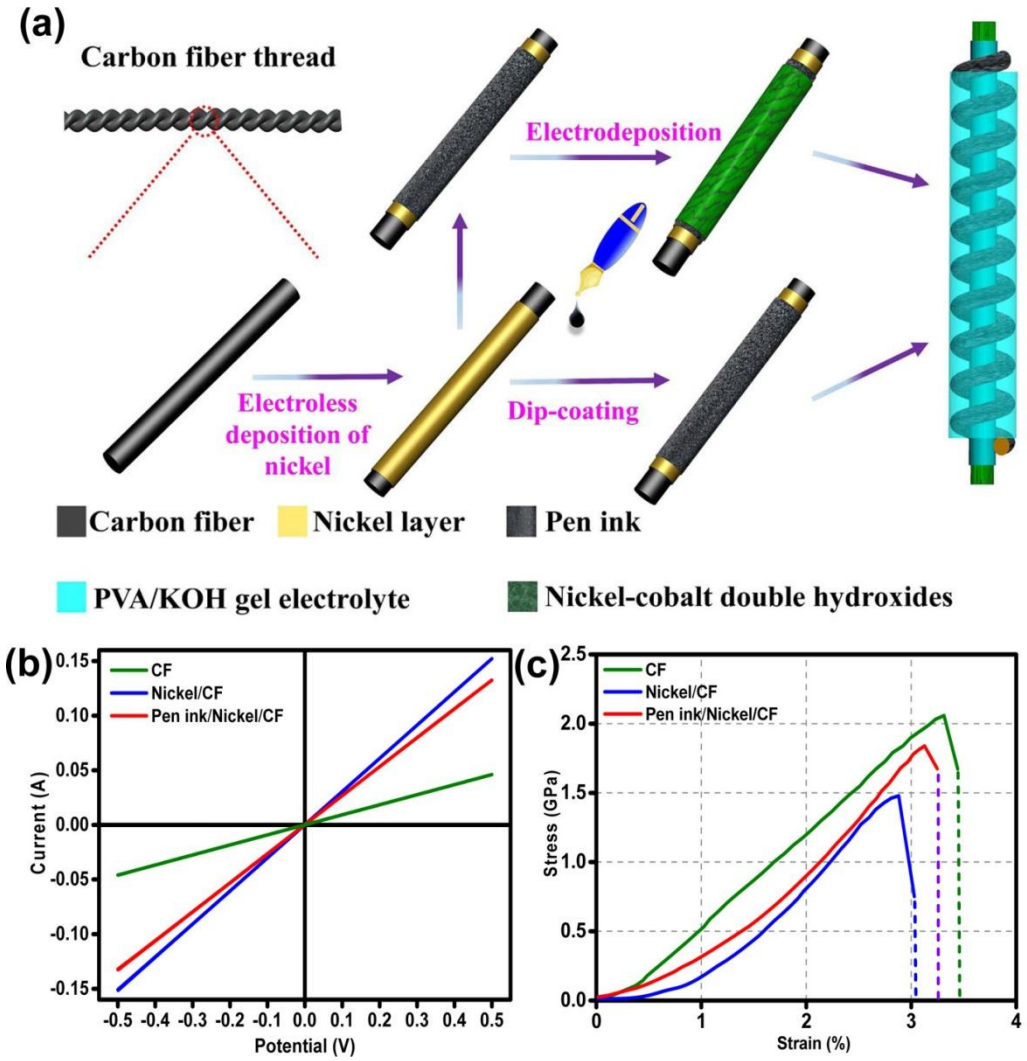

Figure 21: (a) Pictorial representation of fabrication process of flexible fiber-type solid-state asymmetric device; (b) it is conductivity, not two-electrode test; (c) analysis of tensile test. Reproduced with permission from [60] Copyright (2017) American Chemical Society.

The surface morphology of these fabricated hierarchical fiber electrodes is given in **Figure 22**. A single CF filament with a thickness of 6.93 µm holding a smooth surface can be viewed from **Figure 22a** and this CF filament coated with a thin nickel layer having a thickness of 820 nm is shown in **Figure 22b**. Because of the effective chemical penetration towards the core of CF, nickel is going to deposit uniformly on CF thread bundle is given in **Figure 22c**. **Figure 22d** and **e** confirms a uniform distribution of pen ink on nickel/CF thread. From the enlarged view of pen ink film (**Figure 22f**), which represents a porous structure holding a ravine morphology and helped in enhancing the surface area of the electrode nanostructure thereby an enhanced electrochemical reaction to occur. The FESEM image corresponding to Ni-Co LDHS on the substrate is shown in **Figure 22g**. In **Figure 22h**, we can find a thin transparent interconnected network growing over the ink film, which creates a highly electrically conducting network that consists of a large number of electroactive surface regions for the enhanced electrochemical

View Article Online
DOI: 10.1039/D4SU00146J

reaction to occur. The nanosheet microstructure having a rippled silk-like morphology is observed from the high-magnification SEM image depicted in **Figure 22i**.

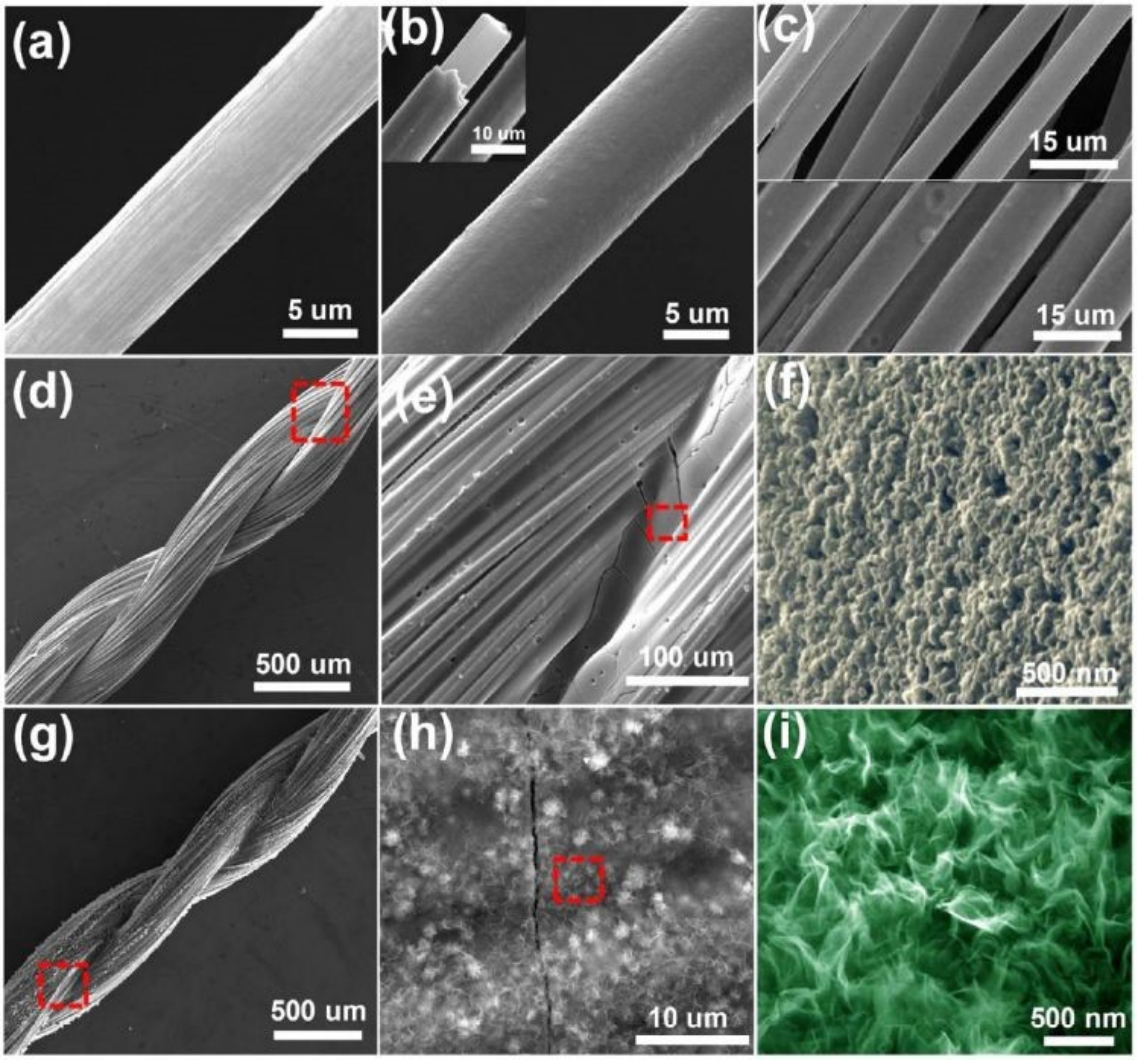

Figure 22: SEM image corresponds to (a) CF with a smooth surface; (b) CF uniformly coated over nickel layer having a smooth surface; (c) top portion of CF bundle and bottom portion is the CF bundle which was coated using Nickel; (d, e) Nickel/CF coated to a pen ink film; (f) porous structure with ravine morphology of pen ink/nickel/CF; (g, h) Ni-Co LDHS creating a uniform conductive network with ink film having porous nature and (i) SEM image with higher magnification. Reproduced with permission from [60] Copyright (2017) American Chemical Society.

An asymmetric SC was fabricated using the Ni-Co LDHS as the x electrode and yy as negative electrode. The CV curves of the as-fabricated asymmetric SC at varying potential window of 0−0.8 V to 0−1.55 V is given in **Figure 23a**. The area under the curve is found to be increased upon widening the potential window, which is obvious. The GCD curves of the as-fabricated asymmetric SC at varying potential window of 0 - 0.8 V to 0 - 1.55 V is given in **Figure 23b** and it can be seen that the SC work in a stable potential window of 0 - 1.55 V without any significant potential drop. The CV curves of the as-fabricated asymmetric SC at different scan rates such as 5 mV/s, 10, 20, 40, 60, 80, 100, and 150 mV/s within a potential window of 0 - 1.55 V is depicted in **Figure 23c**. These CV curves show that the redox-active electrodes with

View Article Online
DOI: 10.1039/D4SU00146J

an efficient reaction kinetics. The GCD measurements of the as-fabricated asymmetric SC at different current densities are shown in **Figure 23d**, which indicates a hybrid charge storage mechanism. The specific capacitance of the SC is found to be 22.94 F/g at a current density of 0.5 A/g and is found to decrease to 7.9 F/g when current density changed to 2 A/g. A high capacitance retention of 86% was also observed for the SC during the cyclic study even after 5000 cycles (**Figure 23e**). The GCD curves at its first and after completing the cycling study are depicted as an inset image of **Figure 23e**. The energy density and power density variation of the SC in the form of Ragone plot is given in **Figure 23f**. From this plot, it can be seen that with an increase in the current density from 0.5 to 2 A/g, there exists a reduction in specific energy density from 7.66 Wh/kg to 3 Wh/kg.

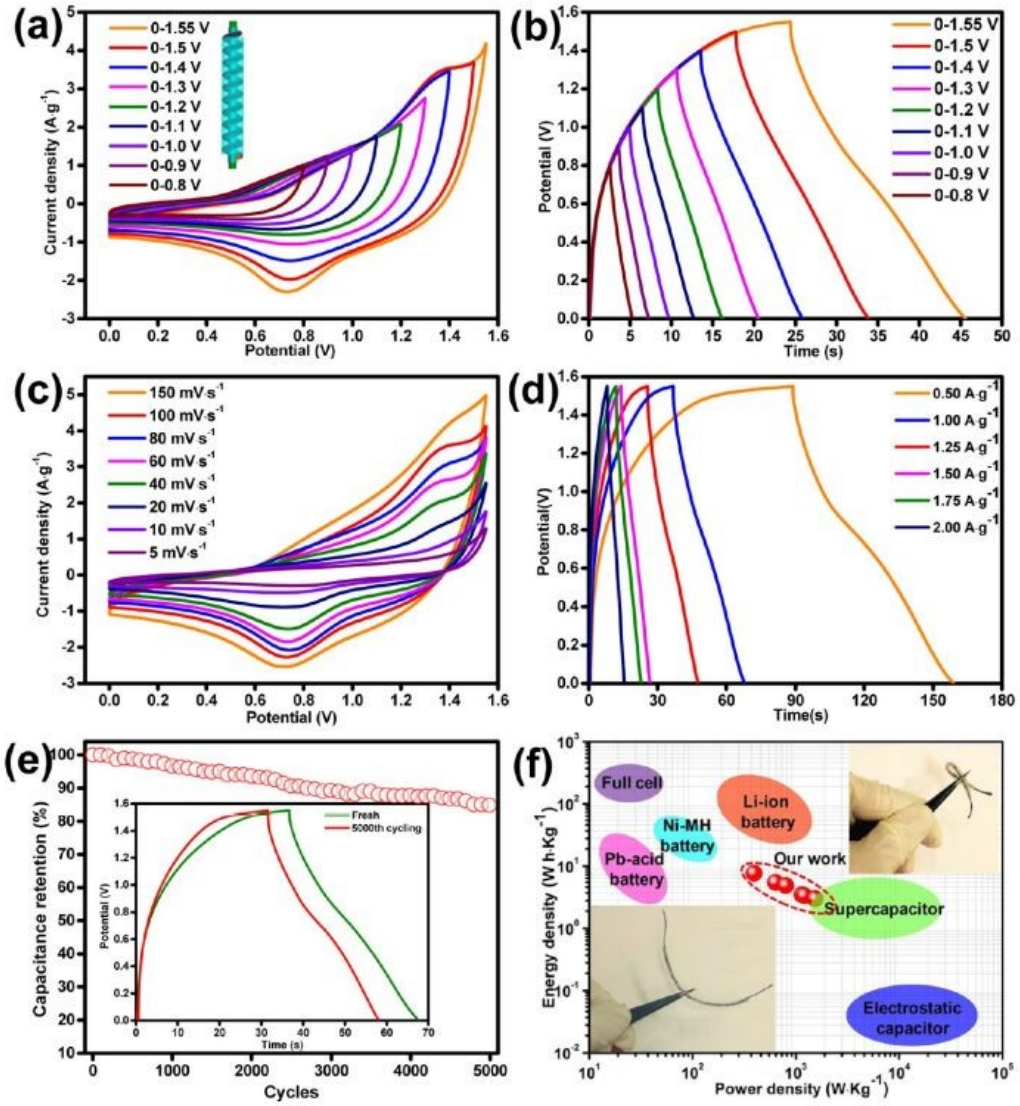

Figure 23: Electrochemical studies of fabricated asymmetric SC in KOH/PVA gel electrolyte (a) CV curve at 100 mV/s scan rate; (b) GCD curve in various voltage window at 1.25 A/g fixed current density; (c) CV curve with scan rate of 5-150 mV/s; (d) GCD curve in current density of f 0.5−2.0 A/g; (e) Cyclic stability analysis of device at current density of 1 A/g with inset representing the GCD curve of device before and after 5000 cycles; (f) Ragone plot, inset corresponding to the optical image of device. Reproduced with permission from [60] Copyright (2017) American Chemical Society.

View Article Online
DOI: 10.1039/D4SU00146J

A solvothermal reaction was opted to synthesize Ni-Co LDHS nanosheets over CF cloth by Wang et al [61]. By using a complex 2-methylimidazole and methanol as solvent, the LDHS nanosheet layer was prepared on CF that exhibited a growth in the (003) direction with an expansion of interlayer spaces. This resulted in the formation of a 3D porous structure having a thickness of 5 - 7 nm. The pictorial representation of charge storage mechanism of the SC electrode is shown in **Figure 24**.

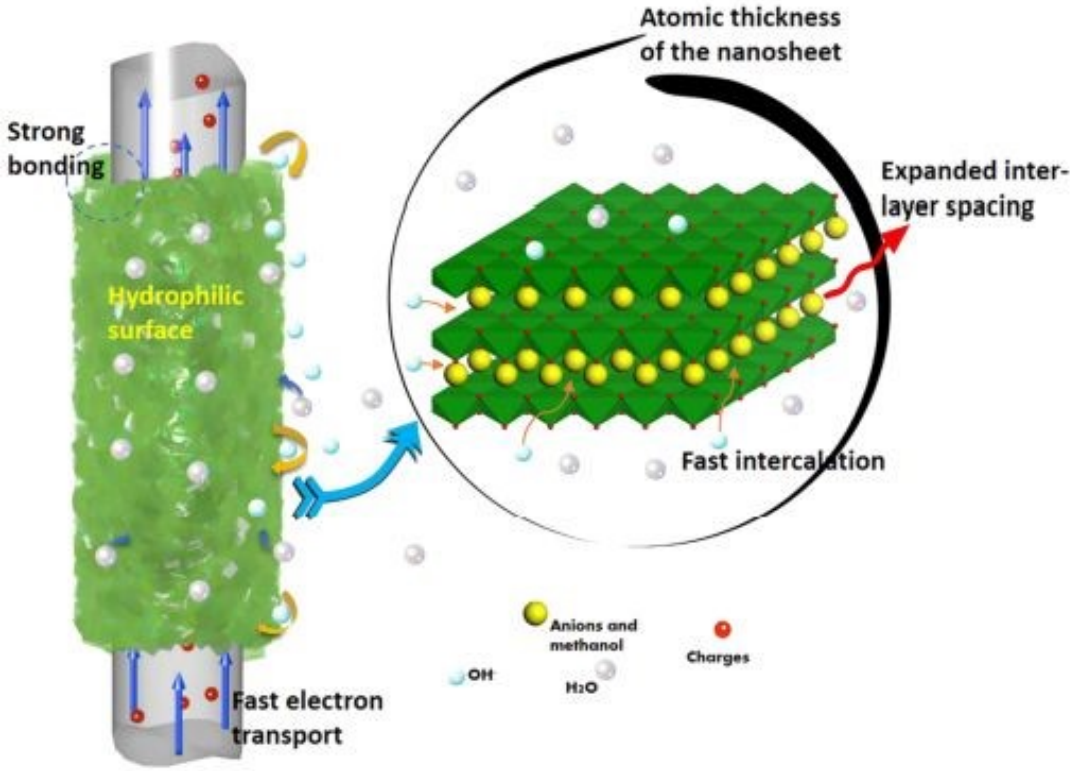

Figure 24: Diagrammatic representation of charge storage mechanism in electrode material. Reproduced with permission from [61] Copyright (2017) American Chemical Society.

A SC was fabricated using the Ni-Co LDHS as the x electrode and yy as negative electrode. The CV curves of the as-fabricated SC at varying potential window of 0 - 0.8 V to 0 - 1.6 V is given in **Figure 25a**. The SC could work within a potential window of 0 - 1.6 V without any deterioration in its behavior but the authors selected a slightly lower potential window of 0 - 1.4 V. The CV curves of the as-fabricated SC at different scan rates within a potential window of 0 – 1.4 V is given in **Figure 25b**. The specific capacitance of the SC was calculated at different scan rates and plotted in **Figure 25c**. A maximum capacitance of 317.9 mF/cm^2 is obtained for the SC at a lower scan rate of 2 mV/s and is found to decrease exponentially at higher scan rates. The Nyquist plot of the SC shown in **Figure 25d** holds a series resistance of 10.15 Ω/cm^2 with a charge transfer resistance of 0.71 Ω/cm^2 representing its excellent conductivity. The as-fabricated SC is found to be highly flexible when the bending test is carried at different bending angles. The CV curves obtained at different bending angles from 15^o to 180^o showed no significant variation, which represents its excellent flexibility. Jagadale et al. [62] reported the synthesis of CoAl LDHS on CF yarns using electrodeposition approach and use it as electrode-active material for fabricating a solid-state SC. The solid-state SC was fabricated using CoAl LDHS on CF yarns as electrode and KOH-PVA gel electrolyte. The

View Article Online
DOI: 10.1039/D4SU00146J

electrochemical performance of the solid-state SC is tested and an area specific capacitance of about 195 mF/cm^2 and a volumetric energy density of 1.6 mWh/cm^3 were obtained.

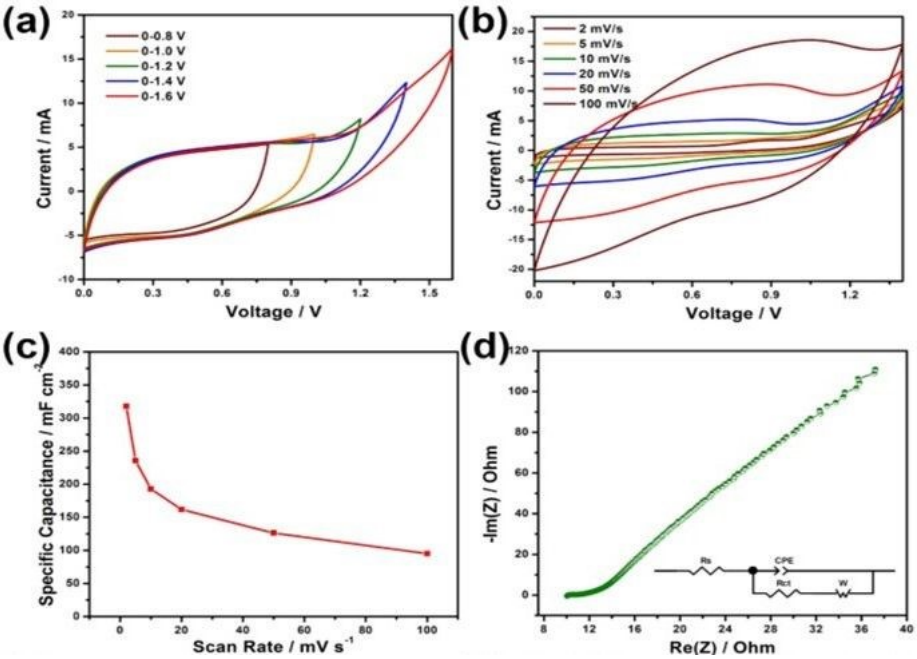

Figure 25: (a) CV curve of device at various voltage windows at a sweep rate 20 mV/s; (b) CV; (c) specific capacitance at various sweep rates; (d) EIS spectrum. Reproduced with permission from [61] Copyright (2017) American Chemical Society.

4.3 Carbon Fibers/Carbon Nanostructures Nanocomposite Electrodes

Carbon-carbon nanocomposites are highly demanded for SC electrode application due to their good electronic conductivity, good chemical and electrochemical stabilities, easy synthesis, etc. Carbon nanostructures such as CNTs, graphene, CNPs, etc are highly exploited as electrode-active materials for SC application in the recent past. Graphene-based SC electrodes has demerit of restacking of graphene layers during the electrode preparation. This leads to the closure of the pores available in the electrode nanostructure, which eventually deteriorates its electrochemical performance. To avoid the restacking of graphene layers while employing it as an electrode-active material for SC fabrication, a new strategy is reported to align graphene sheets vertically on CF substrate [32]. This novel strategy is found to be a versatile method of preparing graphene electrodes by the vertical attachment of graphene sheet to CF (VGCF) thereby the specific surface area of graphene available for electrochemical reactions to occur become enhanced. The VGCF hybrid electrode is synthesised using electrophoretic deposition as given in **Figure 26a-c**, where CF having an average diameter of 6 µm is applied as the substrate for depositing graphene sheets. An electrophoretic deposition is performed whereby the transportation of graphene sheets which are positively charged due to the adsorption of nickel ions towards CF electrode. The electrophoretic deposition of graphene sheets is carry forwarded by applied a DC potential of 50 V (**Figure 26b**) and a 3D VGCF hybrid electrode is obtained (**Figure 26c**). The electron transport in the VGCF hybrid SC electrode is schematically portraited in **Figure 26d**.

View Article Online
DOI: 10.1039/D4SU00146J

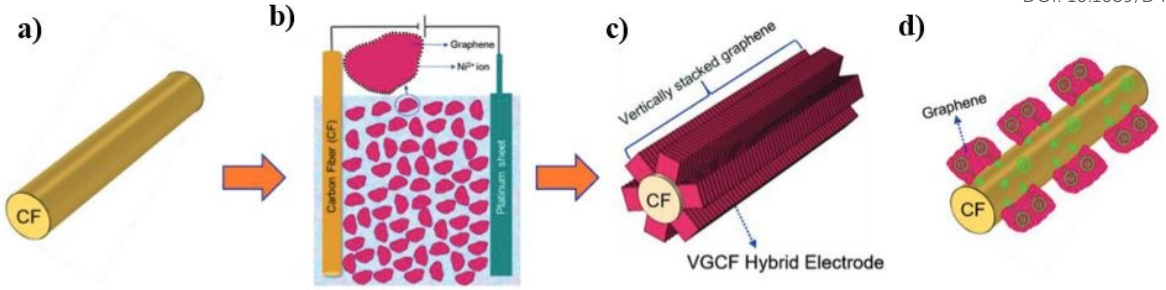

Figure 26: Pictorial representation of synthesis of VGCF electrode (a) CF substrate for electrophoretic deposition; (b) electrophoretic deposition with CF as negative electrode, Pt as positive electrode, and a bath consists of dispersion of graphene sheets in isopropyl alcohol with nickel nitrate hexahydrate; (c)VGF hybrid after electrodeposition; (d) Pictorial representation of electron transport from graphene to CF. Reproduced with permission from[32] Copyright (2019) WILEY-VCH Verlag GmbH & Co. KGaA, Weinheim.

In order to analyse the application of this VGCF hybrid electrode material for industrial purposes, the authors of this work fabricated a symmetric SC using aqueous 1M H_3PO_4 as electrolyte. Nyquist plot of the VGCF hybrid electrode is given in **Figure 27a** and the Nyquist plot at the high-frequency region is given as an inset image, which showed that the electrode exhibited a low electrolyte series resistance. The CV curves obtained for the VGCF hybrid SC (**Figure 27 b**) showed that the hybrid electrode exhibits a redox-type charge storage induced by the presence of oxygen-containing surface functional groups on the graphene sheet as well as the α-$Ni(OH)_2$. The charge storage contribution from the surface-controlled and the diffusion-controlled mechanism is calculated by using Dunn's method and found that the electrode material has 70% surface-controlled and 30% diffusion-controlled charge storage, as depicted in **Figure 27c**. The GCD curves obtained for the VGCF hybrid SC shown in **Figure 27d** exhibited a charge/discharge profile with two slopes, this is due to the different charge storage mechanisms introduced by the electrode. The CV study performed within a potential window of 0 - 1.6 V (**Figure 27e**) depict the efficient charge storage capability of the SC. The VGCF hybrid SC exhibited a capacitance retention of 99.4% even after 17000 cycles (**Figure 27f**) and the inset CV curves show that there is no significant change in the area under the curve in the first cycle and the last cycle. The flexibility of the SC was analysed by bending it at different bending angles such as 30º, 45º, 60º, 90º, 135º, and 180º and from the CV curves (inset image), it is clear that the SC device has a capacitance retention of 100% even at a severe bend of 180º (**Figure 27g**). The SC is found to retain its capacitance even after completing 1000 bending cycles (**Figure 27h**). The inset image is the digital photograph at a bending angle of 90º. A device prototype of this fabricated SC which operating a toy drone propeller fan is given in **Figure 27i** and the running of the fan is given as an inset. In another work, a free-standing helically-coiled CNTs (HCNTs) grown on CF (HCNTF) is used as an electrode-cum-current collector for the fabrication of a flexible SC [63]. The authors of this work synthesized HCNTF hybrid by CVD method using thiophene as the defect induced catalyst for the growth of HCNTF. The flexibility of this SC is analysed by choosing the bending angles 0, 30, 60, 90, and 120º. The rate performance of fabricated electrode with HCNT density of 5.77 mg/cm^3 is verified by GCD measurements performed at various current densities. It is worth to note that the HCNTF hybrid electrode can be charged at a relatively higher current density of 8.33 mA/cm^2. A solid-state SC was fabricated by using HCNTF hybrid electrode-cum-current collector and PVA/LiCl gel electrolyte. The SEM image (**Figure 28a**) shows a mesoporous

open network of HCNTs. A TEM image of a single strand of HCNT is depicted in **Figure 28b**. The SAED pattern (**Figure 28c**) shows that the HCNT is not crystalline due to the defect-induced growth. A schematic representation of the fabricated solid-state SC is given in **Figure 28d**. A digital image of SC module comprising of two similar solid-state HCNTF SCs connected in series is shown in **Figure 28e** and this module is bent at an angle of 180° is shown in **Figure 28f**. The practical application of this SC module in wearable electronic devices is demonstrated by lighting-up an LED at its normal position (**Figure 28g**) and at a severe bend of 180° (**Figure 28i**), which shows that no change in the light intensity.

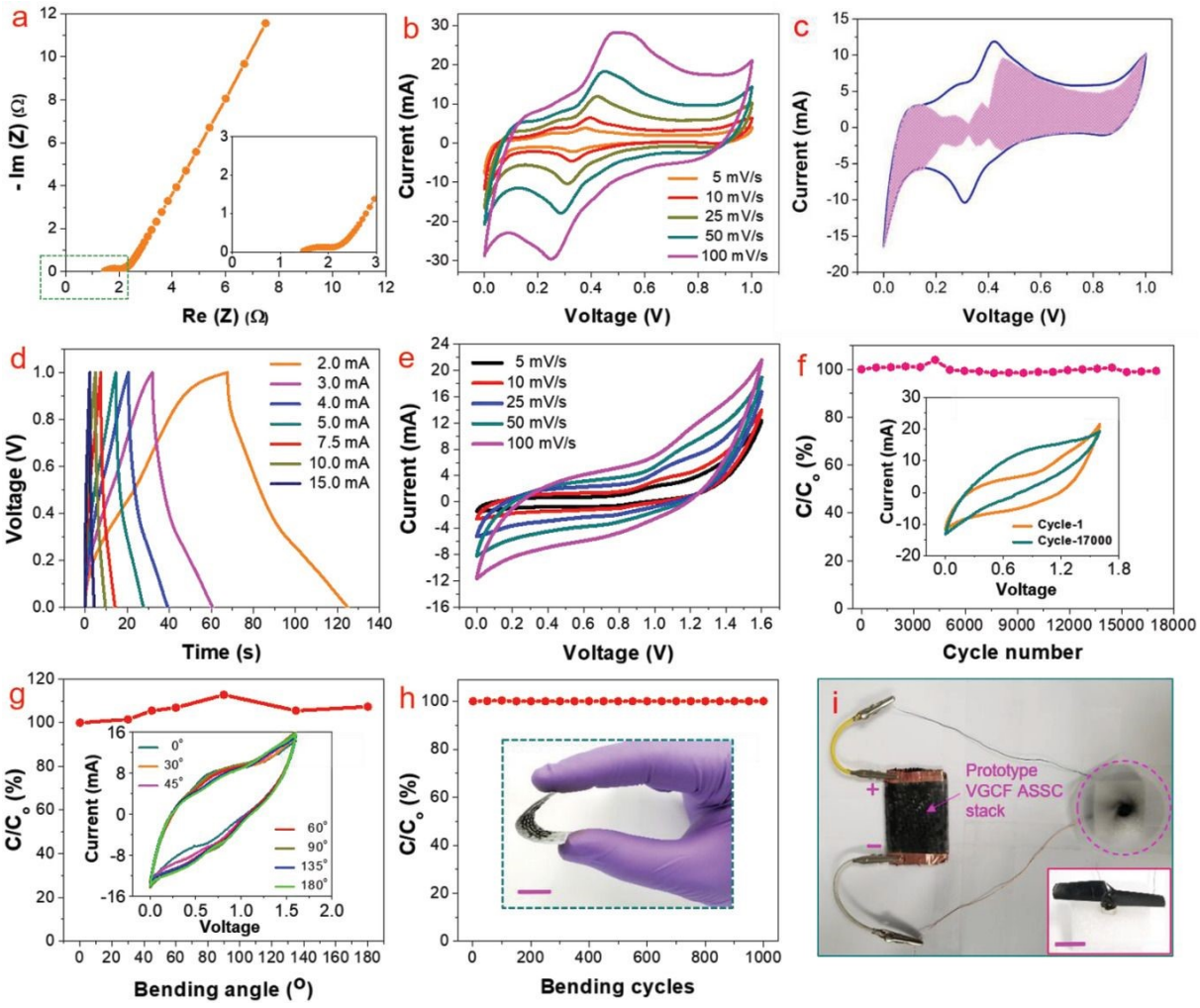

Figure 27: Electrochemical analysis of VGCF SC (a) Nyquist plot (high resolution view of high frequency region); (b) CV with different scan rates; (c) calculation of contribution of capacitance at a scan rate of 25 mV/s; (d) GCD curve at various current density; (e) CV at various scan rate ; (f) capacitance retention with cycle number for 17000 cycles; (g) capacitance retention at various bending angle (inset is the CV at various bending angle at 100 mV/s scan rate); (h) capacitance retention at 1000 bending cycle (inset is the digital photograph at an angle of 90°); (i) device prototype. Reproduced with permission from [32] Copyright (2019) WILEY-VCH Verlag GmbH & Co. KGaA, Weinheim.

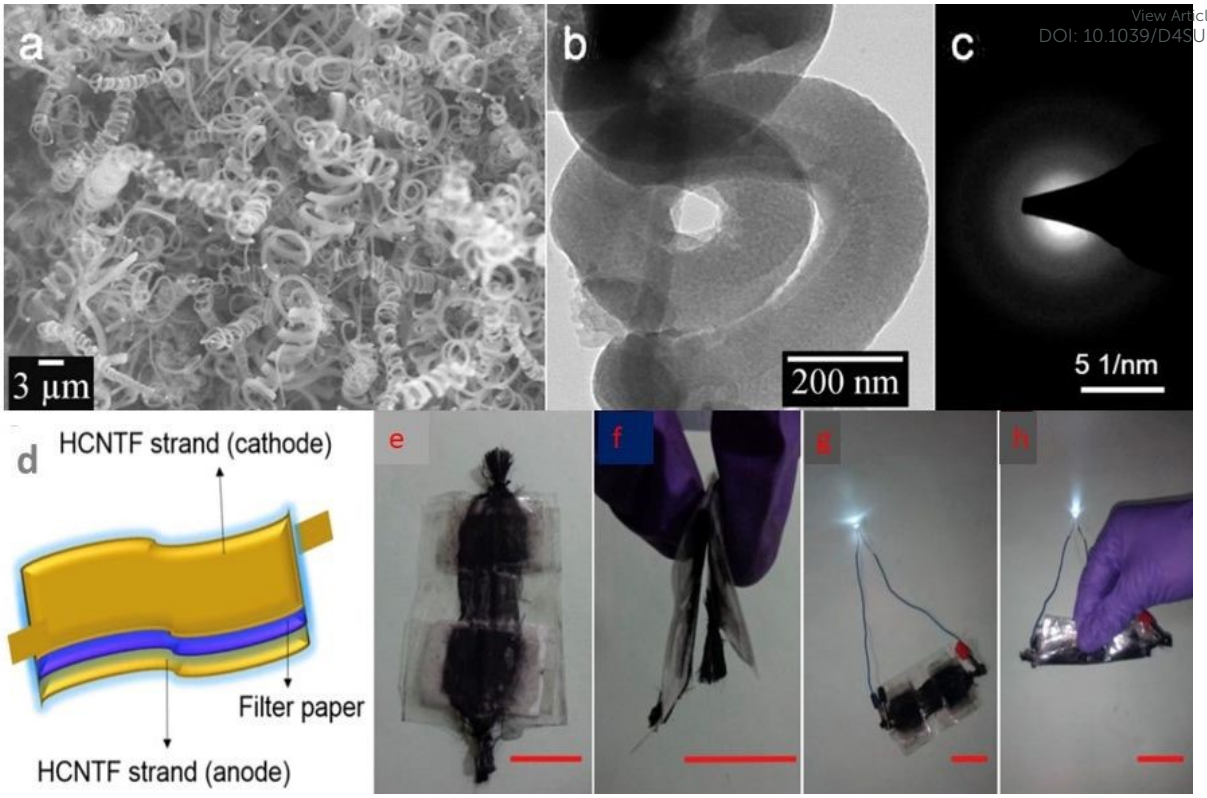

Figure 28: (a) SEM; (b)TEM; (c) SAED spectrum of HCNTF having HCNT density 5.77 mg/cm^3; (d) Pictorial representation of fabricated device; (e) series connection of two solid state flexible HCNTFs; (f) bending of module at 180º; (g) discharging of module by LED; (h) discharging of module by a white LED with bending at 180º. Reproduced with permission from [63] Copyright (2016) Elsevier.

Yang et al. [64] developed a sandwich patterned reduced graphene oxide (rGO)/carboxylated multi-walled CNT (MWCNT) (RGO/cMWCNT) hybrid film and polypyrrole supported with CF paper (CFP/PPy) using vacuum infiltration method and electrochemical deposition. An asymmetric SC was fabricated using RGO/cMWCNT as negative electrode and CFP/PPy as positive electrode, and potassium polyacrylate/KCl gel electrolyte. This asymmetric SC exhibited an energy density of 28.6 W h/kg at a corresponding power density of 15.1 kW/kg at a working cell voltage of 1.6 V. The device holds a capacitance retention of 93% with long cycle life after 2000 cycles. Using a two-step solution process consisting of hydrothermal and chemical bath deposition, Liu et al. [65] synthesized SnO_2@MO_x heterostructure over CF cloth in order to fabricate a high-performance SC. This heterostructure possesses the features of good electronic conductivity of SnO_2 nanosheets as backbone for the deposition of MO_x. The as-fabricated SC showed a higher discharge area specific capacitance of 980 mF/cm^2 at a current density of 1 mA/cm^2 along with an efficient rate capability of about 767 mF/cm^2 when tested at a comparatively higher current density of 20 mA/cm^2. The SC hold an efficient cyclic stability of ~21.9% retention after completing 6000 cycles when performed at a current density of 1 mA/cm^2. Feng et al. [66] synthesized MnO_2 tube-in-tube arrays supported over CF cloth using a facile template-assisted electrodeposition route. The solid-state SC fabricated with PVA/LiCl shows a high area specific capacitance of about 322 mF/cm^2 at a current density of 0.125 A/g. This SC exhibited a volumetric energy density of 0.073 mW h/cm^3 at a corresponding power density of 25W/kg along with a capacitance retention of 96.4% even after completing 2000 cycles. An asymmetric fiber-shaped SC in a weavable and flexible pattern using CF bundle@CNT-NiCo(OH)$_x$ (CF@CNC) as positive electrode and CF bundle

View Article Online
DOI: 10.1039/D4SU00146J

@activated carbon (CF@AC) as negative electrode was reported by Lu et al. [67]. In order to remove the demerits of the hydrophobic nature, reduced electrical conductivity and low surface area, a treatment with air plasma and modification with CNT is performed during the CF@CNC fabrication. This asymmetric SC exhibited an energy density of 0.84 mWh/cm^3 energy density at a corresponding power density of 19.1 mW/cm^3. A high capacitance retention of 100% is also observed even after completing 8000 charge/discharge cycles. Using electrospinning and carbonization process on a CNF membrane, flexible polypyrrolone/polyimide composite (PBPICF) was prepared by Liu et al. [68]. For the preparation of PBPICF, polycarboxylic acid ammonium salt (PCAAS) and polyamic acid (PAA) is mixed in different proportions. The prepared nanofibers are exhibiting a network form structure having a uniformity in diameter of about 400-500 nm. Prepared PBPICF membrane hold an efficient flexibility and it can able to bent and fold without producing any break. This report shows that the prepared SC holds a specific capacitance of 172.44 F/g at a current density of 0.2 A/g. These results show that these binder free, flexible membrane is capable to fabricate a SC with good performance. Here the prepared PBPICF membrane have efficient power density value of 90 W/kg at 19.4 Wh/kg energy density with capacitance retention of 96% after 10000 cycles at a current density of 1 A/g.

With the aid of a multi-step transformation procedure, Tong et al. [69] fabricated an elm-seed structured NiS_2 nanosheets on the surface of coal-based CF. Here, the silica/coal-based fiber is prepared by electrospinning a mixed solution consists of oxidized coal, polyvinyl alcohol and tetraethyl orthosilicate in water/N,N-dimethylformamide followed by carbonization. Due to the large surface area and novel structure, the as-prepared binder-free hybrid electrode for SC and this electrode exhibited a high value of specific capacitance of about 635.1 F/g at a current density of 1 A/g. Also, the SC electrode showed a capacitance retention of about 96.4% after 5000 cycles. Ding et al. [70] fabricated a fiber electrode where acidified CF is modified by rGO/g-C_3N_4. The symmetric SC fabricated from this electrode exhibits an arial capacitance of 61 mF/cm^2 with a capacitive retention of 90% after 5000 cycles. Using hydrothermal approach, Yu et al. [71] created a 3D nanostructure with combination of vertical polyaniline (PANI) nanowire array nitrogen plasma etched-carbon fiber cloth (eCFCs) in order to use it as an electrode for flexible SC. The flexible SC shows a higher specific capacitance of 1035 F/g at a current density of 1 A/g. It possesses an efficient capacitance retention of 88% even at a comparatively higher current density of 8 A/g with a long cyclic stability of 5000 cycles. The flexibility of assembled PANI/eCFC was evaluated at a fixed mechanical stress and its performance is evaluated. They observed that this assembled device has efficient flexibility and mechanical properties and it undergoes different bending angles. The proposed performance durability is relating to higher mechanical flexibility of electrode and it possess strong connection between nitrogen doped eCFC and PANI arrays, indicates their application in flexible electronics.

4.4 Carbon Fibers-Based Wired Electrodes

Wired SCs have received tremendous hope in current era due to its rapid discharge capacity, flexibility, weavable structure, long cycle life and it can be easily be integrated with on-body wearable electronic devices. Ai et al. [72] fabricated a solid-state wired SC by using nanostructured $CoNiO_2$@CF nanocomposite electrode and activated carbon@CF electrode having length greater than 1 m. A schematic representation of the fabrication of this asymmetric solid-state SC is given in **Figure 29**. Here, the anode and cathode fiber are twisted on a polymethylmethacrylate (PMMA) backbone using KOH-PVA gel electrolyte and PDMS layer as shell. The as-fabricated asymmetric SC exhibits efficient flexibility, wearability and toughness.

View Article Online
DOI: 10.1039/D4SU00146J

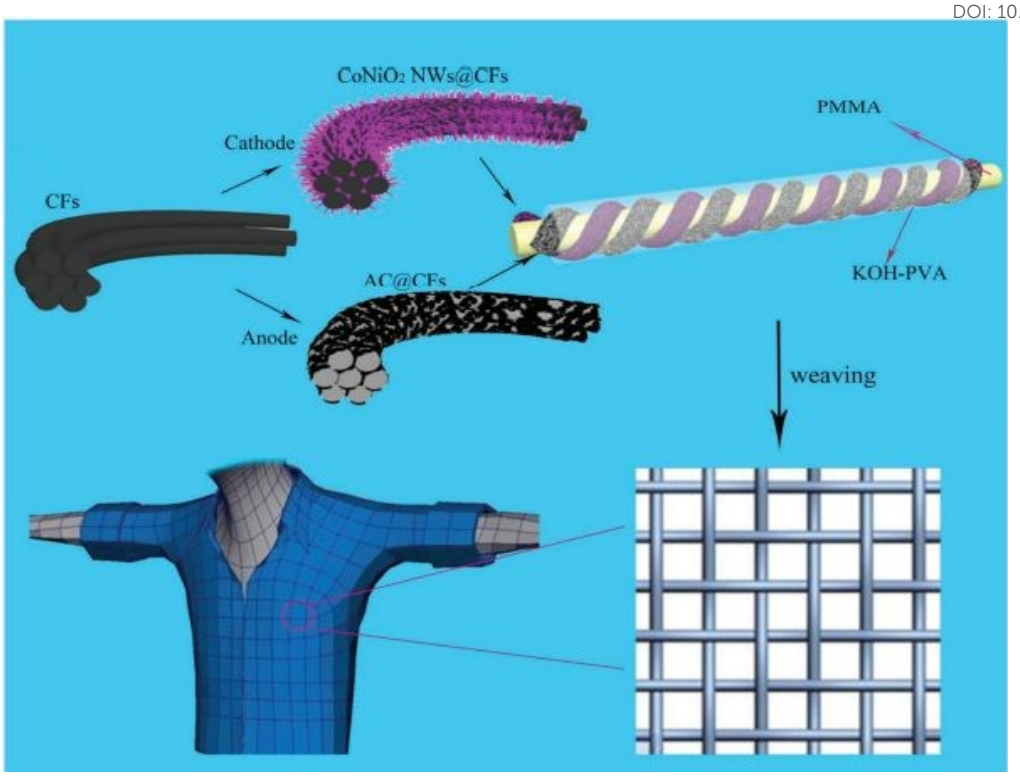

Figure 29: Pictorial representation of fabrication process of wired asymmetric SC. Reproduced with permission from [72] Copyright (2016) WILEY-VCH Verlag GmbH & Co. KGaA, Weinheim.

The electrochemical characteristics of the asymmetric SC is analysed by taking a 10 nm length as given in **Figure 30a**. The CV measurements are carried out within a potential window 0 - 1.8 V and the CV curves (**Figure 30b**) obtained at different scan rates from 5 mV/s to 500 mV/s showed a quasi-rectangular nature. The discharge curves of the asymmetric SC within a potential window of 0 - 1.8 V is given in **Figure 30c**. The specific capacitances calculated from the discharge curves are 16.75, 16.55, 16.14, 15.91, 15.45, 14.95, 14.41, 13.89, 13.32, and 10.24 mF at different current densities such as 0.5, 1, 1.5, 2, 2.5, 3, 3.5, 4, 4.5, and 5 mA, respectively (**Figure 30d**). The wire-shaped SC having an energy density of 0.95 mWh/cm^3 is obtained at a power density of 1.14 mW/cm^3 (**Figure 30e**) and the SC possesses a capacitance retention of about 97% after completing 5000 cycles (**Figure 30f**). The mean variation tendency for capacitance exhibited by the wired asymmetric SC is given in **Figure 30g**.

View Article Online
DOI: 10.1039/D4SU00146J

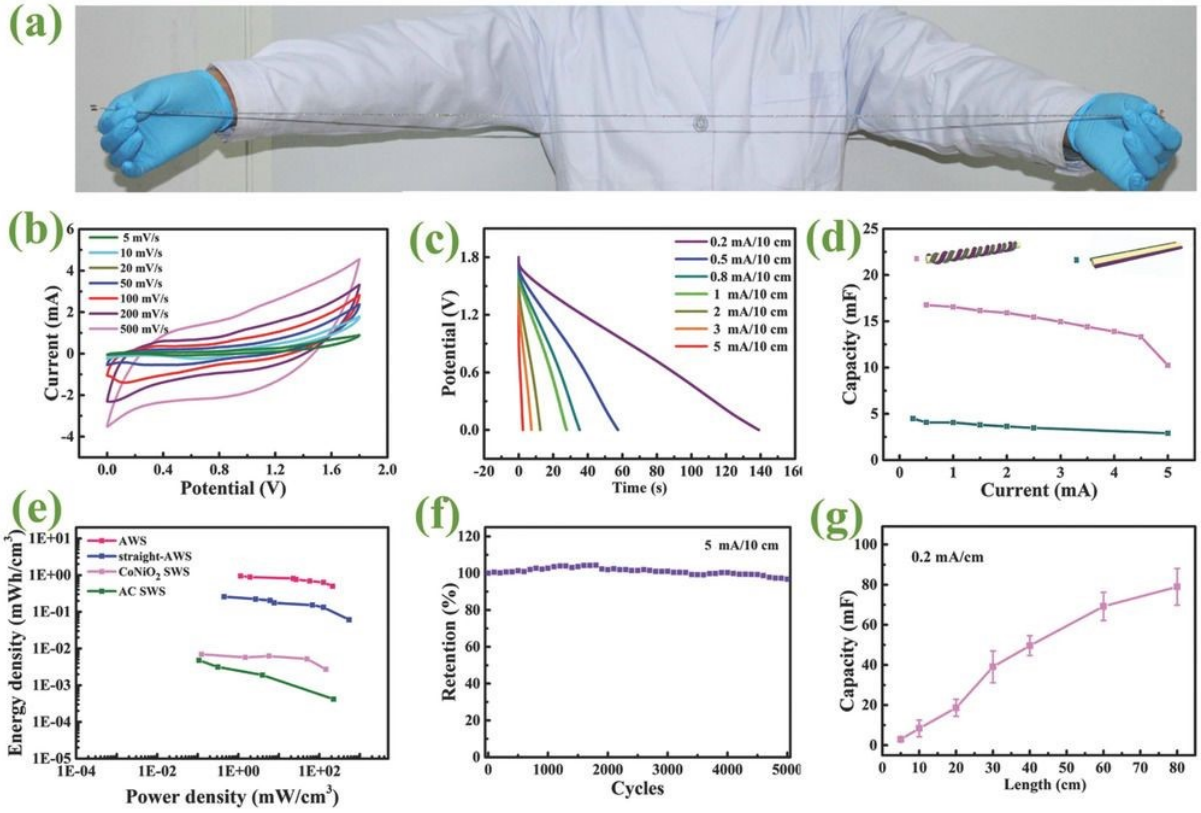

Figure 30: (a) Digital image of asymmetric wired SC with length 1.2 m; (b) CV and (c) GCD curve of SC device; (d) capacitance comparison of spiral double-helix twisted asymmetric wire supercapacitor with those of the straight twisted asymmetric wire supercapacitor; (e) Ragone plot; (f) cyclic stability analysis; (g) change in capacitance of device with length condition measured in similar condition. Reproduced with permission from [72] Copyright (2016) WILEY-VCH Verlag GmbH & Co. KGaA, Weinheim.

Harvesting of wind power in association with SCs have received great attention due to their sustainable energy conversion and storage features. The energy obtained from the wind turbines can be easily be stored in a SC but a major requirement for the same is that the Sc should exhibit high energy density. But the fabrication of a SC with high energy density and reduced internal resistance is a tedious task. Shi et al. [73] developed a strategy to merge wind driven generator (WDG) with an asymmetric wire-shaped SC (WSSC), where the WDG part responsible for the conversion of energy and the asymmetric WSSC responsible for storing the energy. Asymmetric WSSC was assembled using $CoNi_2S_4$ nanosheets arrays and vertical FeOOH coated to flexible CF tubes (CFTs) as a negative and positive yarn electrode, respectively (**Figure 31a**). Here, the vertically aligned cross-linked porous network is introduced by the electroactive nanosheet array is found suitable for diffusion of the ions as well as transportation of charges. **Figure 31b** and **c** represents the FESEM images of FeOOH/CFTs yarn electrode at different magnifications. Here, we can observe that the CFTs are fully covered by the FeOOH (**Figure 31b**). In the case of high-magnification FESEM image (**Figure 31c**), it can be seen that the vertically aligned FeOOH nanosheet with an average thickness in the range of 20 nm is obtained. These nanosheets tend to be interconnecting to each other without producing any agglomeration effect. In the case of $CoNi_2S_4$/CFTs yarn

electrode, a network architecture over CFT is introduced by a uniform construction of $CoNi_2S_4$ nanosheet vertical arrays (**Figure 31d** and **e**).

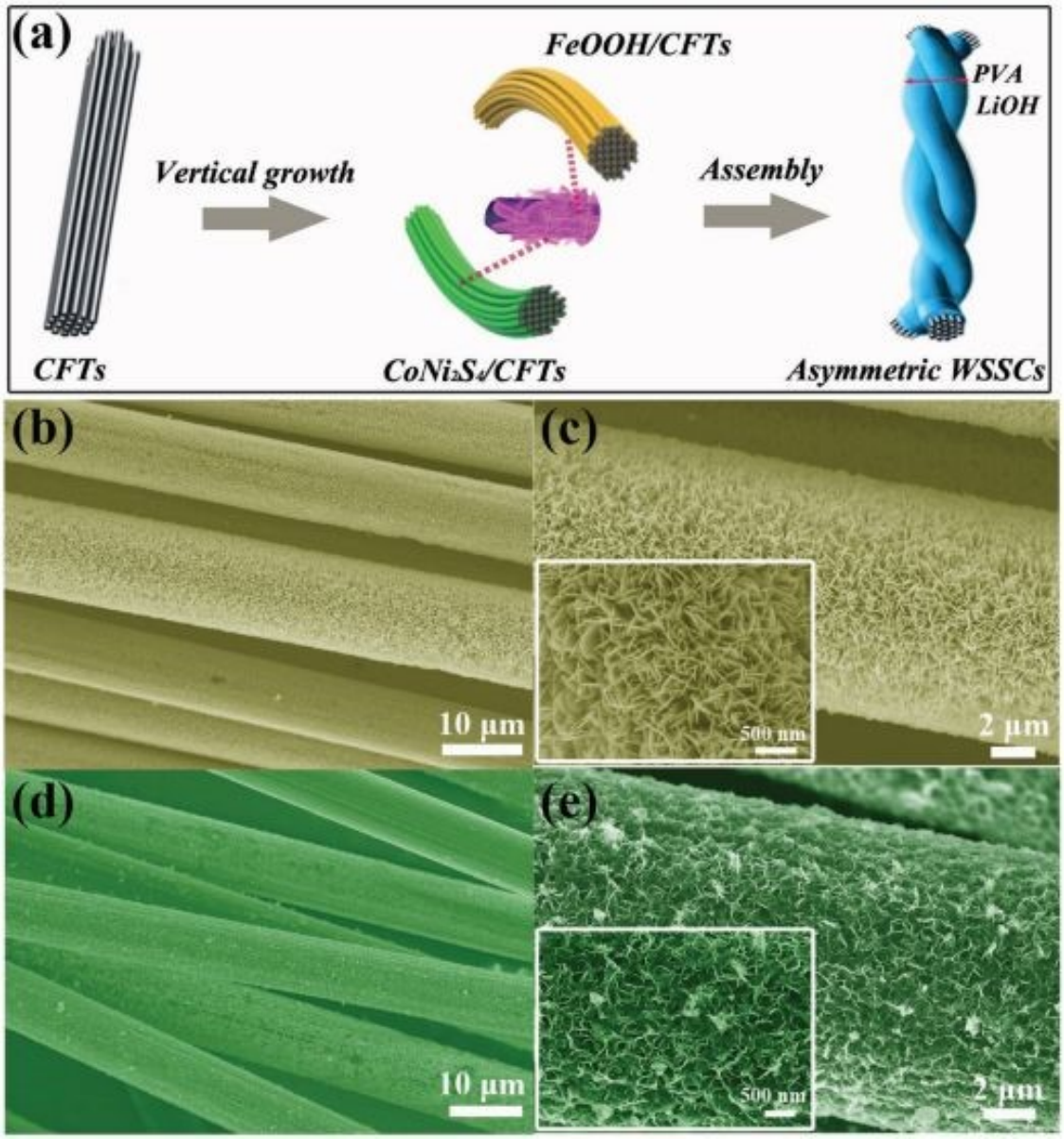

Figure 31: (a) Schematic diagram of an asymmetric WSSC. (b,c) FESEM images of FeOOH. (d,e) FESEM images of $CoNi_2S_4$ vertical nanosheets grown over CF tubes. Reproduced with permission from [73] Copyright (2017) WILEY-VCH Verlag GmbH & Co. KGaA, Weinheim.

The electrochemical performances of as-fabricated SC for harvesting the wind energy were examined by consecutive experiments. The pictorial representation of an integrated system consists of miniaturized WDG, electronic regulator and two asymmetric WSSCs connected in series combination is depicted in **Figure 32a**. The output electric signal generated from the WDG is rectified by a regulator with 3 V output (**Figure 32b**) and there exist a conversion of alternating current to direct current of 600 mA, and the WSSC was charged steadily. Within 8 s, the WSSC module is rapidly charged to 3 V. After completely charging WSSC module, it is discharged via a red LED is given in **Figure 32c**. This process is not only mentioning an effective method to harvest the wind power to charge the WSSC module but also indicating

View Article Online
DOI: 10.1039/D4SU00146J

the fabrication of a WSSC with high energy density. After the completion of 5000 charging/discharging cycles, there is only a slight change in the capacitance observed, which is clear from **Figure 32d**. After the cycling study, the electrochemical series resistance (ESR) of the module is found to be increased slightly (2.8 Ω) whereas the ESR before the cycling was 2.2 Ω (inset of **Figure 32d**).

The preparation of a 3D nanoarchitecture over flexible current collector is a suitable method for the fabrication of portable and wearable power source. Li et al. [74] developed a flexible and efficient electrode with electrospun CF substrate possessing a hierarchical porous V_2O_5 nanosheets by solvothermal method. The formation of a 3D network is clear from the FESEM image given in **Figure 33a**. A cross-sectional view of the prepared electrospun CF indicates that the substrate is holding a thickness of about 87 μm, which is given as an inset image in **Figure 33a**. An average diameter of around 270 nm is obtained for the electrospun nanofiber and it possesses a smooth surface (**Figure 33b**). A uniform 1D hierarchical architecture can be observed from the FESEM micrograph shown in the inset of **Figure 33c**. From the enlarged view of this SEM image (**Figure 33c**), it is found that the 1D architecture is composing of ultrathin sheet-like subunits which producing a uniform growth over the surface of electrospun CF.

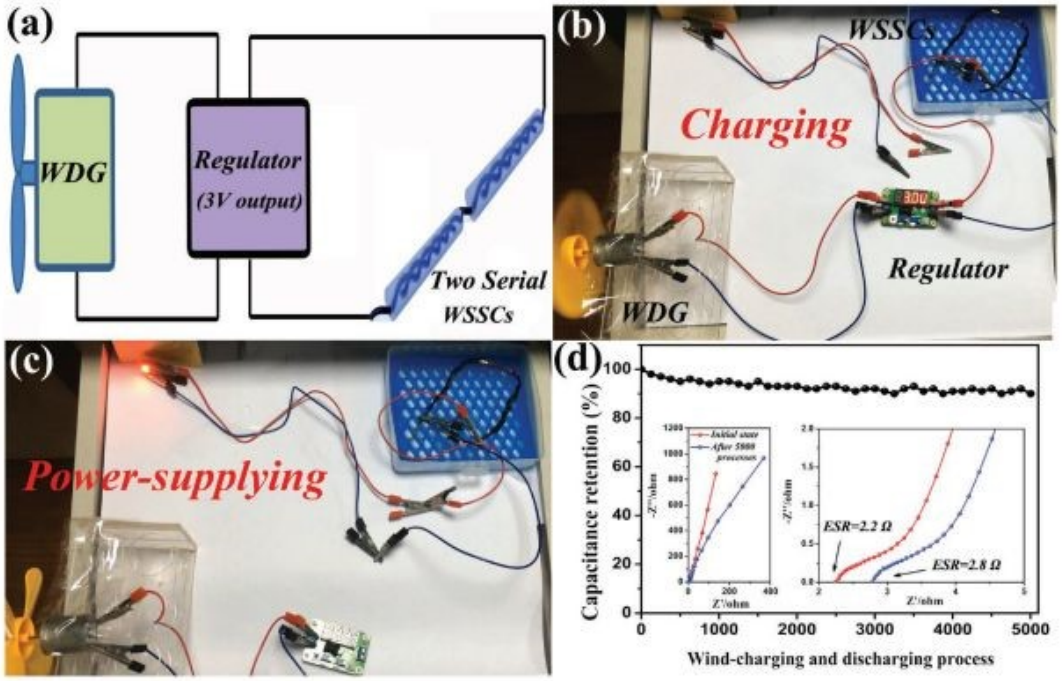

Figure 32: (a) A pictorial representation of the fabrication of wind-charging system, (b) real-time picture of charging process in WSSCs by the harvesting of wind energy, (c) digital photograph of lighting of red lamp with WSSCs after completely charging, (d) retention of capacitance after wind-charging and discharging procedures. Inset representing the Nyquist plot of device before and after 5000 cycles. Reproduced with permission from [73] Copyright (2017) WILEY-VCH Verlag GmbH & Co. KGaA, Weinheim.

After a low temperature annealing in air, the V-O precursor is fully converted to a V_2O_5 crystalline nanosheets. The CF is found to impart a robust support. The morphology of as-prepared V_2O_5 architecture is still maintained after the annealing procedure (**Figure 33d**). The magnified images of V_2O_5 architecture provided in **Figure 33e**,**f** shows a perpendicularly cross-linked V_2O_5 with porous structure, which exhibited a sheet-like morphology. It consists of an

open space between the individual nanosheets, which helps in an easy penetration of electrolyte-ions and hence it produces an efficient electrochemical performance while using it as an electrode-active material in a SC. An asymmetric hybrid supercapacitor device is assembled by using V_2O_5-electrospun CF as anode and electrospun freestanding CF as cathode. The assembled hybrid SC hold an excellent cyclic stability of 10000 cycles with a decay of 10.7% capacitance after completing the cycling study. The SC possesses an excellent energy density of 22.3 Wh/kg at a corresponding power density of 1500 W/kg and efficient mechanical flexibility. The flexibility of SC was evaluated by bending it at different bending angles and possessed excellent mechanical stability during the testing. The electrochemical characteristics of this SC is maintained even after bending it for 200 times, which demonstrates prominent mechanical robustness for practical applications. This study portraits an effective fabrication of hybrid electrodes for flexible SCs.

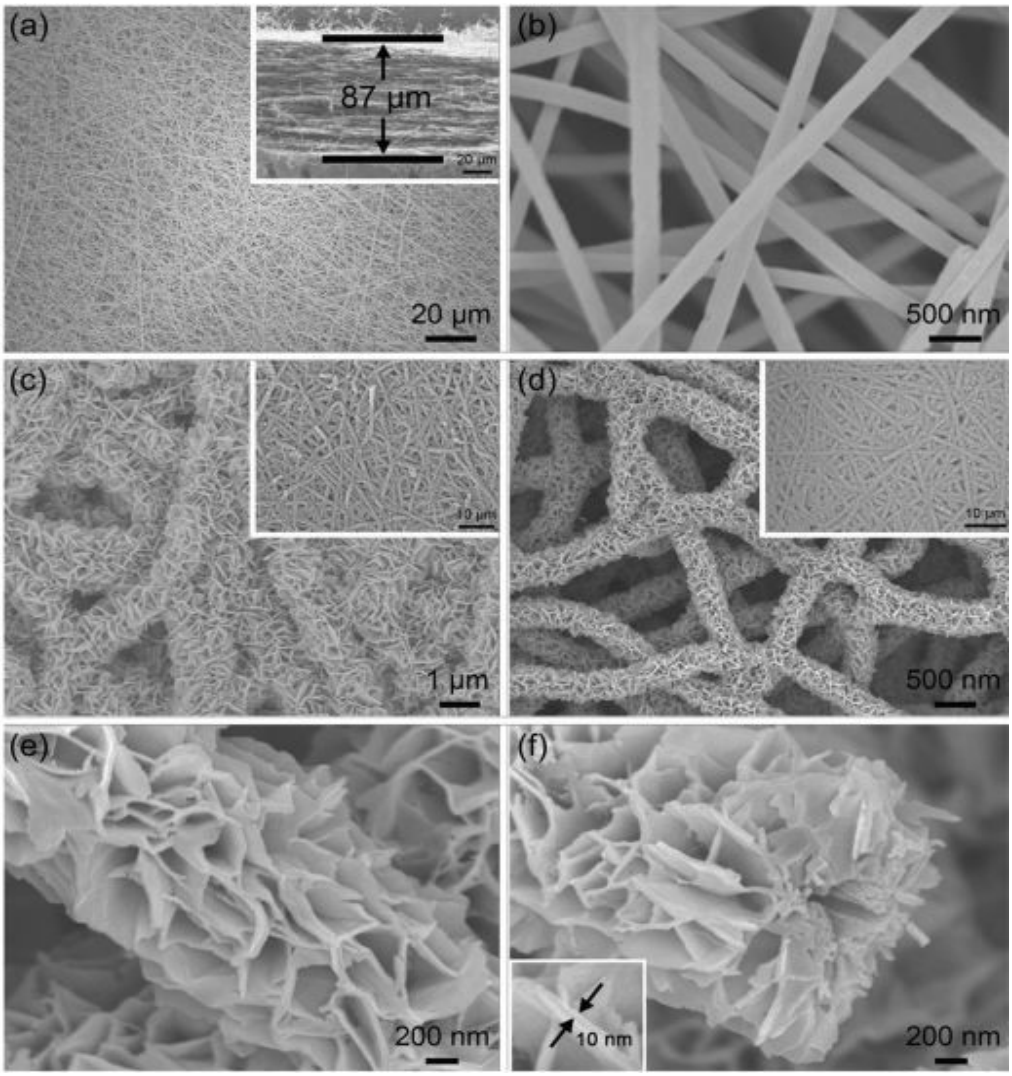

Figure 33: FESEM image of (a,b) electrospun CF substrate in different magnifications (inset image a) cross-sectional view of ECF)), (c) V-O precursor nanosheet array with inset as its large arial view (d-f) crystalized V_2O_5 in various magnification , inset of d) showing the large arial view and inset of, (f) showing the nanosheet with magnified structure. Reproduced with permission from [74] Copyright (2015) WILEY-VCH Verlag GmbH & Co. KGaA, Weinheim.

Textile energy storage systems utilizing the features of wearable electronics is rapidly growing but the development of CF electrode with better capacitance to generate a higher energy density and power density is still remains a challenge. Qin et al. [75] fabricated a carbon cloth (CC) enriched by nitrogen/oxygen (N/O) possess a large surface area and accurate pore volume by electrochemical oxidation approach. The CC electrochemically treated for a duration of 3 minutes (3-CC), pristine CMF bundles and electrochemically-treated CF bundles (3-CMF) possess good mechanical strength and flexibility through the deformation test. The CC and 3-CC did not undergo any breakage when it was wounded on a glass rod with a diameter of ~6 mm and unfolded it afterwards. The CC and 3-CC is found to withstand its original structure (**Figure 34a-c**). The bare CF bundle and electrochemically-treated CF bundle was able to fold onto a logo surface (**Figure 34d**,**e**) and it was weaved into a cloth with area ~1-5 cm^2 using cotton threads (**Figure 34f**). The CMF bundle holding crossed warp and weft composed possessed a diameter of ≈400 μm and it can be observed from the SEM image (**Figure 34g**). After completing the oxidation procedure, the grooves over the surface and embossments are found to be deeper and clear in comparison with the bare one (**Figure 34h**,**i**).

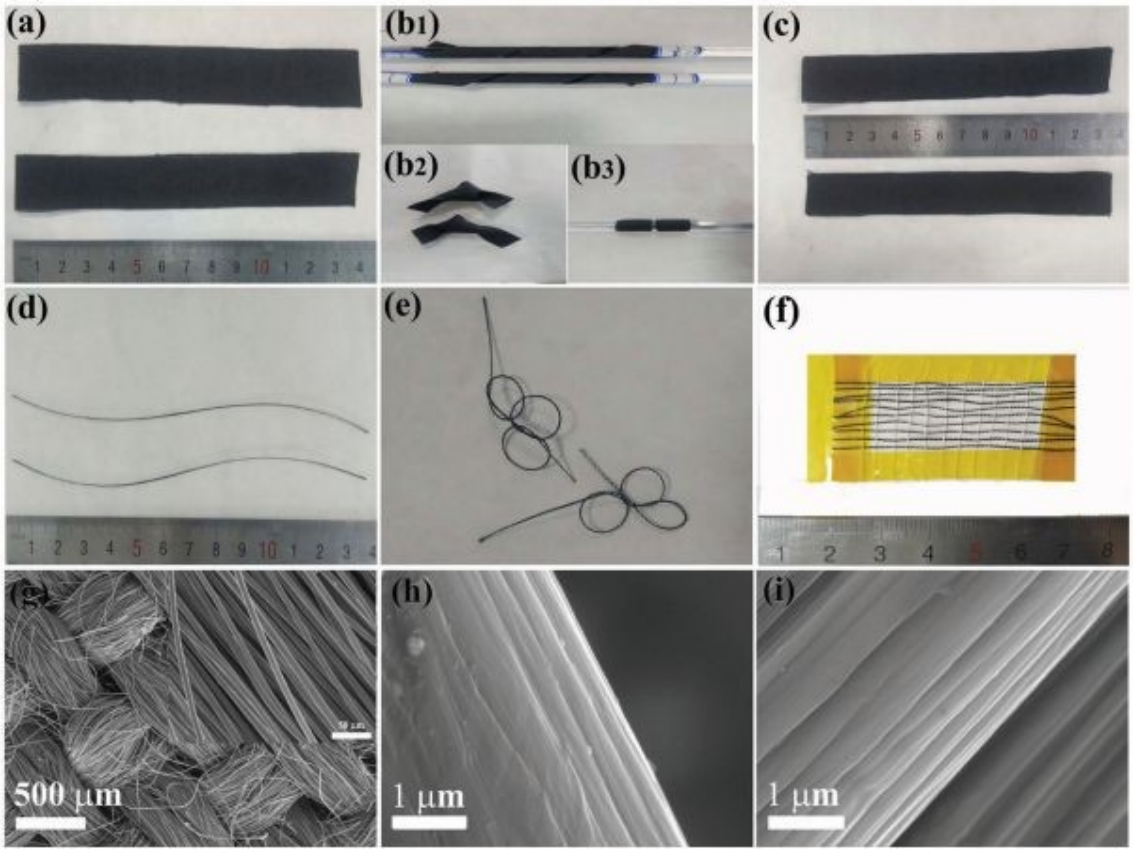

Figure 34: Morphological study of CF, CC and and 3-CC. (a) Optical images of CC (up) and 3-CC (down) before shape changing, b1, b3) wounded on glass rod, b2) kinked, (c) after shape changing; (d) bundles of pristine CF (up) and CF with electrochemical treatment (down), (e kinked; (f) weaved with white cotton threads; (g) SEM images of CC (the inset: its high magnification image) and (h) of pristine CF fiber at high magnification and i) with electrochemical treatment. Reproduced with permission from [75] Copyright (2017) WILEY-VCH Verlag GmbH & Co. KGaA, Weinheim.

The CC and 3-CC electrode-based fiber-shaped and fabric-based SCs were fabricated as shown in **Figure 35a**. The fiber-shaped SC exhibited a higher capacitance of 32 mF/cm^2 than a SC

fabricated with CC (20 mF/cm) (**Figure 35b**). The cyclic stability analysis using GCD measurement is given in **Figure 35c** from which it can be seen that the SC based on CC and 3-CC electrodes exhibited a capacitance retention of 99% and 90%, respectively. These results show that the SCs exhibit excellent cycling stability. The volumetric energy density of the SC fabricated with 3-CC electrode is about 6.8 mWh/cm^3, which is found to be greater than the SC fabricated with CC electrode (≈1.6 mW h/cm^3), as given in **Figure 35d**. The SCs maintained their capacitance while bending it to different bending angles, which indicates its better stability for their implementation in wearable textile devices. The fiber-shaped SCs fabricated with both 3-CC and CC electrodes retained its efficient electrochemical properties while bending it for different cycle numbers, indicates the good flexibility. As an example, about 94% and 85% capacitance value is maintained during bending of the SC fabricated with CC and 3-CC electrodes, respectively (**Figure 35e**). In addition to this, there exists a maintenance of capacitance hold by the Sc fabricated with 3-CC electrode to ~97% even after completing 900 cycles kept at 720º, which is found to be higher than that of the SC fabricated with CC electrode (about 79%), as shown in **Figure 35f**. These hierarchical nanostructured electrodes contain large number of active-sites, which helps in enhancing the capacitance of SCs.

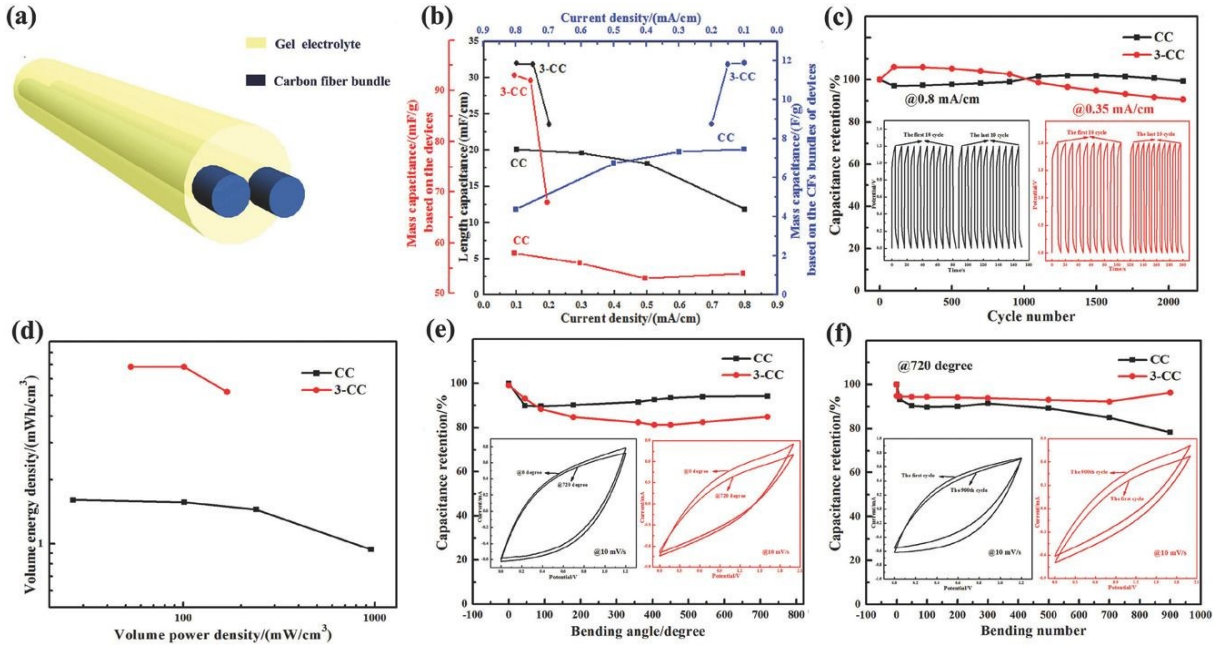

Figure 35: Electrochemical analysis of two-fiber shaped SC with CC and 3-CC bundles (a) schematic of fiber shaped SC; (b) rate calculation based upon GCD with various current density; (c) cyclic stability; (d) ragone plot. Retention of capacitance with (e) bending in 0º and 720º (inset corresponds to CV before and after bending), (f) stability in bending at 720º (inset representing the CV before and after bending). Reproduced with permission from [75] Copyright (2017) WILEY-VCH Verlag GmbH & Co. KGaA, Weinheim.

4.5 Carbon Fibers-Based Hybrid Electrodes

Using in-situ growth method, Yang et al. [33] prepared $(Ni_xCo_{1-x})_9Se_8$ solid solution series on CFC substrate. The $(Ni_{0.1}Co_{0.9})_9Se_8$ nanodendrite arrays were found to exhibit a dense growth over the CFC substrate. Before initiating the growth, there exists a pre-treatment for the CFC

View Article Online
DOI: 10.1039/D4SU00146J

substrate by soaking it on nitic acid and sulfuric acid mixture to introduce a non-uniform surface, which is favourable for its growth. The SEM images given in **Figure 36a** and **b** show the surface morphology of the hierarchical 3D nano-dendrite arrays grown over the CFC substrate. The CV analysis of the SC electrode is performed in a three-electrode cell configuration at different scan rates such as 5, 10, 15, 20, 25, and 30 mV/s and the resultant CV curves are depicted in **Figure 36c**. The CV curve of the system is working in a potential window of 0.05-0.55 V an at a current density of 5 A/g it delivers a specific capacitance of about 591.1 F/ g. The as-fabricated SC electrode can be stranded, folded, pulled, and twisted and the CV curves obtained in each state at a constant scan rate of 50 mV/s is shown in **Figure 36d**. The CV curves are found to be identical in each procedure, which shows excellent flexibility. In the case of assembled device, the GCD measurements were repeated at these states (such as stranded, folded, pulled, and twisted) and the resultant discharge curves are depicted in **Figure 36e** and it can be seen that the discharge curves exhibited a deviation in various states. The asymmetric SC retained a capacitance retention of 88.8% after 3500 cycles (**Figure 36f**). An asymmetric SC was fabricated in a $(Ni_{0.1}Co_{0.9})_9Se_8$@CFC//PVA/KOH//GO@CFC fashion and two such SCs are connected in series lighted-up an LED is given in **Figure 36g**. The asymmetric SC exhibited an energy density of 17 Wh/kg at a corresponding power density of 3.1 kW/kg and 13.7 Wh/kg at a corresponding power density of 10 kW/kg (**Figure 36h**) and these performance metrics shows that this asymmetric SC is capable to meet the growing demand in wearable electronics. Jost et al. [76] developed a textile SC with knitted-CF and activated carbon ink. This textile SC exhibited a specific capacitance of 0.51 F/cm^2 at a scan rate of 10 mV/s. The electrochemical performance of this textile SC is comparable with the standard activated-CF electrode in similar conditions with good flexibility.

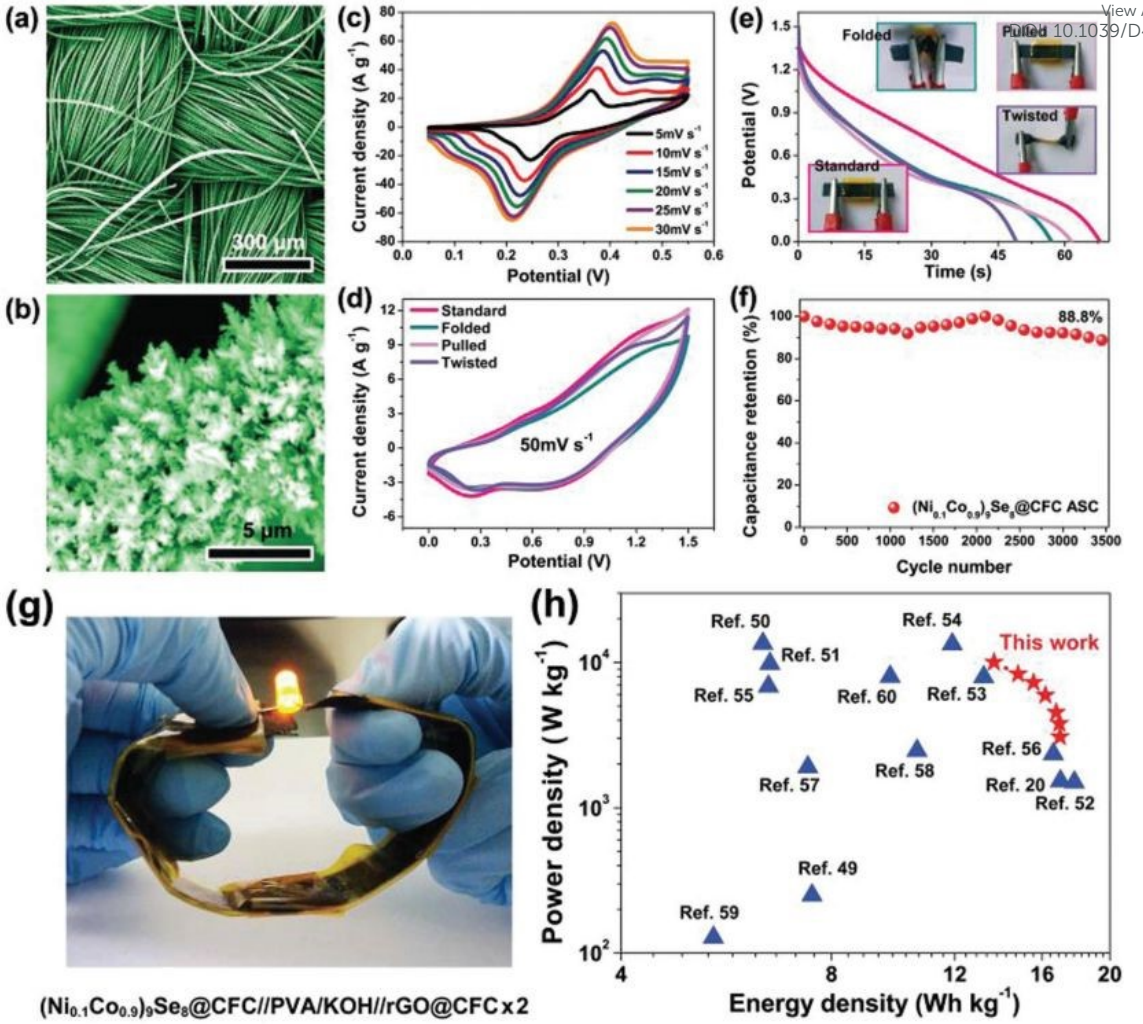

Figure 36: (a, b) SEM image of $(Ni_{0.1}Co_{0.9})_9Se_8$ nanodendrite array grown over CFC; (c) CV and; (d) CV curve for a scan rate of 5 mV/s; (e) GCD curve at 1A/g of the asymmetric flexible SC in various bending conditions; (f) capacitance retention curve; (g) LED indicator lighted by two $(Ni_{0.1}$ Co $_{0.9})_9Se_8$@CFC//PVA/KOH//rGO@CFC asymmetric supercapacitors connected in series (h) Ragone plot in comparison with other reports of nickel-cobalt sulfides and selenides. Reproduced with permission from [33] Copyright (2018) WILEY-VCH Verlag GmbH & Co. KGaA, Weinheim.

By employing ammonia activation and direct procedure of carbonization, Zhan et al. [77] synthesized blow spun activated CF and further used it as an electrode-active material to fabricate a flexible asymmetric hybrid SC. The salient features of this electrode such as highly conducting network, availability of doping with nitrogen, controlled pore structure and surface properties, helped in achieving good electrochemical performance. The asymmetric SC exhibited a high energy of 98 Wh/kg and 9 Wh/kg at a corresponding power density of 400 W/kg and 34 kW/kg, respectively. With the application of dipping-drying method, Zhang et al. [78] introduced CNT/MnO_2 onto activated CF felt substrate. The fabricated flexible SC exhibited an area specific capacitance of 4148 mF/cm^2 with an energy density of 141 µWh/cm^2 at a corresponding power density of 4466 µWh/cm^2. The flexibility of this SC was evaluated while bending it for 100 cycles, indicating its high flexibility. Zhou et al.[79] proposed an effective strategy to develop molten-$NaNH_2$ activated CF cloth for the fabrication of a flexible asymmetric SC. Here, a commercially available CF cloth is oxidized with the aid of wet-

View Article Online
DOI: 10.1039/D4SU00146J

chemical approach and activated with molten-$NaNH_2$. The as-prepared electrode-active material holds many features such as efficient wettability, large surface area, good conductivity and high mechanical strength. The SC electrode delivered a high area specific capacitance of 744.5 mF/cm^2 at a current density of 1 mA/cm^2 with a capacitive retention of 96.94% in 6 M KOH after 10000 cycles. In another report, a flexible solid-state SC was fabricated using a free-standing and porous nanohybrid aerogel containing carbon nanosphere fiber (CNPF)/molybdenum disulfide (MoS_2)/rGO as electrodes and H_2SO_4/PVA gel electrolyte [80]. The CNPF/MoS_2/rGO SC electrode exhibited a specific capacitance of 1144.3 F/g at a scan rate of 2 mV/s. A capacitance retention of 98% was obtained even after completing 10000 cycles at current density of 5 mA/cm^2. The CNPF/MoS_2/rGO SC electrode delivered an energy density of 57.5 µWh/cm^2 at a corresponding power density of 28.8 Wh/kg along with good bendability. Wei et al. [81] fabricated a hybrid Zn-ion SC using polypyrrole/p-phenylenediamine/CF electrode. The as-fabricated hybrid SC delivered a large specific capacity of about 47.6 mAh/g at a current density of 0.2 A/g and found to maintain a capacitance of 85.4% immediately after 1000 cycles and 78.5% after completing 5000 cycles. A coaxial fiber-type electrode was fabricated by Xu et al. [82] by wrapping carbon paper over a MnO_2-modified nanoporous gold wire. The fabricated SC exhibited an area specific capacitance of 12 mF/cm^2 and an energy density of 5.4 µWh/cm^2 with a long cyclic stability. With the aid of an in-situ growth for conductive wrapping mapproach, Tao et al. [83] fabricated a polypyrrole/MnO_2/CF-based hybrid electrode. A SC fabricated with this hybrid electrode structure exhibited a volume specific capacitance of 69.3 F/cm^3 at a current density of 0.1A/cm^3. Also, this SC delivered an energy density of 6.16x10^3 Wh/cm^3 at a corresponding power density of 0.04 W/cm^3. In order to introduce an efficient durability and longer cycle life, Shin et al.[84] fabricated a veil-based flexible SC electrode by using activated-CF (ACF). An optical image of ACF veil is given as **Figure 37a** and it comprising of a porous network structure of non-uniformly distributed ACF holding a thickness in the range of 100 µm (**Figure 37b** and **c**). The permeability of this electrode was examined and found that the permeability of ACF veil electrode is almost the same to that of linen, cotton and nylon (**Figure 37d**) represents its potential in wearable textile application. The synthesis procedure of ACF veil SC electrode fabrication involve various steps including activation of carbon, dispersion, filtration and extraction, as shown in **Figure 37e**.

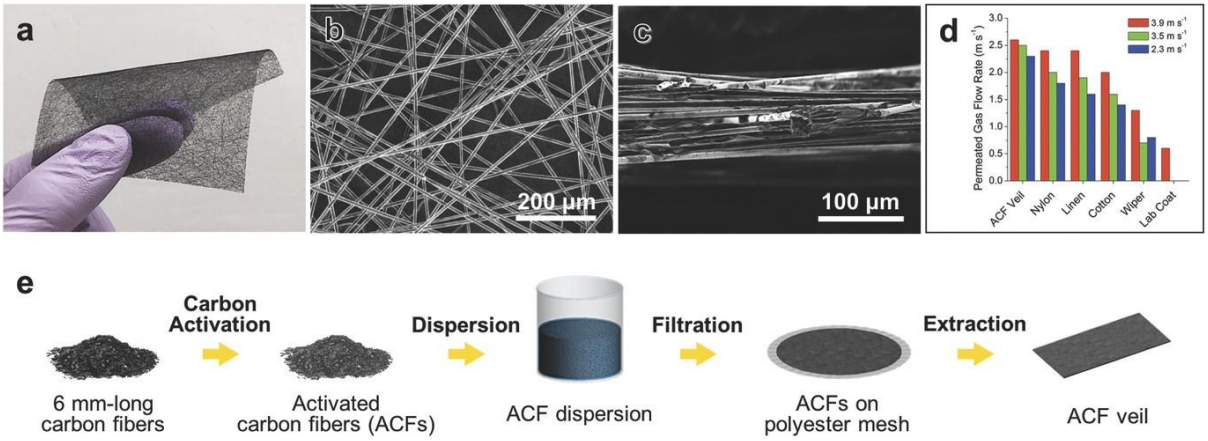

Figure 37: (a) Optical image of ACF veil. SEM images, (b) top view, (c) side view, (d) permeability of air in the network; (e) synthesis process of ACF veil. Reproduced with permission from [84] Copyright (2018) WILEY-VCH Verlag GmbH & Co. KGaA, Weinheim.

View Article Online
DOI: 10.1039/D4SU00146J

The electrochemical performance evaluation of the ACF veil SC electrode is conducted in a two-electrode cell configuration using PVA/H_3PO_4 gel electrolyte, as shown in **Figure 38a**. The CV (**Figure 38b**) and GCD (**Figure 38c**) measurements were also performed at different scan rates such as 1, 3, 5, and 10 mV/s and at different current densities ranging from 77.7 to 466.4 mA/g, respectively, within a potential window of 1 V. The rectangular CV curves and triangular GCD curves proved that the charge storage is by means of EDL formation. The Nyquist plot obtained for the SC is depicted in **Figure 38d** from which it can be seen that at a higher frequency region, a diffuse resistance is generated due to a slower ion diffusion. A rapid reduction in open circuit voltage can also be observed in the prepared SC, where a 50% of energy is conserved after a charging of 5.5 h (**Figure 38e**). The observed potential drop is proportional to the square root of time (**Figure 38f**), which indicates the diffusion-controlled ion concentration variation is prominent mechanism of self-discharge. In another study, Pan et al. [85] reported the preparation of a flexible textile SC electrode based on CNT/PANI fiber composite, which delivered a specific capacitance of 272.7 F/g. This composite electrode was further integrated to generate an energy textile, it makes a conversion of solar energy toward electrical energy other than storing and producing a photoelectric conversion and storage efficiency of 2.1%.

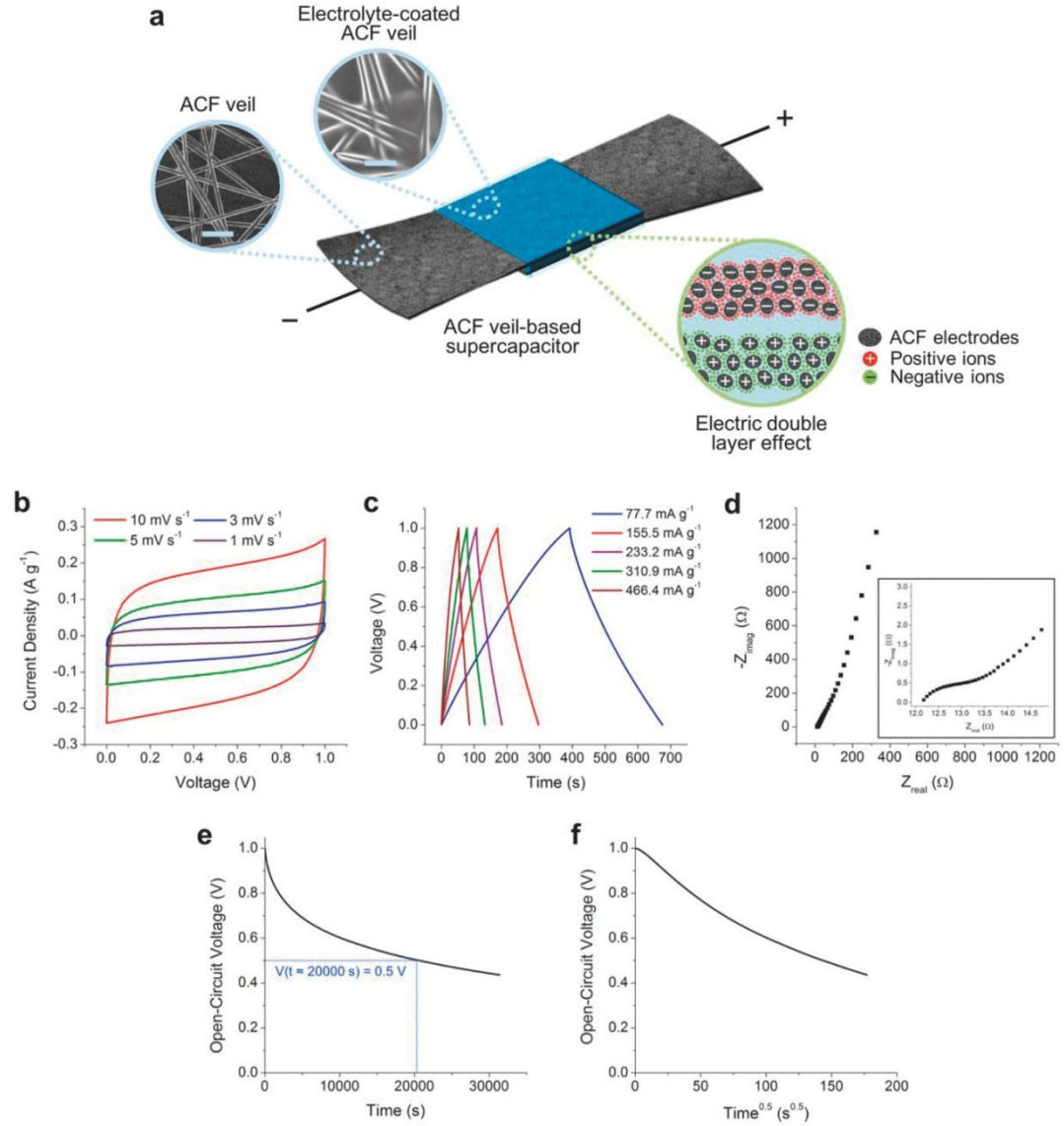

View Article Online
DOI: 10.1039/D4SU00146J

Figure 38: (a) Schematic representation of veil-based SC; (b) CV; (c) GCD; (d) Nyquist plot. Inset represents the high frequency region (e) reduction of OCV with time; (f) OCV with square root of time. Reproduced with permission from [84] Copyright (2018). WILEY-VCH Verlag GmbH & Co. KGaA, Weinheim.

From the above discussion, it can be seen that CF can be used both as a substrate for SC electrode as well as an electrode-active material to fabricate a SC. The prominent features of CF such as flexibility and electrochemical stability, it can be considered as a suitable material for the fabrication of flexible and wearable SC along with other electrode-active materials. **Table 1** provides the salient features of CF-based SC reported in the literature.

Table 1: Salient features of CF-based SCs in the literature.

Sl. No.	Electrode Material	Synthesis Method	Major Observations	Ref.
1.	Coaxial MnO_2-CNF cable mat	Electrodeposition	Coin cell symmetric SC gives a specific capacitance of 47 F/g at 0.5 A/g in a potential window of 0 to 1.6V	[86]
2.	MnO_2/CF hybrid fiber	Electrochemical deposition	Solid state device shows a volumetric energy density 3.8 mWh/cm^3 at a power density 89 mW/cm^3 It possesses an efficient flexibility 85.8% capacitance retention after 10000 cycles	[87]
3.	Meso-macroporous nano-CF	Electrospun method	Symmetric device with NCF having 138 F/g at 5 mV/s and 98 F/g at 100 mV/s	[88]
4.	Free-standing porous coaxial carbon nanofiber	Coaxial electrospinning and template method	Energy density of 48.6±3 Wh/kg and power density 67.5±1 Wh/kg in a two-electrode system	[89]
5.	Polypyrrole-doped with dodecyl benzene sulfonate	Electrochemical deposition	Energy density and power density of 1.20 mWh/cm^3 and 0.59 W/cm^3 at a discharge current density of 1.50 A/cm^3 using LiCl/PVA electrolyte	[90]
6.	Ni-Co selenide on CF paper	Selenization approach	Symmetric SC device possesses volumetric capacitance of 14.55 F/cm^3 at 1 mA/cm^2 and 0.47 mWh/cm^3	[91]

View Article Online
DOI: 10.1039/D4SU00146J

			volumetric energy density at 10 mA/cm^2	
7.	CNT fiber/3D porous CNTs/PANI	Electrophoretic deposition and electrochemical polymerization	Specific capacitance of 67.31 mF/cm^2 at 0.5 mA/cm^2 and it maintains a capacitance of 99.8% even bending it to 180º for 500 cycles	[92]
8.	MnO_2 with cotton derived carbon cloth	Pyrolysis treatment	Area specific capacitance of 202 mF/cm^2 with area specific energy density 30.1 µWh/cm^2 at a power density of 0.15 mW/cm^2. It shows a capacitance retention of 87.7% after 5000 cycles	[93]
9.	$NiCo_2O_4$@MnO_2 core shell	Hydrothermal deposition method	Area specific capacitance of 1.55 F/cm^2 at 2 mA/cm^2 with higher energy density of 1.983 mWh/cm^2 at a power density of 1.72 mW/cm^2 having good stability over 8000 cycles at 50 mA/cm^2 current density	[94]
10.	NiCo layered double hydroxide	In-situ growth with substitution	Flexible device holds a specific capacity of 1377 mC/cm^2 at 1 mA/cm^2 with 70% capacitance retention and 99% coulombic efficiency over 10000 cycles	[95]
11.	Hollow N-doped CF embedded with graphene nanosheet	Coaxial electrospinning and thermal treatment	In a three-electrode system it delivers a specific capacitance of 249 F/g at 1 A/g with capacitance retention of 99% over 5000 cycles in a two-electrode arrangement	[96]
12.	BN co-doped CNTs grown over the surface of CF around carbon cloth	Single step pyrolysis based thermal chemical vapour deposition	It delivers a volumetric capacitance of 21.4 F/cm^3 with 741.8 mWh/cm^3 energy density and 1 kW/cm^3 power density	[97]
13.	3D nanocomposite of CNTs-carbonized cotton fiber-PANI	Single step chemical vapour deposition	Area specific capacitance of 3.1 F/cm^2 at 2 mA/cm^2 current density with a	[98]

			cyclic stability of 91% after 2000 cycles	
14.	$CuCo_2O_4$@$Ni(OH)_2$ /CFC	Simple step procedure	Asymmetric SC device gives a higher energy density 58.9 Wh/kg at a power density of 400 W/kg	[99]
15.	Ni_3S_2/polyaniline on CF	Electrodeposition and in-situ polymerization	Flexible asymmetric SC gives an energy density of 35.7 Wh/kg at a power density of 850 W/kg	[100]
16.	$NiCo_2S_4$ nanotube grown over CF	Hydrothermal method	Asymmetric device gives energy density of 24.78 Wh/kg at a power density of 1770.13 W/kg	[101]
17.	$NiCo_2O_4$ decorated PAN/lignin-based CF	Electrospinning, stabilization, carbonization followed by hydrothermal method	Asymmetric SC device gives a specific capacitance of 134.3 F/g at 1 A/g current density with an energy density of 47.75 Wh/kg at a power density of 799.53 W/kg	[102]
18.	$Ni_{0.4}Co_{0.6}(OH)_2$ grown over CF	Hydrothermal method	Symmetric solid-state SC delivers a specific capacitance of 1816 F/g at 1 A/g with a capacitance retention of 98.3% after 5000 cycles	[103]
19.	$Ti_3C_2T_x$ MXene/CF	Electrospinning of PAN	Gravimetric capacitance of 120 F/g at 2 mV/s with 98% capacitance retention after 10000 cycles	[104]
20.	Crystalline tetraaniline nanofiber deposited over oxidized CFC	Solution based self-assembly approach	Device delivers a capacitance retention of 99.97% after 10000 cycles in H_2SO_4/Na_2SO_4/PVA electrolyte	[105]
21.	V_2O_5 nanosheet assembled over 3D CF	Hydrothermal method	Freestanding asymmetric SC gives energy density of 0.928 mWh/cm^3 at 17.5 mW/cm^3 power density with a capacitance retention of 89.7% after 2000 cycles	[106]
22.	FeNiP@CoNi-LDH grown over carbon cloth	Hydrothermal and phosphorization treatment	Aqueous symmetric SC gives an energy density of 87.3 Wh/kg at power	[107]

			density of 408.8 W/kg with capacitance retention of 73.9% after 20000 cycles	
23.	2D 1T-MoS_2/1D $Cu(OH)_2$ over CF paper	In-situ growth	It exhibits an energy density of 0.13 mWh/cm^2 at a power density of 0.375 mW/cm^2. The device holds 90.8% capacitance retention after 20000 cycles	[108]
24.	Polypyrrole@CF yarn electrode	Electrosynthesis	It delivers a specific capacitance of 50.08 F/cm^3 with an energy density of 4.45 mWh/cm^3 and it maintains a capacitance retention of 89% after 5000 bending cycles	[109]
25.	Polyaniline/manganese hexacyanoferrate	Electrochemical co-polymerization method	Specific capacitance of 730 F/g at 1 A/g current density with a capacitance retention of 85% after 1000 cycles	[110]
26.	Carbon nanofibers@ polypyrrole@ graphene film	Electrochemical deposition	Specific capacitance of 336.2 F/g at 2 mV/s with capacitance retention of 98% after 2500 cycles	[111]
27.	Ultrathick CNT fiber	Sonochemical process	Volumetric capacitance of 523.3 F/cm^3 with a flexibility of 98.4% at a bending angle 90º	[112]
28.	CF surface-grown over helical CNTs and polyaniline	Catalytic CVD and in-situ polymerization	Specific capacitance of 439 F/g at 0.05A/g current density and capacitance retention of 95.4% over 500 cycles	[113]
29.	Micro-nano integrated core sheath CF electrode	Space confined hydrothermal method	Volumetric capacitance of 27 F/cm^3 with energy density of 3.75 mWh/cm^3 and a power density of 612 mW/cm^3	[114]
30.	MnO_2 nanograsses on porous CFC	Simple wet-chemical method	Delivers an energy density of 841 µWh/cm^2 with a capacitance retention of 96% after 20000 cycles	[115]

5. Future Perspectives

View Article Online
DOI: 10.1039/D4SU00146J

CF-based flexible SCs are futuristic devices for widespread wearable electronic applications. The utilization of CF as a flexible substrate to a wearable SC is a facile way to use it for on-body applications. But one of the major demerits underlying with the use of CF in SC fabrication is depends upon its precursor hence the purity. Although CF is highly flexible at its virgin state, during various treatment processes, there is a high chance to reduce its flexibility, structural pattern, etc., thus it is very compulsory to optimize the experimental parameters before using it. Another parameter which depends upon the CF performance is the synthesis method adopted. An optimized concentration of precursor materials is necessary for the introduction of CF with a porous morphology to establish high performance in SC fabrication. The synthesis of CF in a low-cost approach is mandatory, such as synthesis from a biomass derived material where only a small number of reports based on synthesis of CF from biomass materials can be seen from the literature. The derivation of CF from biomass ingredients opens-up a facile pathway for its environment-friendly route. A widespread study on suitable biomaterial that are favourable to synthesis CF may open-up a facile and cost-effective approach to its large-scale synthesis. A long-term stability of CF-based electrode is a major criterion which depicts their durability in application. There exists a probability in reduction of stability hold by CNF due to restacking and other structural distortions, which hurdle their performance in long-run functioning. Another demerit of CNF is the less eco-friendly nature of synthesis hence the synthesis of CNF from less toxic materials is appreciated in the future, such as synthesis from biomass-based materials. By considering these features, CF can be used as a potential electrode candidate in the futuristic wearable supercapacitors with high flexibility and long cyclic stability.

6. Summary

CF is considered a promising sustainable material for a variety of applications due to their high flexibility, ease in synthesis, good mechanical strength, etc. to name a few. In this review, we described the salient features of CF in order to use it in the preparation of SC electrodes. The various synthesis methods of CF were discussed by emphasizing the microstructure and surface morphology of the CF. The various precursors used for the CF synthesis was explained with uniqueness in obtaining a particular morphology. Further, the application of CF in flexible SC application was explained in detail with the help of literature data. Various synthetic methods such as drop-casting or spin-coating approaches were opted for the synthesis of flexible electrodes. The capability of CF-based SC for their easy integration with flexible and wearable electronic devices was examined with the help of various electrochemical analysis tools such as CV and GCD measurements performed at various bending angles and at different states such as folded, pulled, twisted, stranded, etc. We discussed the recent developments on the CF-based electrode-active materials for wearable SCs. CF-based electrode materials enabled excellent flexibility and electrochemical performance to the fabricated flexible SCs including symmetric and asymmetric SCs. The various synthetic approaches to prepare flexible electrodes using polymer-based solid-state gel electrolytes is discussed in detail. The CF-based electrode-active materials should be synthesized in a cost-effective, facile and eco-friendly manner in order to make it a sustainable material for the future. The preparation of CF-based hybrids or nanocomposites for SC electrode application helped in achieving high specific capacitance was included. The demonstration of CF-based SC electrodes in order to meet the requirements of flexible electronic device demonstrations such as in the field of telecommunication, health-monitoring systems, etc were also provided. The CF-based flexible SCs are highly recommended for flexible and miniaturized-devices to compete our daily life. A further development and utilization of CF-based wearable SCs is indeed for the sustainable on-body wearable devices in the future.

View Article Online
DOI: 10.1039/D4SU00146J

Conflicts of interest

The authors declare no conflict of interest.

References

1. Guo, Z., et al., *Flexible self-standing carbon fabric electrode prepared by using simple route for wearable applications.* 2020. **31**(2): p. 1554-1565.
2. Thomas, S.A. and J. Cherusseri, *Boron Carbon Nitride (BCN): Emerging Two-Dimensional Nanomaterial for Supercapacitors.* Journal of Materials Chemistry A, 2023.
3. Wu, C., et al., *Free-standing graphene-based porous carbon films with three-dimensional hierarchical architecture for advanced flexible li–sulfur batteries.* 2015. **3**(18): p. 9438-9445.
4. Han, Y., et al., *Review of flexible supercapacitors using carbon nanotube-based electrodes.* Applied Sciences, 2023. **13**(5): p. 3290.
5. Thomas, S.A. and J. Cherusseri, *A Review of Nb2CT x MXene as an Emerging 2D Material: Synthesis, Applications in Rechargeable Batteries and Supercapacitors, Progress, and Outlook.* Energy & Fuels, 2023.
6. Sim, H.J., et al., *Biomolecule based fiber supercapacitor for implantable device.* 2018. **47**: p. 385-392.
7. Zhang, Y., et al., *Flexible and stretchable lithium-ion batteries and supercapacitors based on electrically conducting carbon nanotube fiber springs.* 2014. **53**(52): p. 14564-14568.
8. Thomas, S.A. and J. Cherusseri, *Strategically designing layered two-dimensional SnS2-based hybrid electrodes: A futuristic option for low-cost supercapacitors.* Journal of Energy Chemistry, 2023.
9. Banerjee, S., et al., *Capacitor to supercapacitor*, in *Handbook of Nanocomposite Supercapacitor Materials I*. 2020, Springer. p. 53-89.
10. Thomas, S.A., et al., *MXene based hybrid materials for supercapacitors: Recent developments and future perspectives.* 2022. **55**: p. 105765.
11. Krishnan, S.G., et al., *Energy storage in metal cobaltite electrodes: Opportunities & challenges in magnesium cobalt oxide.* Renewable and Sustainable Energy Reviews, 2021. **141**: p. 110798.
12. Krishnamoorthy, K., et al., *Supercapacitive properties of hydrothermally synthesized sphere like MoS2 nanostructures.* Materials Research Bulletin, 2014. **50**: p. 499-502.
13. Cherusseri, J., et al., *Flexible supercapacitor electrodes using metal–organic frameworks.* 2020. **12**(34): p. 17649-17662.
14. Li, L., et al., *Advances and challenges for flexible energy storage and conversion devices and systems.* 2014. **7**(7): p. 2101-2122.
15. Thomas, S.A., et al., *Translation of supercapacitor technology from laboratory scale to commercialization*, in *Supercapacitors*. 2024, Elsevier. p. 371-395.
16. Bruce, P.G., B. Scrosati, and J.M.J.A.C.I.E. Tarascon, *Nanomaterials for rechargeable lithium batteries.* 2008. **47**(16): p. 2930-2946.
17. Thomas, S.A., J. Cherusseri, and D. N. Rajendran, *2D Nickel Sulfide Electrodes with Superior Electrochemical Thermal Stability along with Long Cyclic Stability for Supercapatteries.* Energy Technology: p. 2301641.
18. Thomas, S.A., J. Cherusseri, and D. N. Rajendran, *Rapid Synthesis of Hierarchical Tin Disulfide (SnS2) Nanostructures by a Microwave-Assisted Hydrothermal Method for High-Performance Supercapatteries.* ACS Applied Electronic Materials, 2024.
19. Krishnan, S.G., et al., *2D Materials for supercapacitor and supercapattery applications*, in *Adapting 2D Nanomaterials for Advanced Applications*. 2020, ACS Publications. p. 33-47.

View Article Online
DOI: 10.1039/D4SU00146J

20. Jeong, G., et al., *Prospective materials and applications for Li secondary batteries.* 2011. **4**(6): p. 1986-2002.
21. Fergus, J.W.J.J.o.p.s., *Recent developments in cathode materials for lithium ion batteries.* 2010. **195**(4): p. 939-954.
22. Thomas, S.A., et al., *"Water-in-salt" electrolyte—toward high-voltage aqueous supercapacitors*, in *Supercapacitors*. 2024, Elsevier. p. 289-315.
23. Yan, Z., et al., *Recent advances in flexible wearable supercapacitors: properties, fabrication, and applications.* Advanced Science, 2024. **11**(8): p. 2302172.
24. Badawi, N.M., et al., *A review of wearable supercapacitors fabricated from highly flexible conductive fiber materials.* New Carbon Materials, 2023. **38**(2): p. 211-225.
25. Cherusseri, J., et al., *Recent trends in transition metal dichalcogenide based supercapacitor electrodes.* 2019. **4**(4): p. 840-858.
26. Mishra, A., et al., *Carbon cloth-based hybrid materials as flexible electrochemical supercapacitors.* 2019. **6**(23): p. 5771-5786.
27. Pallavolu, M.R., et al., *Scalable synthesis of binder-free hierarchical MnCo2O4 nanospikes/Ni (OH) 2 nanosheets composite electrodes for high-capacity supercapatteries.* Journal of Energy Storage, 2023. **73**: p. 108999.
28. Khadem, A.H., *Recent Advances in Functional Fabric-Based Wearable Supercapacitors.* Advanced Materials Interfaces, 2024. **11**(7): p. 2300724.
29. Lee, S. and G.-H. An, *Interface engineering of carbon fiber-based electrode for wearable energy storage devices.* Advanced Fiber Materials, 2023. **5**(5): p. 1749-1758.
30. Liang, Y., D. Wu, and R. Fu, *Carbon microfibers with hierarchical porous structure from electrospun fiber-like natural biopolymer.* Scientific reports, 2013. **3**(1): p. 1119.
31. Ren, J., et al., *One-pot synthesis of carbon nanofibers from CO2.* Nano letters, 2015. **15**(9): p. 6142-6148.
32. Cherusseri, J., et al., *Vertically aligned graphene–carbon fiber hybrid electrodes with superlong cycling stability for flexible supercapacitors.* 2019. **15**(44): p. 1902606.
33. Yang, P., et al., *Fractal (NixCo1− x) 9Se8 Nanodendrite Arrays with Highly Exposed () Surface for Wearable, All-Solid-State Supercapacitor.* 2018. **8**(26): p. 1801392.
34. Ojeda-López, R., et al., *Tailoring synthesis conditions of carbon microfibers to enhance the microporosity, CO2 and CH4 adsorption by using the response surface methodology.* Microporous and Mesoporous Materials, 2020. **305**: p. 110333.
35. Wang, L., et al., *Mesoporous carbon microfibers for electroactive materials derived from lignocellulose nanofibrils.* ACS sustainable chemistry & engineering, 2020. **8**(23): p. 8549-8561.
36. Saxena, K., P. Kumar, and V. Jain, *Synthesis of carbon microfibers by chemical vapor deposition during the catalytic decomposition of turpentine oil.* New carbon materials, 2011. **26**(5): p. 356-360.
37. Taer, E., W. Mustika, and R. Taslim. *Synthesis of a carbon-activated microfiber from spider webs silk*. in *IOP Conference Series: Earth and Environmental Science*. 2017. IOP Publishing.
38. Yang, Z., et al., *Molten salt guided synthesis of carbon Microfiber/FeS dielectric/magnetic composite for microwave absorption application.* Carbon, 2023. **202**: p. 225-234.
39. Zhihua, L., et al., *Hypha-templated synthesis of carbon/ZnO microfiber for dopamine sensing in pork.* Food Chemistry, 2021. **335**: p. 127646.
40. Su, F., et al., *Template synthesis of mesoporous carbon microfibers as a catalyst support for methanol electrooxidation.* Industrial & engineering chemistry research, 2007. **46**(26): p. 9097-9102.
41. Jiang, X., *CVD growth of carbon nanofibers.* physica status solidi (a), 2014. **211**(12): p. 2679-2687.
42. Zheng, G.-B., et al., *A model for the structure and growth of carbon nanofibers synthesized by the CVD method using nickel as a catalyst.* Carbon, 2004. **42**(3): p. 635-640.

View Article Online
DOI: 10.1039/D4SU00146J

43. Che, G., et al., *Chemical vapor deposition based synthesis of carbon nanotubes and nanofibers using a template method.* Chemistry of Materials, 1998. **10**(1): p. 260-267.
44. Deeney, C., et al., *Template-assisted synthesis of luminescent carbon nanofibers from beverage-related precursors by microwave heating.* Molecules, 2019. **24**(8): p. 1455.
45. Deeney, C., et al., *Templated microwave synthesis of luminescent carbon nanofibers.* RSC advances, 2018. **8**(23): p. 12907-12917.
46. Gopalakrishnan, A., P. Sahatiya, and S. Badhulika, *Template-assisted electrospinning of bubbled carbon nanofibers as binder-free electrodes for high-performance supercapacitors.* ChemElectroChem, 2018. **5**(3): p. 531-539.
47. Matsumoto, Y., et al., *Preparation of carbon nanofibers by hot filament-assisted sputtering.* Materials Science and Engineering: B, 2000. **74**(1-3): p. 218-221.
48. Onuma, Y., et al., *Preparation of carbon nanofibers by hot-filament-assisted sputtering.* Japanese Journal of Applied Physics, 2000. **39**(7S): p. 4577.
49. Ahmed, Y.M., et al., *Synthesis and characterization of carbon nanofibers grown on powdered activated carbon.* Journal of Nanotechnology, 2016. **2016**.
50. Gaud, B., et al., *Synthesis of carbon nano fiber from organic waste and activation of its surface area.* Int. J. Phys. Res. Appl, 2019. **2766**: p. 2748.
51. Kotanjac, Ž., et al., *Synthesis of carbon nanofibers on large woven cloth.* C, 2015. **1**(1): p. 2-15.
52. Ling, X., et al., *Core–shell structure γ-MnO2-PANI carbon fiber paper-based flexible electrode material for high-performance supercapacitors.* 2021. **99**: p. 317-325.
53. Niu, F., et al., *Coral-like PEDOT nanotube arrays on carbon fibers as high-rate flexible supercapacitor electrodes.* 2020. **3**(8): p. 7794-7803.
54. Cherusseri, J. and K.K.J.J.o.M.C.A. Kar, *Ultra-flexible fibrous supercapacitors with carbon nanotube/polypyrrole brush-like electrodes.* 2016. **4**(25): p. 9910-9922.
55. Zhou, Y., et al., *Reclaimed carbon fiber-based 2.4 V aqueous symmetric supercapacitors.* 2019. **7**(5): p. 5095-5102.
56. Ramu, M., et al., *A self-branched lamination of hierarchical patronite nanoarchitectures on carbon fiber cloth as novel electrode for ionic liquid electrolyte-based high energy density supercapacitors.* 2020. **30**(6): p. 1906586.
57. Li, J., et al., *Flexible All-Solid-State Supercapacitor Fabricated with Nitrogen-Doped Carbon Nanofiber Electrode Material Derived from Polyacrylonitrile Copolymer.* 2021. **4**(6): p. 5830-5839.
58. Cherusseri, J. and K.K.J.J.o.M.C.A. Kar, *Hierarchically mesoporous carbon nanopetal based electrodes for flexible supercapacitors with super-long cyclic stability.* 2015. **3**(43): p. 21586-21598.
59. Hu, W., et al., *Electrochemical Performance of Coaxially Wet-Spun Hierarchically Porous Lignin-Based Carbon/Graphene Fiber Electrodes for Flexible Supercapacitors.* 2021. **4**(9): p. 9077-9089.
60. Gao, L., et al., *Flexible fiber-shaped supercapacitor based on nickel–cobalt double hydroxide and pen ink electrodes on metallized carbon fiber.* 2017. **9**(6): p. 5409-5418.
61. Wang, T., et al., *2-Methylimidazole-derived Ni–Co layered double hydroxide nanosheets as high rate capability and high energy density storage material in hybrid supercapacitors.* 2017. **9**(18): p. 15510-15524.
62. Jagadale, A.D., et al., *Binder-Free Electrodes of CoAl Layered Double Hydroxide on Carbon Fibers for All-Solid-State Flexible Yarn Supercapacitors.* 2016. **4**(8): p. 997-1004.
63. Cherusseri, J., R. Sharma, and K.K.J.C. Kar, *Helically coiled carbon nanotube electrodes for flexible supercapacitors.* 2016. **105**: p. 113-125.
64. Yang, C., et al., *All-solid-state asymmetric supercapacitor based on reduced graphene oxide/carbon nanotube and carbon fiber paper/polypyrrole electrodes.* 2014. **2**(5): p. 1458-1464.

65. Liu, Y., et al., *Enhanced electrochemical performance of hybrid SnO 2@ MO x (M= Ni, Co, Mn) core–shell nanostructures grown on flexible carbon fibers as the supercapacitor electrode materials.* Journal of Materials Chemistry A, 2015. **3**(7): p. 3676-3682.
66. Lu, X.-F., et al., *High-performance supercapacitors based on MnO 2 tube-in-tube arrays.* 2015. **3**(32): p. 16560-16566.
67. Lu, X., et al., *A high-performance flexible and weavable asymmetric fiber-shaped solid-state supercapacitor enhanced by surface modifications of carbon fibers with carbon nanotubes.* 2016. **4**(46): p. 18164-18173.
68. Liu, S., et al., *Flexible polypyrrolone-based microporous carbon nanofibers for high-performance supercapacitors.* RSC advances, 2018. **8**(45): p. 25568-25574.
69. Tong, F., et al., *NiS nanosheets with novel structure anchored on coal-based carbon fibers prepared by electrospinning for flexible supercapacitors.* 2020. **22**(9): p. 1625-1632.
70. Ding, M., et al., *Reduced graphene oxide/gC 3 N 4 modified carbon fibers for high performance fiber supercapacitors.* 2021. **45**(2): p. 923-929.
71. Yu, P., et al., *Polyaniline nanowire arrays aligned on nitrogen-doped carbon fabric for high-performance flexible supercapacitors.* 2013. **29**(38): p. 12051-12058.
72. Ai, Y., et al., *Meters-Long Flexible CoNiO2-Nanowires@ Carbon-Fibers Based Wire-Supercapacitors for Wearable Electronics.* 2016. **1**(8): p. 1600142.
73. Shi, M., et al., *Integrated Sustainable Wind Power Harvesting and Ultrahigh Energy Density Wire-Shaped Supercapacitors Based on Vertically Oriented Nanosheet-Array-Coated Carbon Fibers.* 2017. **1**(5): p. 1700044.
74. Li, L., et al., *A flexible quasi-solid-state asymmetric electrochemical capacitor based on hierarchical porous V2O5 nanosheets on carbon nanofibers.* 2015. **5**(17): p. 1500753.
75. Qin, T., et al., *Flexible and wearable all-solid-state supercapacitors with ultrahigh energy density based on a carbon fiber fabric electrode.* 2017. **7**(20): p. 1700409.
76. Jost, K., et al., *Knitted and screen printed carbon-fiber supercapacitors for applications in wearable electronics.* 2013. **6**(9): p. 2698-2705.
77. Zhan, C., et al., *Blow-spun N-doped carbon fiber based high performance flexible lithium ion capacitors.* 2020. **10**(17): p. 9833-9839.
78. Zhang, J., et al., *Comprehensive approaches to three-dimensional flexible supercapacitor electrodes based on MnO2/carbon nanotube/activated carbon fiber felt.* 2017. **52**(10): p. 5788-5798.
79. Zhou, S., et al., *Molten-NaNH2 activated carbon cloth with high areal capacitance and exceptional rate stability for flexible asymmetric supercapacitors.* 2019. **54**(12): p. 9111-9123.
80. Lv, Y., et al., *Nanocellulose-derived carbon nanosphere fibers-based nanohybrid aerogel for high-performance all-solid-state flexible supercapacitors.* 2019. **30**(9): p. 8585-8594.
81. Wei, B., et al., *Highly flexible Zn-ion hybrid supercapacitors based on carbon fibers covalently combined with polypyrrole.* 2022: p. 1-10.
82. Xu, H., et al., *Flexible fiber-shaped supercapacitors based on hierarchically nanostructured composite electrodes.* 2015. **8**(4): p. 1148-1158.
83. Tao, J., et al., *Solid-state high performance flexible supercapacitors based on polypyrrole-MnO2-carbon fiber hybrid structure.* 2013. **3**(1): p. 1-7.
84. Shin, D., et al., *Breathable 3D supercapacitors based on activated carbon fiber veil.* 2018. **3**(11): p. 1800209.
85. Pan, S., et al., *Novel wearable energy devices based on aligned carbon nanotube fiber textiles.* 2015. **5**(4): p. 1401438.
86. Liu, C.-S., et al., *MnO2-based carbon nanofiber cable for supercapacitor applications.* 2021. **33**: p. 102130.
87. Zhang, J., et al., *High-performance all-solid-state flexible supercapacitors based on manganese dioxide/carbon fibers.* 2016. **107**: p. 844-851.

View Article Online
DOI: 10.1039/D4SU00146J

88. Fan, L., et al., *Nitrogen-enriched meso-macroporous carbon fiber network as a binder-free flexible electrode for supercapacitors.* 2016. **107**: p. 629-637.
89. Xiao, Y., et al., *Coaxial electrospun free-standing and mechanically stable hierarchical porous carbon nanofiber membranes for flexible supercapacitors.* 2020. **160**: p. 80-87.
90. Zhou, W., et al., *Polypyrrole doped with dodecyl benzene sulfonate electrodeposited on carbon fibers for flexible capacitors with high-performance.* 2015. **176**: p. 594-603.
91. Xu, P., et al., *3D Ni-Co selenide nanorod array grown on carbon fiber paper: towards high-performance flexible supercapacitor electrode with new energy storage mechanism.* 2017. **241**: p. 41-49.
92. Liu, J.-h., et al., *A high performance all-solid-state flexible supercapacitor based on carbon nanotube fiber/carbon nanotubes/polyaniline with a double core-sheathed structure.* 2018. **283**: p. 366-373.
93. Wan, C., et al., *A high-performance, all-textile and spirally wound asymmetric supercapacitors based on core–sheath structured MnO2 nanoribbons and cotton-derived carbon cloth.* 2018. **285**: p. 262-271.
94. Wu, X., et al., *High flexibility and large energy density asymmetric fibered-supercapacitor based on unique NiCo2O4@ MnO2 core-shell nanobrush arrays electrode.* 2019. **295**: p. 532-539.
95. Xuan, X., et al., *In-situ growth of hollow NiCo layered double hydroxide on carbon substrate for flexible supercapacitor.* 2019. **321**: p. 134710.
96. Li, X., et al., *Flexible all-solid-state supercapacitors based on an integrated electrode of hollow N-doped carbon nanofibers embedded with graphene nanosheets.* 2020. **332**: p. 135398.
97. Paul, R. and A.K.J.E.A. Roy, *BN-codoped CNT based nanoporous brushes for all-solid-state flexible supercapacitors at elevated temperatures.* 2021. **365**: p. 137345.
98. Xing, D., et al., *Development of CNTs-carbonized cotton fiber/PANI 3D-nanocomposites for flexible energy storage and electromagnetic shielding applications.* 2022. **427**: p. 140847.
99. Zhu, D., et al., *Rationally designed CuCo2O4@ Ni (OH) 2 with 3D hierarchical core-shell structure for flexible energy storage.* 2019. **557**: p. 76-83.
100. Wang, L., et al., *Construction of ultra-stable trinickel disulphide (Ni3S2)/polyaniline (PANI) electrodes based on carbon fibers for high performance flexible asymmetric supercapacitors.* 2020. **577**: p. 29-37.
101. Liu, C. and X.J.M.R.B. Wu, *NiCo2S4 nanotube arrays grown on flexible carbon fibers as battery-type electrodes for asymmetric supercapacitors.* 2018. **103**: p. 55-62.
102. Lei, D., et al., *NiCo2O4 nanostructure-decorated PAN/lignin based carbon nanofiber electrodes with excellent cyclability for flexible hybrid supercapacitors.* 2017. **132**: p. 31-40.
103. Wu, X., et al., *A novel and facile step-by-step hydrothermal fabrication of peony-like Ni0. 4Co0. 6 (OH) 2 supported on carbon fiber cloth as flexible electrodes for advanced electrochemical energy storage.* 2018. **174**: p. 325-332.
104. Hwang, H., et al., *High-rate electrospun Ti3C2Tx MXene/carbon nanofiber electrodes for flexible supercapacitors.* 2021. **556**: p. 149710.
105. Wang, D., et al., *High-crystalline tetraaniline nanofibers deposited carbon cloth as flexible electrode for high-performance solid-state supercapacitors.* 2021. **424**: p. 127626.
106. You, M., et al., *V2O5 nanosheets assembled on 3D carbon fiber felt as a free-standing electrode for flexible asymmetric supercapacitor with remarkable energy density.* 2021. **47**(3): p. 3337-3345.
107. Wan, L., et al., *Construction of FeNiP@ CoNi-layered double hydroxide hybrid nanosheets on carbon cloth for high energy asymmetric supercapacitors.* 2020. **465**: p. 228293.
108. Zhang, G., et al., *3D hetero-nanostructured electrode constructed on carbon fiber paper with 2D 1T-MoS2/1D Cu (OH) 2 for flexible asymmetric solid-state supercapacitors.* 2022. **523**: p. 231031.

View Article Online
DOI: 10.1039/D4SU00146J

109. Liu, X., et al., *Design and fabrication of high performance flexible supercapacitor with polypyrrole@ carbon fiber yarn electrode and redox active dopants.* 2021. **271**: p. 116654.
110. Babu, R.S., et al., *Novel polyaniline/manganese hexacyanoferrate nanoparticles on carbon fiber as binder-free electrode for flexible supercapacitors.* 2018. **143**: p. 141-147.
111. Chen, L., et al., *Flexible all-solid-state supercapacitors based on freestanding, binder-free carbon nanofibers@ polypyrrole@ graphene film.* 2018. **334**: p. 184-190.
112. Lee, S., et al., *Flexible supercapacitor with superior length and volumetric capacitance enabled by a single strand of ultra-thick carbon nanotube fiber.* 2023. **453**: p. 139974.
113. Luo, H., H. Lu, and J.J.J.o.E.C. Qiu, *Carbon fibers surface-grown with helical carbon nanotubes and polyaniline for high-performance electrode materials and flexible supercapacitors.* 2018. **828**: p. 24-32.
114. Zhai, S., et al., *Hydrothermal assembly of micro-nano-integrated core-sheath carbon fibers for high-performance all-carbon micro-supercapacitors.* 2017. **9**: p. 221-228.
115. Wang, H., et al., *MnO2 nanograsses on porous carbon cloth for flexible solid-state asymmetric supercapacitors with high energy density.* 2017. **8**: p. 127-133.